A study of high energy flash rubes and their application to ruby lasers

Smith, M. A.

A Study of High Energy Flash Tubes and their Application to Ruby Lasers

By

M.A. Smith, B.Sc., A. Inst. P.

A thesis submitted in candidature for the degree of Master of Science

University of Durham

1968.

Abstract

The design of $6\frac{1}{2}$" arc length xenon filled flash tubes capable of withstanding energy inputs up to 10000 joules is described. The lamp performance is investigated as a function of filling pressure, bore size of lamp between 10 mm and 15 mm, operating voltage, energy input and circuit parameters.

The lamp life has been related to input energy, flash duration and the inner wall area of the lamp. Above a given lamp wall loading, the lamp is likely to shatter in the first few discharges.

Lamp efficiency measurements show that for a fixed capacitor bank, operating voltage variation between 1.0 and 2.4 kV does not change the efficiency and that the efficiency is lower when a lamp is lightly loaded.

Flash duration is almost independent of bank voltage and tube bore. The peak light intensity is increased and the flash duration decreased by a factor 2 when the lamp series inductance is changed from 450 μH to 100 μH.

Design aspects of a laser system using ruby rods $6\frac{1}{2}$" long x $\frac{1}{2}$" diameter are studied and the output characteristics of six ruby rods of varying optical quality measured. The laser performance does not necessarily depend on the rod optical quality.

Measurements of the variation of laser performance with lamp operating parameters show a linear relationship between output energy and input energy above laser threshold. For maximum efficiency, the lamp should be operated with a low bank capacity, a high bank voltage and short flash duration provided the lamp wall loading limit is not exceeded. The 10 mm bore lamp gives the highest efficiency.

Measurement of the output beam divergence shows that the ruby rods giving the lowest beam divergence are of the best optical quality.

Acknowledgements

The author wishes to thank the management of Thermal Syndicate Ltd. for permission to submit his research work for the Company in this thesis. The valuable advice of G.W. Stephenson is gratefully acknowledged. Thanks are also due to Dr J. Thorp for his supervision and for reading the proof. The assistance of the tracer and the photographic department in preparing the figures and the work of the typist is greatly appreciated.

M. A. Smith.

Contents

Chapter 1. Fundamental Theory of Lasers

1.1 Emission and Absorption of Radiation

Emission of light from any type of source involves transfer of energy in some form to the atoms which eventually provide the output light. This input energy can be thermal, electrical, mechanical or another form of light. For a black body radiation source, such as an incandescent light filament, the input energy is electrical and the light is emitted over a broad spectrum according to the Stefan-Boltzmann radiation laws. For a line spectrum source such as a mercury or sodium discharge lamp, the atoms absorb the input electrical energy and are then said to be in an excited state. It is well known that an atomic system can exist in certain stationary states, each corresponding to a definite value of the energy possessed by the atom, ion or molecule. These states are called the energy levels of the atomic system and are represented by quantum numbers. Transitions between states can occur (subject to certain rules) with emission or absorption of energy as radiation or with energy transfer to or from another system. The frequency, υ, of a radiative transition is given by the Bohr frequency relation,

$$h\upsilon_{21} = E_2 - E_1 \qquad (1.1)$$

where h is Planck's constant and E_2 and E_1 are the energies of the two levels. The ground state is the level of the system with the lowest energy; every other level is an excited state. When the atomic system is not in the ground state, an atom may change without external cause to a lower level. The radiation emitted, completely random in phase and direction, is known as spontaneous emission. All light sources other than the laser radiate by spontaneous emission of photons.

The idea of a second type of emission or absorption was advanced by Einstein in 1917. Quantum mechanical analysis shows that under the influence of external radiation υ_{21} an atom can either gain energy by undergoing a $1 \rightarrow 2$ transition or lose energy by a $2 \rightarrow 1$ transition. In the latter case the atom is stimulated to emit radiation of the same phase and in the same direction as the incident radiation. The probability of an atom in state 2 giving up

energy to the radiation field is exactly equal to the probability of an atom in state 1 absorbing the same amount of energy from the field. Thus if an atomic system contains N_1 atoms per unit volume in state 1 and N_2 in state 2, the field is attenuated if $N_1 > N_2$ and amplified if $N_2 > N_1$. In the latter case, stimulated emission predominates and this forms the basis of the laser. Laser is an acronym for Light Amplification by Stimulated Emission of Radiation.

Two conditions are necessary for light amplification; the excess of atoms in the excited state 2 known as population inversion and a cavity resonance.

1.2 Population Inversion

Under conditions of thermal equilibrium, an atomic system at an absolute temperature T has a population ratio given by the Boltzmann relation:

$$\frac{N_2}{N_1} = \exp^{-\frac{(E_2-E_1)}{kT}} \qquad (1.2)$$

where k is Boltzmann's constant. Normally therefore, $N_2 < N_1$ and the condition for light amplification can never be satisfied. To achieve a non-equilibrium population inversion, several conditions must be fulfilled. Laser materials must possess a metastable level from which all normal transitions to a lower level are forbidden. An atom entering this level will therefore remain for a time long compared with the normal transition time. Figure 1a shows the pertinent energy levels of a three level laser system such as ruby. Level 1 is the ground state and 3 represents an absorption band of the material. Most of the absorbed energy W_{13} is transferred by a fast radiationless transition S_{32} to the intermediate sharp level 2 which is metastable. If the exciting radiation is discontinued, emission will still go on from level 2 as fluorescence consisting of spontaneous emission A_{21} with some stimulated emission W_{21}. Since the rates of $W_{13} + S_{32} \ll A_{21}$, there will be a build up of atoms in level 2 when the exciting radiation is sufficiently intense. In the particular case of a three level laser, amplification cannot occur until at least 50% of the atoms are in level 2 because the transition probabilities of W_{21} and W_{12} are equal. In practice, losses in an actual system require more than 50% population inversion. The amount of energy required to just achieve light amplification is called the laser threshold energy.

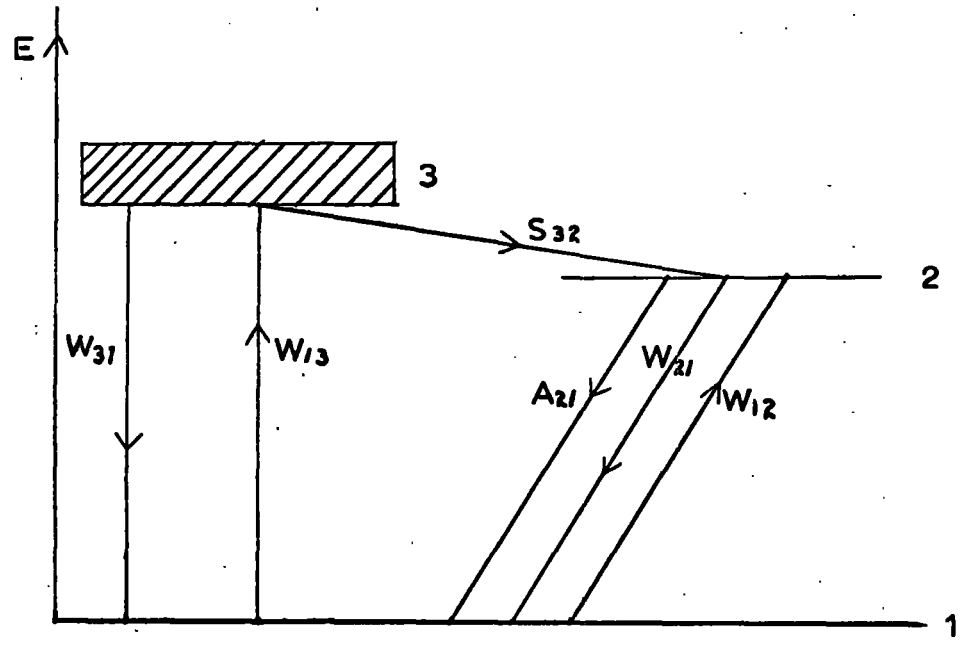

FIG. 1a. 3 LEVEL SYSTEM

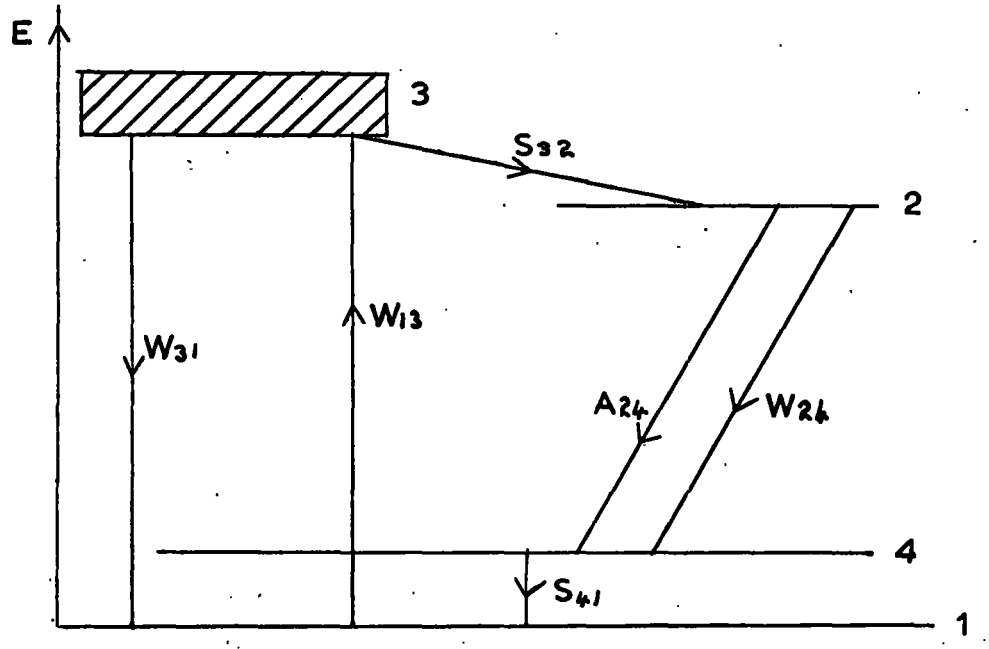

FIG. 1b. 4 LEVEL SYSTEM

Figure 1 b shows the energy levels of a four level laser system. The essential difference lies in the laser transition terminal level 4 which is normally unoccupied at the operating temperature. Provided transition S_{41} is sufficiently rapid, the probability of stimulated absorption is negligible. Light amplification can now occur as soon as there is sufficient occupation of metastable level 2 to overcome oscillator losses.

The total stimulated transition rate W_{12} is given by:

$$W_{12} = \frac{C_1^2}{8\pi h \upsilon^3 t_s} \; g(\upsilon) \; I \qquad (1.3)$$

where I is the inducing flux density, $g(\upsilon)$ a factor depending on the sharpness of the energy level and t_s the spontaneous emission lifetime. C_1 is the velocity of light in the medium. (YARIV and GORDON 1963)

1.3 Line Width

Since the energy levels in a solid are not perfectly sharp, the radiation emitted is spread about frequency υ_{21}. The line width can be estimated using the Heisenburg Uncertainty Principle where the spread in energy of an excited state δE is defined by:

$$\Delta E . \; t_s \approx \frac{\hbar}{2\pi}$$

t_s is the life time of an atom in the state and $t_s = \frac{1}{A_{21}}$

Since $\Delta E = h\Delta\upsilon_{21}$, the line width in terms of frequency is given by:

$$\Delta\upsilon_{21} = \frac{A_{21}}{2\pi} \qquad (1.4)$$

The exact line shape depends on the mechanism which shortens the life time. A Lorenztian line shape results from processes involving the collision of a radiating atom with the lattice. A Gaussian line shape arises from a random variation in the distribution of the atoms. The atomic line shape function $g(\upsilon)$ is defined by YARIV and GORDON (1963). For a Lorenztian line shape with a full width at half peak $\Delta\upsilon$ centred about υ_c.

$$g(\upsilon) = \frac{\Delta\upsilon}{2\pi \left[(\upsilon - \upsilon_c)^2 + \left(\frac{\Delta\upsilon}{2}\right)^2 \right]}$$

Once laser action begins the linewidth is reduced, so for $\upsilon \simeq \upsilon_c$

$$g(\upsilon_c) = \frac{2}{\pi \Delta \upsilon} \qquad (1.5)$$

Similarly for a Gaussian line shape

$$g(\upsilon_c) = \frac{2(\pi \ln 2)^{\frac{1}{2}}}{\pi \Delta \upsilon}$$

A Lorenztian line shape is usually assumed in a solid state laser.

1.4 Cavity Resonance

Resonant cavity design depends upon obtaining optimum amplification characteristics from a pair of highly reflecting surfaces separated by the laser material.

The characteristics of a cavity with a passive medium as the spacer are well known in the form of the Fabry-Perot interferomter, (BORN and WOLF 1959). With a laser, the spacing medium is capable of amplifying the electromagnetic field in the cavity. In the case of a solid state laser, the material is generally formed into a rod whose ends are polished flat and parallel to within a few seconds of arc. In some cases, low loss dielectric reflecting coatings are vapour deposited on the rod ends. However, most high power systems employ external reflectors accurately aligned with the end faces. The laser output is obtained by making one of these mirrors partially transmitting.

The cavity oscillation consists of a standing wave generated by the plane wave I (Equation 1.3) between the reflectors. This wave can be attenuated by a number of factors. These are mainly:

a) transmission and absorption of the mirrors;
b) scattering by optical inhomogeneities in the laser material (KAISER and KECK 1962);
c) absorption in the material due to mechanisms other than W_{12};
d) diffraction losses due to the mirror apertures;
e) losses due to interactions between different oscillator modes.

All loss mechanisms are characterised by a single parameter t_p equal to the decay time constant of the radiation with the amplifying medium neutral

i.e. $N_1 = N_2$. If α is the total loss per pass in the cavity of length L, then:

$$t_p = \frac{L}{\alpha C_1} = \frac{Q}{2\pi\upsilon} \qquad (1.6)$$

where Q is the resonant cavity factor. ($\alpha << 1$).

1.5 Threshold Condition

The increase in intensity I due to stimulated emission is given by:

$$\left(\frac{dI}{dt}\right)_1 = h\upsilon\left(N_2 - N_1 \frac{g_2}{g_1}\right) C_1 W_{12}$$

The factor $\frac{g_2}{g_1}$, where g is the degeneracy of the level, applies where a number of atomic states have the same energy level.

The intensity loss is:

$$\left(\frac{dI}{dt}\right)_2 = -\frac{I}{t_p}$$

For amplification or sustained oscillation,

$$\left(\frac{dI}{dt}\right)_1 + \left(\frac{dI}{dt}\right)_2 \geq 0$$

The threshold condition is therefore:

$$h\upsilon\left(N_2 - N_1\frac{g_2}{g_1}\right)C_1 W_{12} = \frac{I}{t_p}$$

Substituting for W_{12} from (1.3) gives

$$\left(N_2 - N_1\frac{g_2}{g_1}\right) = \frac{8\ \pi\ \upsilon^2}{C_1{}^3 g(\upsilon_c)}\ \frac{t_s}{t_p}$$

which for a Lorenztian line shape using (1.5) gives:

$$\left(N_2 - N_1\ \frac{g_2}{g_1}\right) \geq \frac{4\pi\upsilon^2\Delta\upsilon}{C_1{}^3}\ \left(\frac{t_s}{t_p}\right) = \frac{\Delta N_c}{V} \qquad (1.7)$$

ΔN_c is defined as the critical population inversion at threshold.
ΔN_c is the critical inversion density. (YARIV and GORDON 1963).

1.6 Pump Power Requirement

The threshold pump power per unit volume is:

$$P = \frac{N_2 h\upsilon}{t_s}$$

Substituting for t_s from (1.7) gives:

$$P = \frac{N_2}{\Delta N_C} \cdot \frac{4\pi^2 h\upsilon^3 V \Delta\upsilon}{C_1^3 t_p} \qquad (1.8)$$

For a four level system $N_2 \simeq \Delta N_C$. In the .05% doped ruby normally used, $\Delta N_C \simeq 10^{16}$ and $N_2 \simeq 10^{18}$ so the pump power requirement is increased by a factor 100. In practice there are almost always a multiplicity of possible modes of oscillation in the resonant cavity which complicate the theoretical concepts and the threshold pump power is generally higher than that given by theory. For ruby, assuming a scatter-free crystal, the cavity loss factor t_p can be determined for a single mode. The threshold pump power required is found to be 475 w/cm^3.

MAIMAN (1964) has related the pump power requirement to the brightness temperature of the pump source. The minimum brightness temperature for pumping ruby is shown to be 4800°K in an ideal system. Figure 2 shows the brightness temperature of typical sources and a curve of pump efficiency vs. black body temperature for ruby. The peak pump efficiency for ruby is given by a source equivalent to a black body at 8500°K. This brightness temperature can only be achieved by a pulsed arc. Ruby has been pumped by a C.W. arc (NELSON and BOYLE 1962) although operation is marginal. Recently C.W. operation of ruby has been reported using a mercury vapour lamp with pulses superposed on the normal d.c. excitation. (ROESS and ZEIDLER 1966)

Pulsed discharges, as well as producing radiation of the required colour temperature for ruby laser pumping, offer a reasonably efficient means of converting stored electrical energy into light energy. It has been shown theoretically that the light output of a pulsed discharge in a noble gas varies approximately with the square root of the atomic weight of the gas. Relative efficiency values for Argon, Krypton and Xenon in the ratio 100: 130: 160: are confirmed experimentally. (MARSHAK 1956). Determination of the optimum characteristics of xenon filled discharge tubes is an important factor

Source	Brightness Temperature
Pulsed Arc	5000 - 15000°K
Sun	5800°K
C.W. Arc	4000 - 5500°K
Incandescent Body	2400 - 3400°K

(a) TYPICAL BRIGHTNESS TEMPERATURES

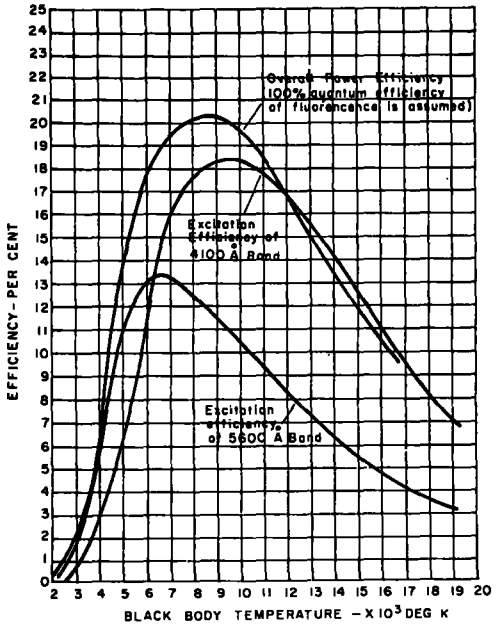

(b) EFFICIENCY CURVES FOR BLACK BODY PUMPING OF RUBY

FIGURE 2

in the design of a high energy ruby laser system.

1.7 Laser Materials

The data in the preceeding paragraphs may be used to consider the essential conditions to be met in a laser material. These are:

(a) a narrow laser line width $\Delta\upsilon$;

(b) long lifetime of the metastable level. The lifetime in ruby ($\simeq$ 3 milliseconds at room temperature) is one of the longest observed in practical laser materials;

(c) a high value of the loss parameter t_p. This implies a scatter free material, a low loss optical cavity and all upward transitions from the metastable state forbidden;

(d) downward transitions from the metastable level should be purely radiative, i.e. t_s = metastable level lifetime;

(e) in a four level laser the terminal level should be unpopulated at the operating temperature. A fast transition between the terminal level and the ground level is thus essential;

(f) the absorption bands of the laser ion must be broad and have a high quantum efficiency. The host lattice may also have absorption bands giving energy transfer to the active ion, e.g. Er_2O_3: Tm^{3+}(SOFFER and HOSKINS 1965). The relatively low threshold in ruby despite its being a three level system is due to the broad absorption bands in the green and blue region of the spectrum (see Figure 3).

Most four level laser materials have narrow absorption bands so although they might have a low threshold, the overall efficiency tends to be low. Others have absorption bands which allow upward radiative transitions from the metastable level with a loss of stimulated photons. The most practical four level laser ion is Nd^{3+} in a host lattice of glass or calcium tungstate. Because large pieces of high optical quality material can be manufactured, high pulse energy outputs ($\simeq$1000 joules) are attainable from large rods (BOWNESS and MISSIO 1963).

A serious disadvantage of this and other four level laser crystals is the tendency to suffer damage under intense pumping due to low thermal shock resistance. Ruby is outstanding in its hardness and high thermal conductivity (exceeding that of copper at low temperatures). It is clear therefore why

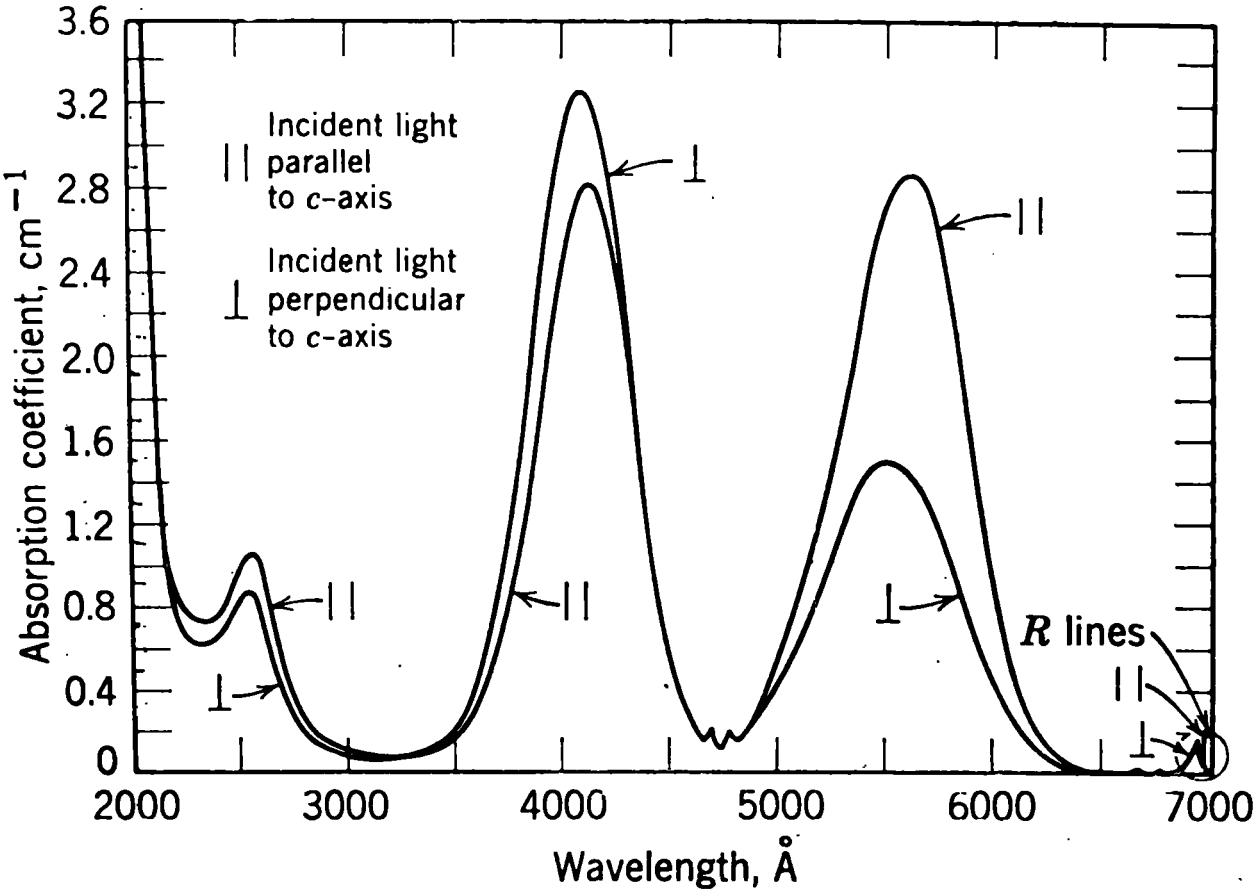

Figure 3: ABSORPTION SPECTRUM OF RUBY

ruby, despite the high threshold, is used for most applications requiring a high pulse energy from a reasonably compact laser system.

1.8 The Solid State Laser

An optically pumped solid state laser may be considered as a multi-stage energy conversion device whose overall efficiency is dependent on four separate stages; the conversion of electrical energy into light energy by the flash tube, the coupling of the light energy into the laser material by the pumping geometry, the laser material itself and, finally, the efficiency of the resonant Fabry-Perot cavity. The efficiency of linear xenon flash tubes as converters of electrical energy into radiation corresponding to the absorption bands of ruby will be studied in chapter 5. The effects of ruby rod quality on laser performance are examined in chapter 8.

Two main pumping goemetries are used for achieving population inversion in a solid state laser; (a) the laser rod is placed along the axis of a helical flash tube surrounded by a cylindrical reflector and (b) a linear flash tube is placed in one focal line of an elliptical reflecting cylinder and the laser rod placed in the other focal line.

The former system was that used by MAIMAN (1960) in the original ruby laser, the latter was first used by CIFTAN et al (1961) who compared the efficiency of both geometries using the same ruby and found a substantial improvement with the elliptical reflector. CONGLETON et al (1963) and KAMIRYO et al (1965) also found that the elliptical cylinder is more efficient in pumping a ruby fine ground on its cylindrical surface. The linear flash tube/elliptical cylinder pumping arrangement is the one used in this work.

The efficiency of the resonant Fabry-Perot cavity depends on the factors set out in 1.4. With a good quality ruby rod, the most important of these is the reflectivity of the partially transmitting output mirror. The variation of output energy with mirror reflectivity has been examined by WHITEMAN (1966). The optimum reflectivity was found to depend also on the length of the ruby rod. For a $6\frac{1}{2}$" x $\frac{1}{2}$" diameter ruby rod, the optimum mirror reflectivity is about 20%. The ability of the reflectors to withstand high energy laser pulses is also important and will be discussed in chapter 7.4.

Chapter 2. Flash Lamp Design and Production

2.1 Envelopes

The production of high quality vitreous silica at Thermal Syndicate permits selection for flash lamp manufacture. Only tubing free from wall defects such as bubbles is used. Attention to this detail ensures that the tubes can withstand the shock waves associated with high energy devices. Figure 4 highlights the differences that can occur in tubing such as striae. Selected A quality or 066 tubing is normally used for discharge lamps since the cost of the higher optical quality Spectrosil would be prohibitive.

2.2 Electrodes

Prototype flash tubes were made using pure Molybdenum and Tungsten electrodes. Condensation of electrode material on the tube wall caused early failure due to tracking of the discharge with subsequent shattering of the envelope. The less volatile tungsten proved a more suitable electrode material. A 1% thoriated tungsten was then tested and found to exhibit less sputtering and to prolong tube life. Thoriated cathodes have a lower work function than pure tungsten.

Investigation of electrode shape showed the necessity for a profile as in Figure 5. This together with a highly polished electrode surface reduces localised erosion by the discharge. Figure 6 shows the cathode deterioration due to a pure tungsten electrode of the wrong shape. Prior to flash tube assembly, the electrodes are cleaned chemically to remove oxide and degassed at high temperature under vacuum.

2.3 Seals

The seals used are a modification to the quartz-lead seal used for high current feed-through insulators in the valve manufacturing industry. A typical seal is shown in Figure 5.

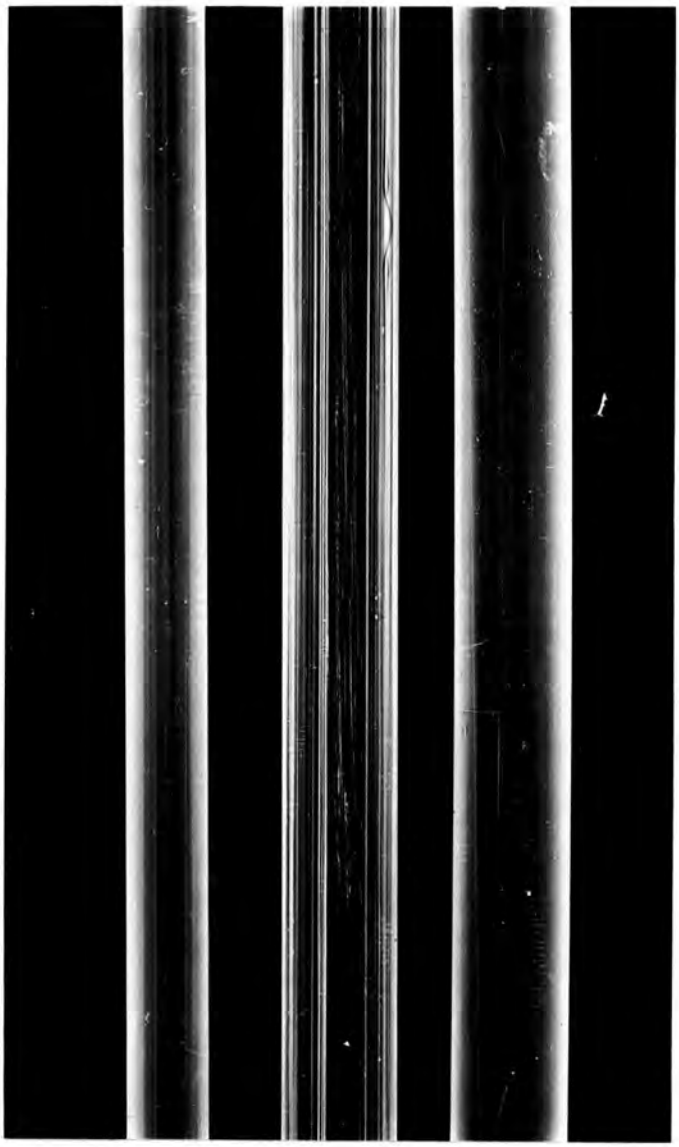

A B C

A : SPECTROSIL
B : NORMAL QUALITY
C : 066 GRADE

Figure 4: COMPARISON OF TUBING QUALITY

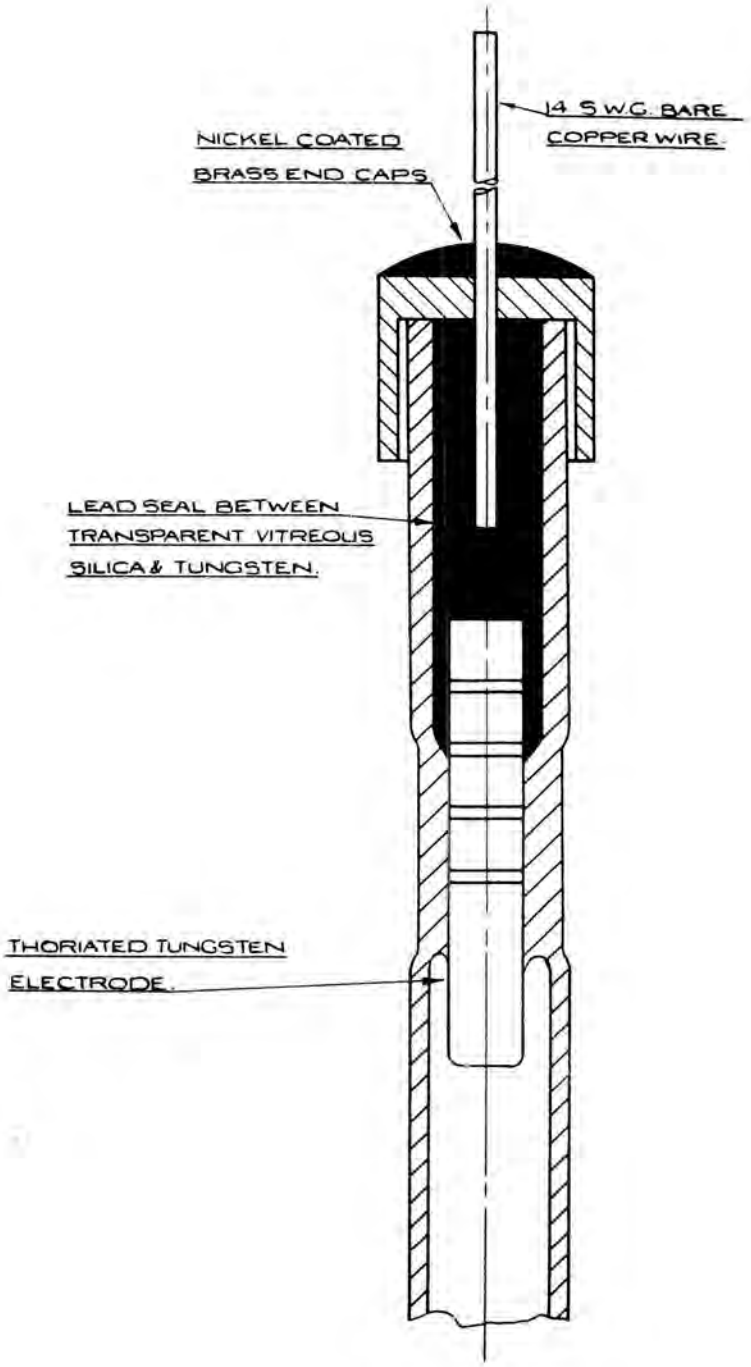

Figure 5: FLASH TUBE LEAD SEAL

A : New flash tube

B : Pure tungsten cathode
50 shots at 10kj

C : Thoriated tungsten cathode
1000 shots at 10kj

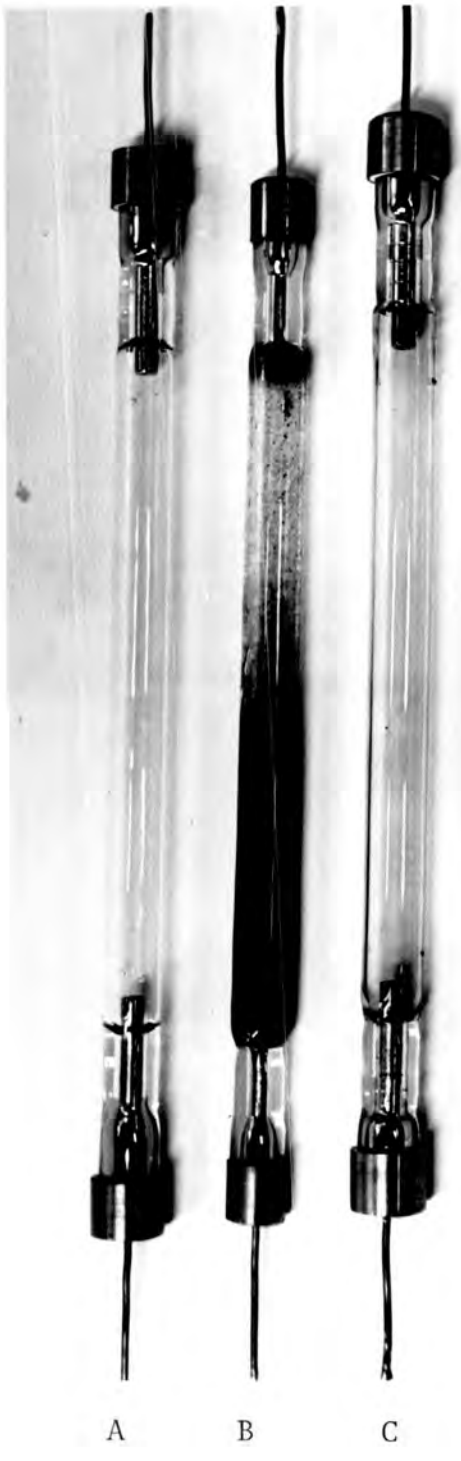

Figure 6: SPUTTERING OF PURE TUNGSTEN CATHODE

These seals:

(a) withstand the high energy shock waves generated during the discharge

(b) accomodate large diameter electrodes

(c) provide an excellent vacuum seal by virtue of the large area contact between the lead and the tube wall

(d) reduce overheating of the electrodes by virtue of their high thermal conductivity

2.4 Lamp Manufacture

The method of manufacture eliminates a seal-off stem in the arc tube, a possible source of weakness. The various stages in fabrication are shown in Figure 7. Attachment of preformed seal tubes to the arc tube by lathe working provides the concentric assembly (7a). The cleaned and degassed electrodes and lead are then introduced and one end of the tube sealed (7b). The tube is attached to a pumping system, evacuated and baked. Specpure xenon gas is then admitted, the required filling pressure being read from a dial gauge. The tube is drawn off from the filling system and the electrodes are manoeuvred into position and fixed by carefully heating the tubing around them. The pressure differential causes the tubing to run down onto the electrodes. The lead is then melted and the tube held upright to allow the lead to form the seal. The seal ends are cut off and the lead at the top of the seal re-melted for insertion of tinned copper connecting wires. (See Figure 7c and d). End caps cemented to the seal and soldered to the copper wire complete the lamp assembly, Figure 4.

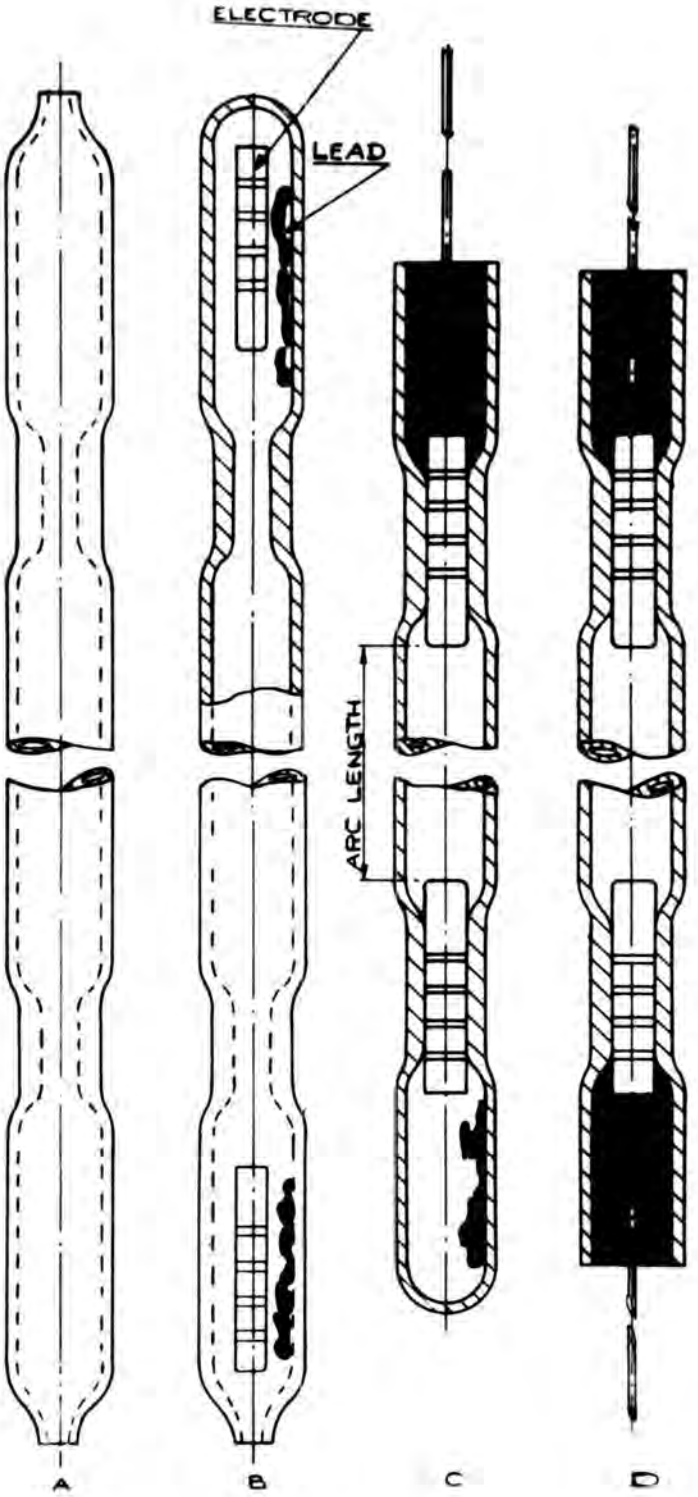

Figure 7: STAGES IN LAMP MANUFACTURE

Chapter 3. Flash Tube Excitation and Monitoring Equipment

3.1 Capacitor Bank

The capacitor unit shown in Figure 8 consists of eight trays of oil filled paper capacitors, each tray having a nominal value of 462 microfarads. A thyratron controlled charging unit provides a D.C. voltage between 1.2 KV and 2.5 KV. An external variac added to the primary circuit of the H.T. transformer allows bank voltages lower than 1.2 KV and slows the charging rate. The bank voltage is observed on a built-in meter. This meter was checked with an AVOMETER 8 connected to the output and found to be accurate to within 2%. With the lower H.T. voltages, the internal trigger supply of the charging unit does not provide sufficient pulse voltage to trigger the flash tube. A more efficient pulse unit has been constructed with a variable voltage output. This is set to trigger satisfactorily at the lowest H.T. voltage used (1 KV). As the manufacturing tolerance of the capacitors lies between -10% and +20% of the stated value, the bank capacity was determined using a Marconi bridge accurate to 3%.

3.2 Series Inductors

The inductors are made from $\frac{1}{2}$" wide $\frac{1}{8}$" thick insulated copper strip wound in a flat spiral. The approximate inductance of the spiral winding was determined as a function of the dimensions. An inductance bridge, accurate to 5%, was used to measure the actual value. Inductors of 100 μH, 235 μH, and 450 μH have been used in this work. The D.C. resistances of the coils and the associated connecting leads were measured using a valve micro-voltmeter and ammeter. The voltage readings were plotted against current and the resistance calculated from the gradient.

3.3 Oscilloscope

A Hewlett-Packard model 175A oscilloscope with a band width of at least 50 Mc/sec is used. With the appropriate plug-in unit this instrument is capable of measuring rise times of less than 7 nanoseconds. The horizontal amplifier ranges extend in 1-2-5 steps from 0.1 μsec/cm to 5 secs/cm with an accuracy of ± 3%. With the 1755 A vertical amplifier,

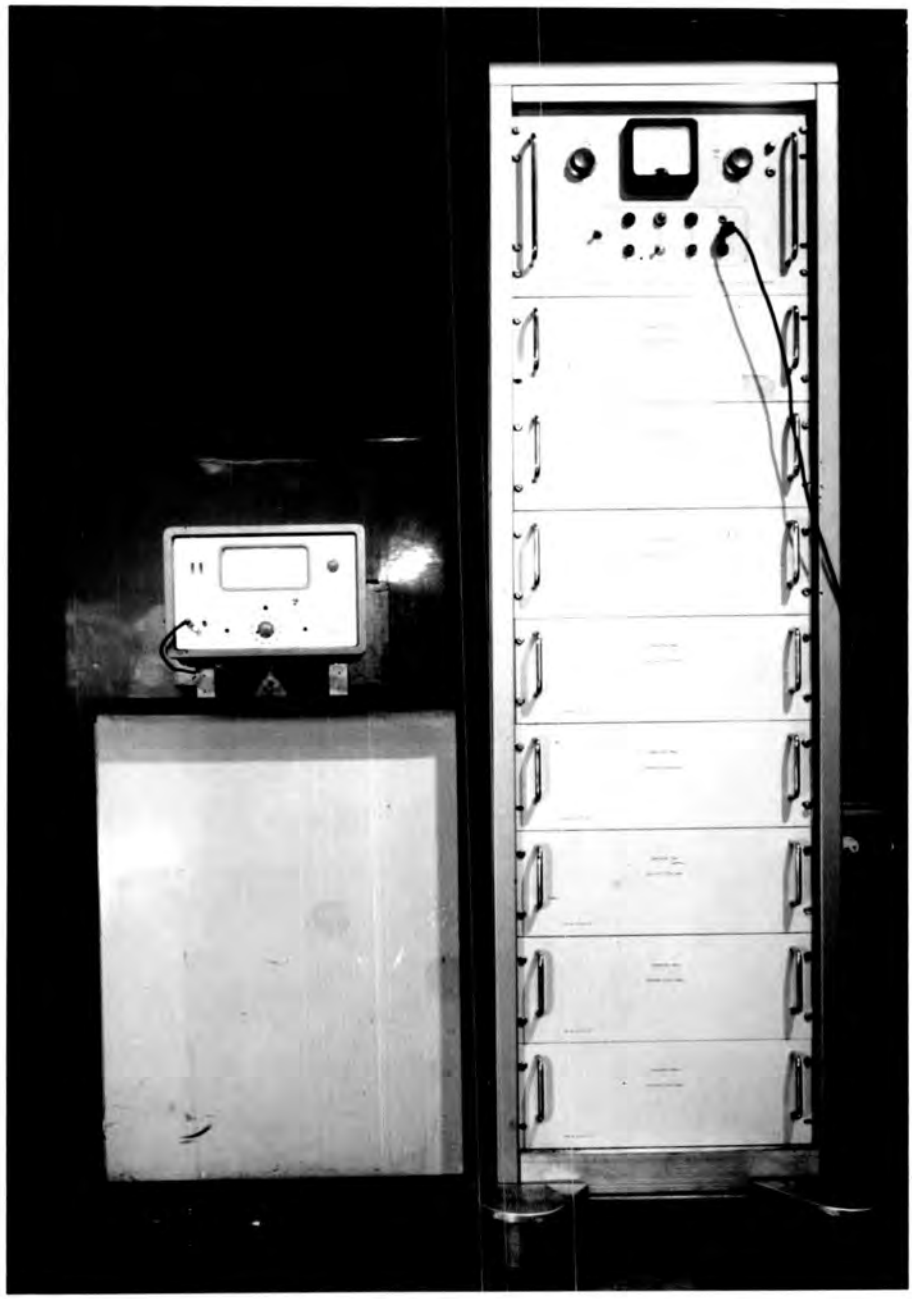

Figure 8: POWER SUPPLY AND CAPACITOR BANK

voltages from 1 mv/cm to 5v/cm can be measured. Down to 5 mv/cm the accuracy is ±3%, below this ±5%. The oscilloscope is provided with a square wave calibrator whose peak to peak voltage of 1 volt or 10 volts is accurate to ±1% at room temperature. Frequent use of this wave form for checking the vertical amplifier attenuators means in practice an accuracy in voltage measurement of ±2%. The waveforms displayed on the 12cm diameter tube with internal graticule are recorded on a camera equipped with a Polaroid film back. A permanent record is thus available 10 seconds after photographing. Measurements may be taken from the films and referred to the oscilloscope settings at that time with a correction for camera optics. This correction is determined by photographing the 1cm x 1cm squares of the graticule and measuring their size on the film.

3.4 Photodiode System

An SD100 photodiode (made by Edgerton, Germeshausen and Grier, U.S.A.) is used to monitor the light output waveform. These diodes are linear to within 5% over seven decades of incident light energy according to the manufacturers specification. The light flux as measured by the diode is dependent on the integrated product of the spectral response of the diode and the spectral intensity of the flash tube radiation. The diode and associated components (See circuit in Figure 9) are built into a machined brass holder attached to a rod mounted in an optical bench saddle. Filters are always used to maintain the photodiode output on the linear part of its response characteristics. The specified maximum peak current of 100ma with the 50 ohm lead limits the peak oscilloscope voltage to 5 volts. The diode rise and fall times are specified as 4 and 15 nsecs respectively. Figure 10 shows the relative spectral response curve of the diode and the V.I. characteristics.

3.5 Ballistic Thermopile

A model 100 ballistic thermopile (manufactured by Technical Research Group U.S.A.) is used to measure integrated light outputs. This instrument consists of two thin hollow cones whose temperature rise is measured with

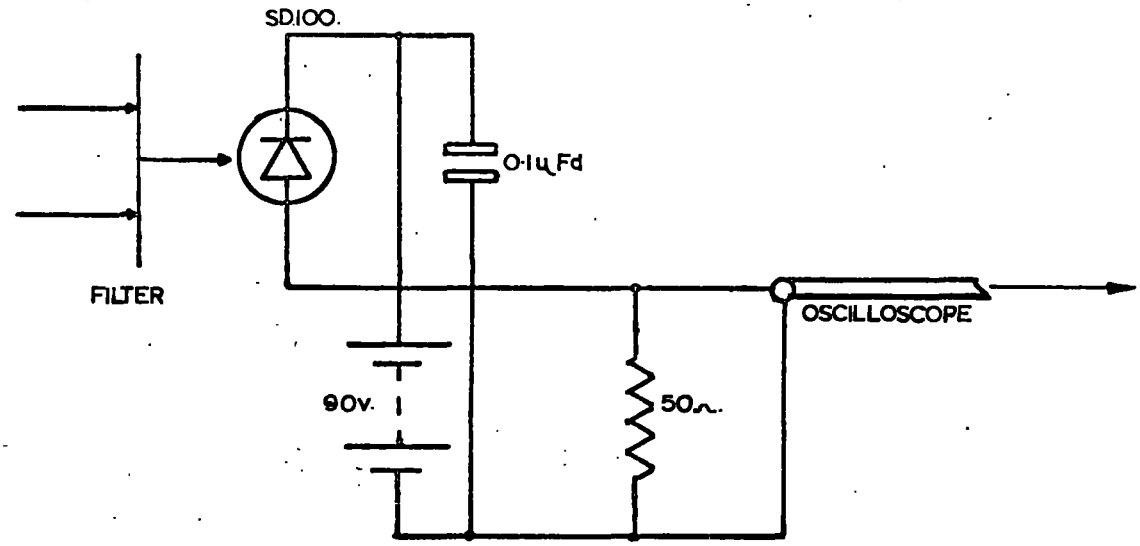

FIGURE 9. PHOTODIODE CIRCUIT.

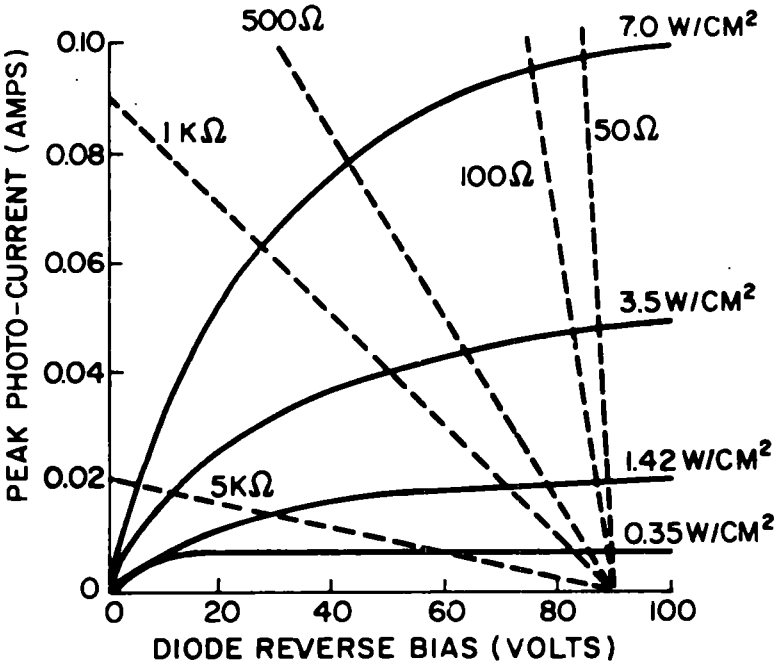

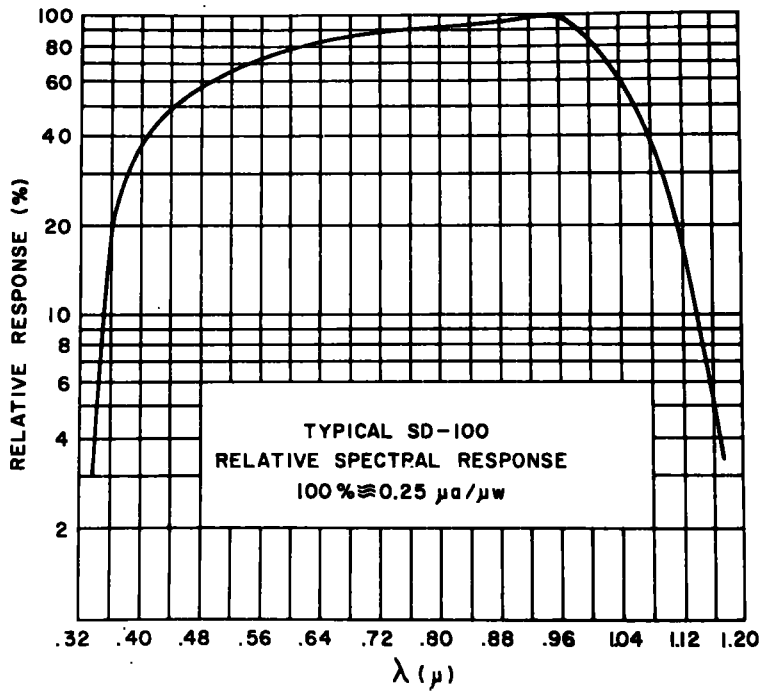

Figure 10: SPECTRAL RESPONSE AND V-I CHARACTERISTIC OF SD100 PHOTODIODE

series connected thermocouples. The junctions are spaced around the outside of the cones, one set attached to the receiver cone and the other to a reference cone of identical dimensions shielded from the incident radiation. In this way the output voltage is compensated for room temperature variation. The silver cones are bright nickel plated and the small cone angle ensures that the radiation undergoes a large number of reflections. A wavelength independent absorption of 98% is obtained. The instrument is calibrated in microvolts per joule.

The output voltage is measured on a valve-voltmeter. The most sensitive scale on this meter of 0 → 100 μV in 1 μvsteps with the makers calibration of the thermopile (232 μv/Joule) permits measurements as low as 4 - 5 millijoules. At this sensitivity the overall accuracy is ±5μv. Above 100μv an accuracy of 5% is specified. The thermopile has a ballistic integrating time of seven seconds which allows easy reading of the peak output voltage to within a half division on the meter scale.

3.6 Filters

Filters with transmission characteristics close to the absorption bands of ruby are used to monitor light intensity from 400 to 500 millimicrons (B) and 500 to 600 millimicrons (G) Spectrophotometer traces of the filters and for comparison, the absorption bands of ruby are shown in Figure 11. A neutral density 1.0 filter (N) in combination with an infra red absorbing filter is used to maintain the SD100 photodiode output on the linear part of its characteristics when monitoring total radiation from 250 to 1250 millimicrons (see Figure 12).

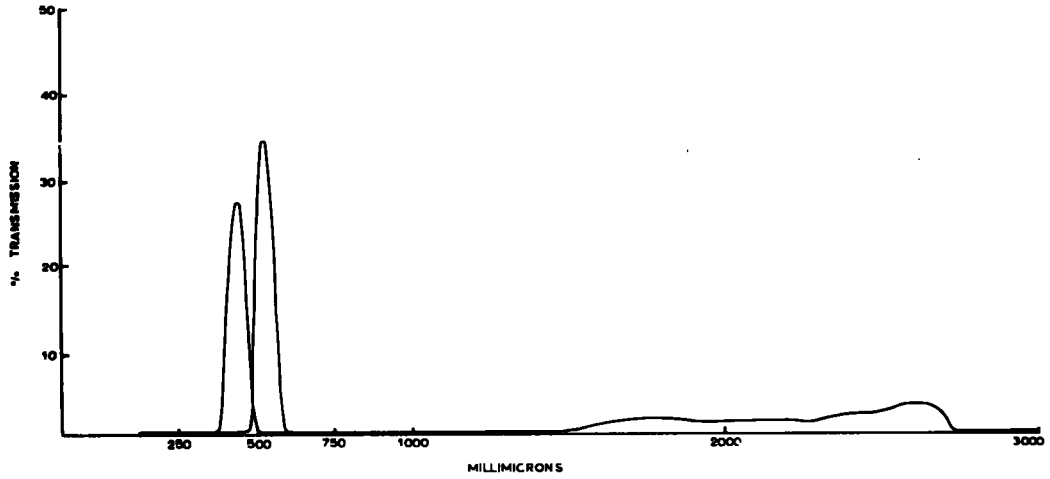

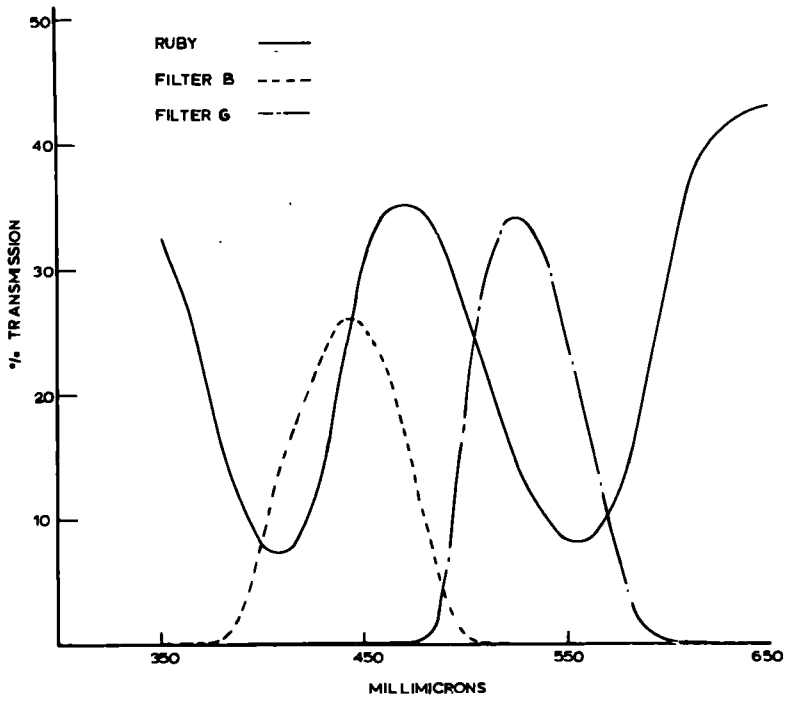

Figure 11: NARROW BAND FILTERS

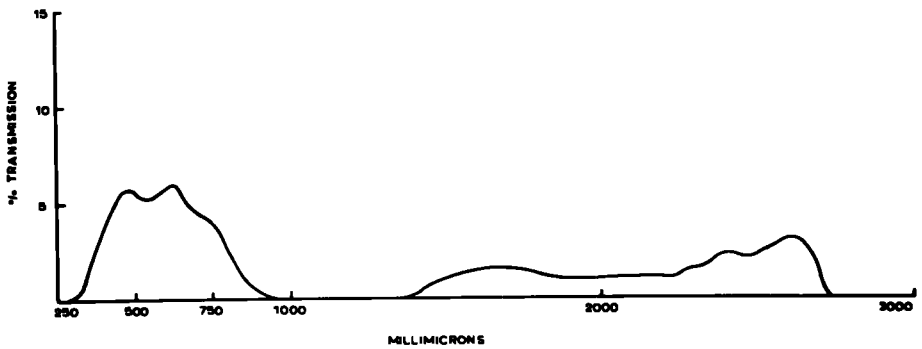

Figure 12: NEUTRAL DENSITY FILTER

Chapter 4. Flash Tube Operation and Appraisal

4.1 Flash Tube Mounting

Flash tubes are mounted on stand-off insulators in a metal box with hinged lid (see Figures 13 and 14). This box serves as protection should the tube shatter. The lid is interlocked with the capacitor unit controls by a microswitch. Lifting the lid discharges the bank and cuts off the charging supply. An optical bench is adjusted at 90^0 to the tube axis and fixed centrally. The light output wave-form is monitored by the photodiode from one side and the integrated output simultaneously recorded from the other side. Careful measurement ensured that the tube axis is always at the same distance from the monitors.

4.2 Discharge Circuit

The flash tube discharge circuit is shown in Figure 15. Capacitor C charged to voltage V discharges its energy $E = \frac{1}{2} CV^2$ into the flash tube through inductor L. The inductor is essential to limit the initial rate of rise of current and prevent shattering at high energy input. Since the self breakdown voltage of all the flash tubes is in excess of 4 KV, a higher voltage trigger pulse (40 KV peak 10 μsec duration) is applied to a thin nickel trigger wire wound spirally between the tube electrodes. This pulse causes an initial ionisation which enables the main discharge (1 - 2.4 KV) to take place. Heavy copper leads are used in the circuit to keep resistive losses to a minimum.

4.3 Light Output Waveform

The basic shape of the light output waveform measured with the SD100 photodiode is shown in Figure 16. Conventionally, flash duration is measured between the one third peak height points on the light output wave-form. The peak voltage output and flash duration are calculated from the oscilloscope films and the values obtained used to compare different flash tubes operated with the same circuit components. The effect of variation of the circuit components on the light output of a given tube is also studied.

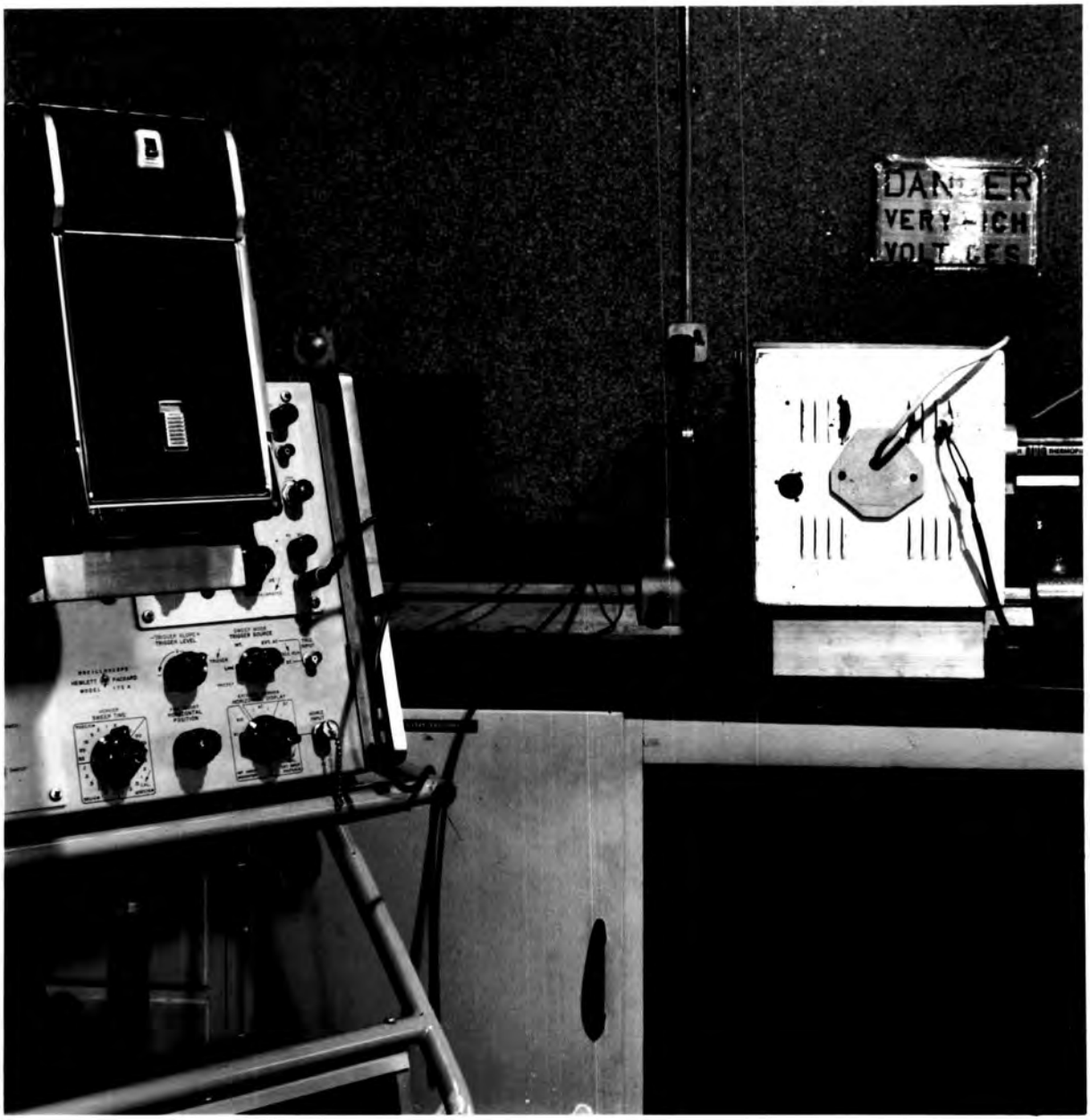

Figure 13: APPARATUS FOR LIGHT OUTPUT MEASUREMENT

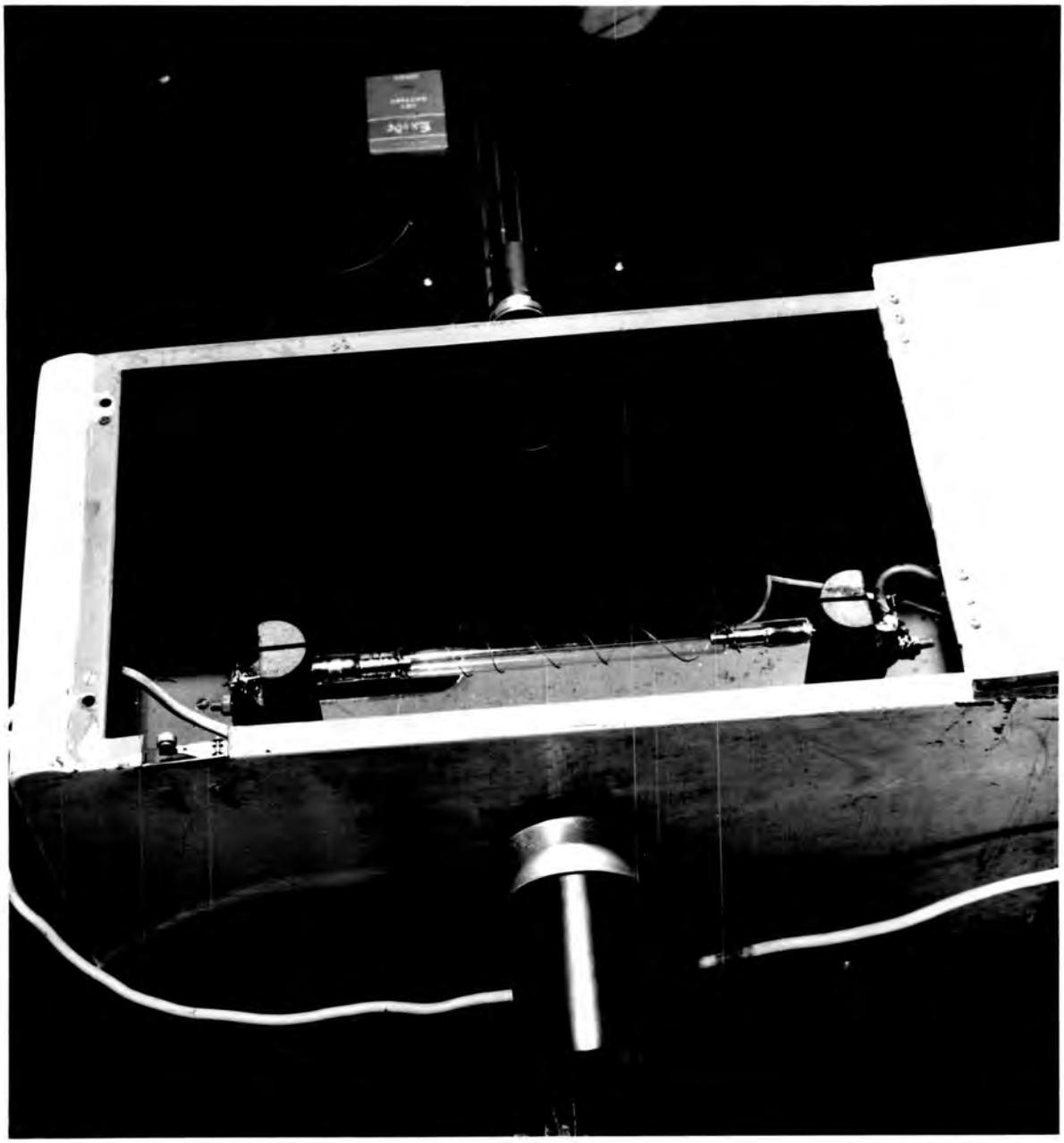

Figure 14: FLASH TUBE MOUNTING

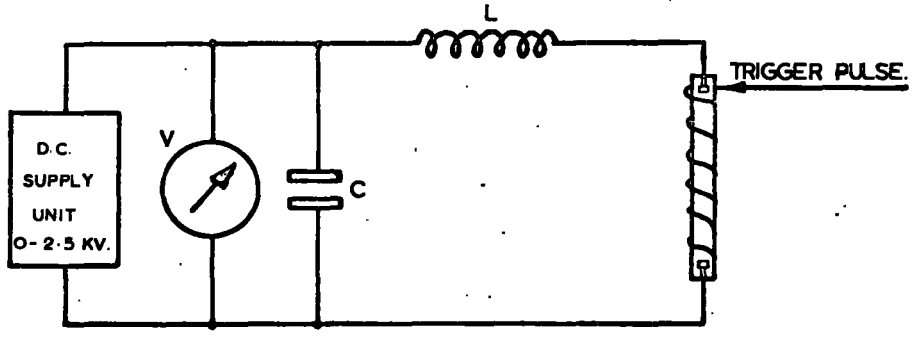

FIGURE 15. FLASH TUBE CIRCUIT.

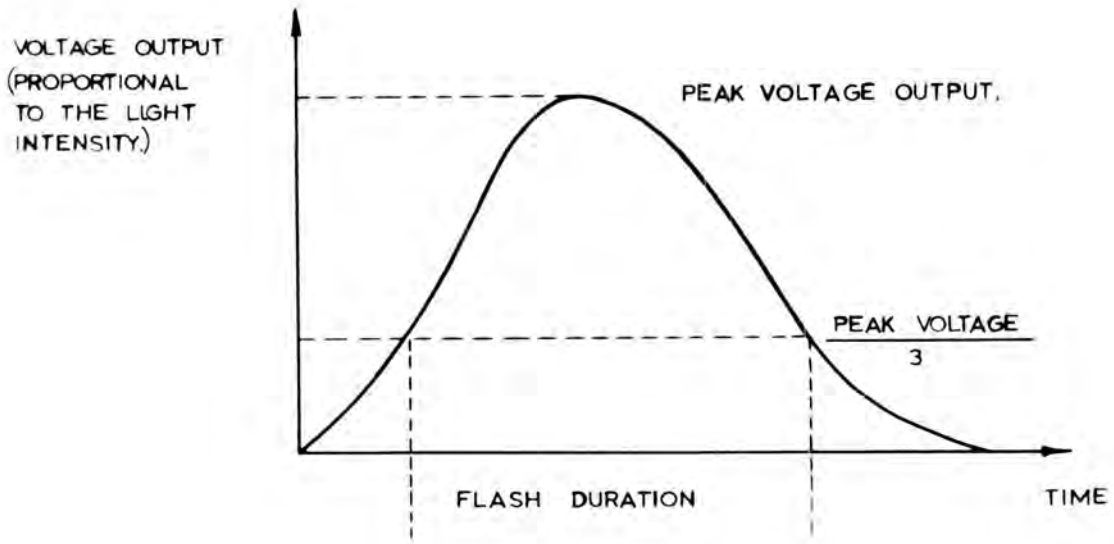

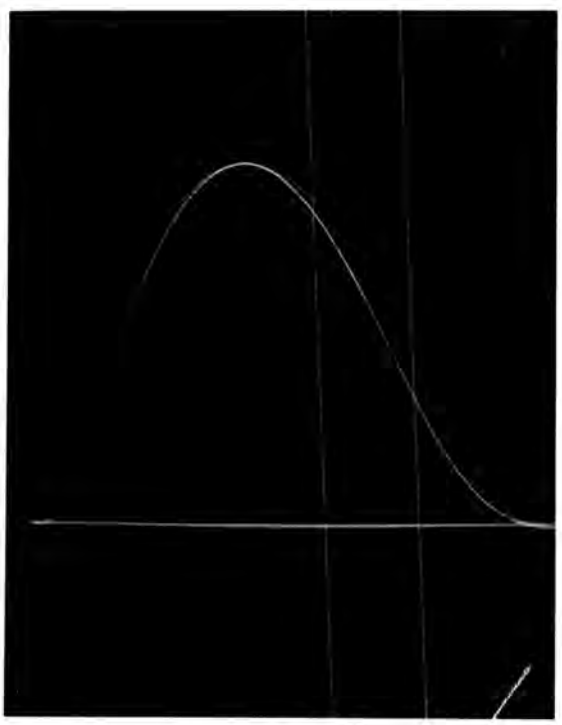

Figure 16: LIGHT OUTPUT WAVEFORM

The height of the photodiode is adjusted so that its centre is in the same horizontal plane as the flash tube axis. A clamping collar on the optical bench mounting rod prevents alteration of this setting. The diode is fixed at a distance of 24cm from the tube axis. A 1" diameter aperture in the side of the protective box (at a distance of 9cm from the diode) limits the radiation received by the detector. Due to the wavelength dependent sensitivity, absolute calibration of the diode and filter combination is not possible.

4.4 Light Output Measurement

In considering light output measurement the following assumptions are made:- (i) The emissivity of the ionised Xenon gas is uniform throughout the volume of the arc.

(ii) The radiation received by the detector is uniform across its aperture A.

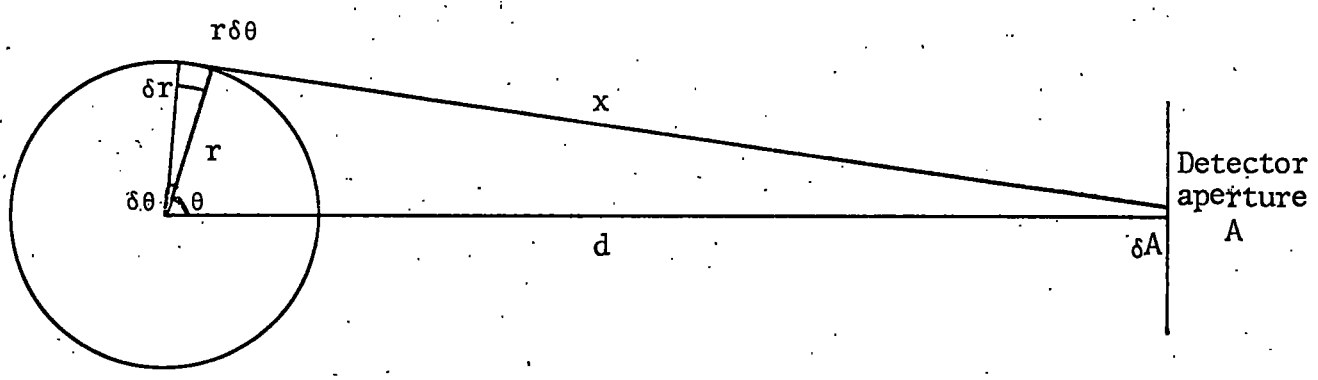

The total energy emitted by the tube will be related to the output voltage of the thermopile.

Considering a section of emitting plasma δt thick at a distance r from the centre of the flash tube.

Flash tube radius = Rcm. Flash tube length = Lcm.

Energy received at δA due to element $\delta t \delta r \delta\theta$

$$= \frac{r\,\delta\theta}{4\pi x^2}\,\delta t \delta r \delta A \frac{W}{\pi R^2 L} \text{ joules,}$$

where W = total energy emitted by the tube (joules)

$\therefore$ Total energy received by aperture A

$$= \frac{A}{4\pi}\frac{W}{\pi R^2 L}\,\delta t \int_{r=0}^{r=R}\int_{\theta=0}^{\theta=2\pi} \frac{r d\theta}{x^2}$$

$$= \frac{A}{4\pi}\frac{W}{\pi R^2 L}\,\delta t \int_{r=0}^{r=R}\int_{\theta=0}^{\theta=2\pi} \frac{r d\theta}{d^2+r^2-2dr\cos\theta}\, dr$$

Provided d is large compared with R and a short length of flash tube is considered, variation in x due to angular deviation of δt will be negligible. For a 1cm length of tube $\delta t = 1$.

$\therefore$ Energy received by detector from 1cm length of tube

$$E = \frac{A}{4\pi}\frac{W}{\pi R^2 L}\int_0^R \frac{2\pi r\, dr}{d^2-r^2}$$

$$= \frac{A}{4\pi}\frac{W}{\pi R^2 L}\,\pi \log\left(1+\frac{R^2}{d^2-R^2}\right)$$

$$= \frac{A}{4\pi}\frac{W}{\pi R^2 L}\frac{\pi R^2}{(d^2-R^2)}$$ - by expansion and considering the first term only since R<1cm and d>13cm.

$$= \frac{A}{4\pi}\frac{W}{L}\frac{1}{(d^2-R^2)} \text{ joules}$$

Calibration factor of thermopile = 232 μV/joule

$\therefore E = \frac{Vp}{232}$ joules where Vp is the peak output voltage (μV)

$$\frac{Vp}{232} = \frac{A}{4\pi}\frac{W}{L}\frac{1}{d^2-R^2}$$

$$W = \frac{Vp}{232}\frac{4\pi L}{A}(d^2-R^2) \text{ joules for 1cm length of tube}$$

The maximum tube radius R. = 0.75cm. R^2 = 0.056cm
Since d > 13cm d^2 > 169cm^2, the contribution of R to the (d^2-R^2) term has been ignored, and the total energy emitted by the tube becomes,

$$W = \frac{4\pi L}{232A} Vp\, d^2 \text{ joules for 1cm length of tube} \quad (4.1)$$

To verify this expression, $1/Vp^{\frac{1}{2}}$ is plotted against d for a fixed energy input to the tube. For values of d greater than 15cm a straight line graph results. (Figure 17)

$$\text{Tube efficiency} = \frac{\text{Energy emitted by tube}}{\text{Energy input to tube}}$$

Since the circuit resistance is small compared with the arc-resistance during discharge, efficiency is calculated from

$$\eta = \frac{\text{Energy emitted by tube}}{\text{Energy stored in capacitor bank}}$$

$$= \frac{W}{\frac{1}{2} CV^2}$$

W is calculated from equation (4.1)

An aperture formed by a 1cm wide slot aligned with the optical bench axis is placed close to the flash tube. The tube diameter and distance of the thermopile aperture to the tube wall are carefully measured and the reading on the optical bench scale correlated with d.

Although the thermopile output is sufficient for efficiency measurements with no filter, readings with the narrow band filters are too low for accurate calculation. The 1cm aperture was removed and d reduced to 13cm. At an input of 10KJ, a reading of only 18μV was obtained with filter B. By moving the flash tube supports close to the side of the protective box d was further reduced to 4cm. The filter material was damaged by the high light flux. Work by GUREVICH, however, has shown that the relative spectral

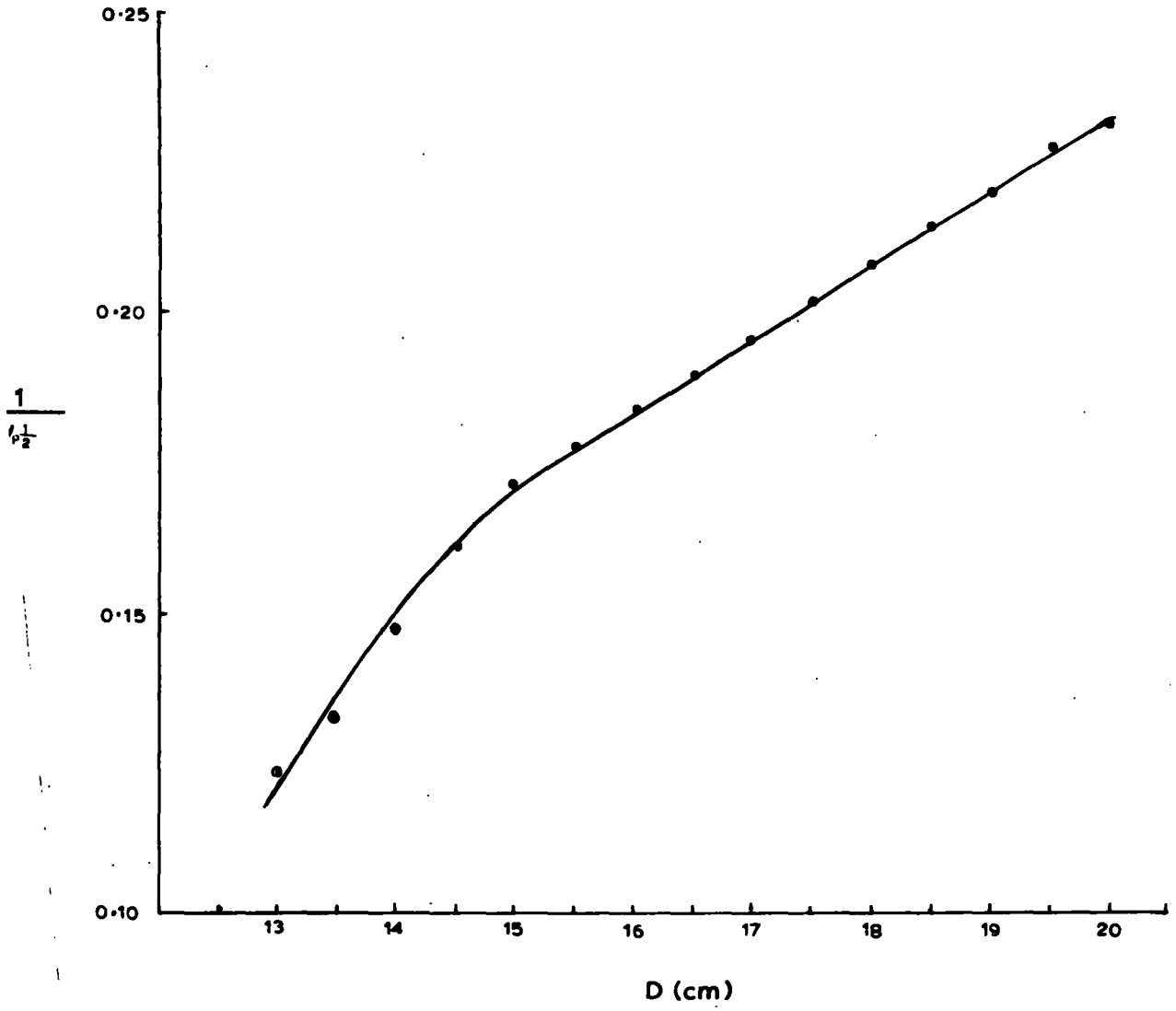

Figure 17: GRAPH OF $1/V_p^{\frac{1}{2}}$ AGAINST D

distribution of the light output does not depend on capacity or changes in tube diameter between 8mm and 15mm. Spectral distribution varies with voltage gradient. Measurements made of the total radiated energy can thus be used to determine the most efficient lamp and operating conditions at a given voltage.

4.5. Flash Tube Load Limits

In order to equate the energy a flash tube can withstand with operational parameters, the following expression has been defined:-

$$\text{Flash tube wall loading (W.L.)} = \frac{\text{Energy input}}{\text{Inner wall area x Flash duration}} \text{ KW/cm}^2$$

$$= \frac{\frac{1}{2} CV^2}{a\tau} \qquad (4.2)$$

The inner wall area between the electrodes is calculated in square centimetres and the flash duration ($^1/_3$ peak points) in milliseconds. Experiments during flash tube development have shown that tubes can be operated safely at wall loadings up to 55KW/cm^2. At this loading tubes have a life of 1,000 discharges before the light output is reduced by more than 10%. Increased loading gives a reduced life. Above an estimated 70-80 KW/cm^2 the tube shatters in the first five discharges. Since determination of the exact load limit would require a large number of tubes, a wall loading of 70 KW/cm^2 is not usually exceeded in these experiments.

For flash durations up to 3 milliseconds, the wall loading limit allows wide operational parameter variation. Increased bank voltage or reduction of series inductance for a fixed energy will increase the wall loading since the flash duration is reduced. To avoid overloading, the energy input must then be reduced. The wall loading limit cannot be verified for pulses longer than 3 milliseconds. This flash duration results from the maximum capacity of 4000μFd at 2.4KV discharged into the tube through the 450μH series inductance. Increase of inductance causes oscillation of the discharge circuit current resulting in two or more light pulses of decreasing amplitude. Production of a single pulse

longer than 3 milliseconds requires a larger capacitor bank charged at a lower voltage. Provided a wall loading of 55 KW/cm is not exceeded, the failure mechanism for longer pulses will probably depend more on overheating and electrode erosion than on instantaneous shattering. However, a flash tube might withstand a shock wave for 3 milliseconds and shatter if the same shock wave is applied for a longer period.

Chapter 5. Results and Discussion of Flash Tube Performance

5.1 Measurement of Capacitor Bank and Inductors

The total capacity, the capacity of each tray and of the four pairs of adjacent trays were measured.

Top	Capacitance Bridge readings		Total
	Separate trays μFd	Adjacent pairs μFd	μFd
Tray 1	489	988	4012
2	501		
3	504	1006	
4	505		
5	498	990	
6	501		
7	502	1000	
8	502		
Total	4002	3984	4012

Mean value = $3999\frac{1}{3}\mu Fd \pm 3\%$. For convenience of calculation a value of 4000μFd has been used.

Microvoltmeter readings at the inductor terminals corresponding to an accurately set current wereplotted against the current value. The d.c. resistances were calculated from the gradients.

Component	450μH	235μH	100μH	Leads
D.C. resistance (ohms)	18×10^{-3}	21×10^{-3}	6×10^{-3}	8×10^{-3}

(Due to non-delivery of $\frac{1}{2}$" x $\frac{1}{8}$" copper strip, the 235μH coil was wound with $\frac{1}{2}$" x $\frac{1}{16}$" section strip).

5.2 Variation of Filling Pressure

The peak light intensity measured by the photodiode output voltage was monitored for tubes filled at pressures from 100 to 500 torr. Filters B,G and N were used to assess the difference in spectral efficiency with pressure. The total radiation was monitored by the thermopile without the 1cm slit to obtain high readings at low energy

input. (The maximum voltage used with 10mm bore tubes and full capacitor bank was 2.0KV since the safe loading is exceeded at higher voltage).

For a fixed voltage input, light output is plotted against filling pressure. Figure 18 shows the variation in peak light intensity with filling pressure for 13mm bore tubes. The shape of the graph is similar for 10mm and 15mm bore tubes. The variation in total radiated output with pressure is shown in figure 19. These results show that irrespective of bore size or spectral composition, the light output increases with filling pressure. The increase is greater for pressures between 100 and 300 torr than between 300 and 500 torr. The difference in output is negligible at 1.0KV and most obvious at the highest voltage used, 2.4KV.

Due to manufacturing problems at higher pressure, 400 torr has been selected as the most suitable filling pressure. The following results apply to tubes filled at 400 torr.

5.3 Efficiency Measurements

With a fixed energy input to the tube and a 1cm slit the thermopile output voltage (Vp) was measured at various distances from the tube axis. The calculated values of $1/Vp^{\frac{1}{2}}$ were then plotted against d (Figure 17). A straight line graph for distances greater than 15cm verifies the theory in chapter 4.4.

The energy emitted by the flash tube was calculated from equation (4.1)

$$W = \frac{4\pi L}{232 A} \cdot Vp\, d^2$$

Arc length of tube L = 16.5cm

Area of thermopile aperture = $\pi(0.5)^2$ cm^2

$\therefore$ W = 1.14 Vp d^2 joules (5.3)

To ascertain further the validity of (5.3), the peak voltage readings monitored by the SD100 photodiode were calculated from oscillographs taken at various distances from the tube axis. The product of the peak photodiode voltage ($\propto$light intensity) and d^2 was constant at a fixed input energy to

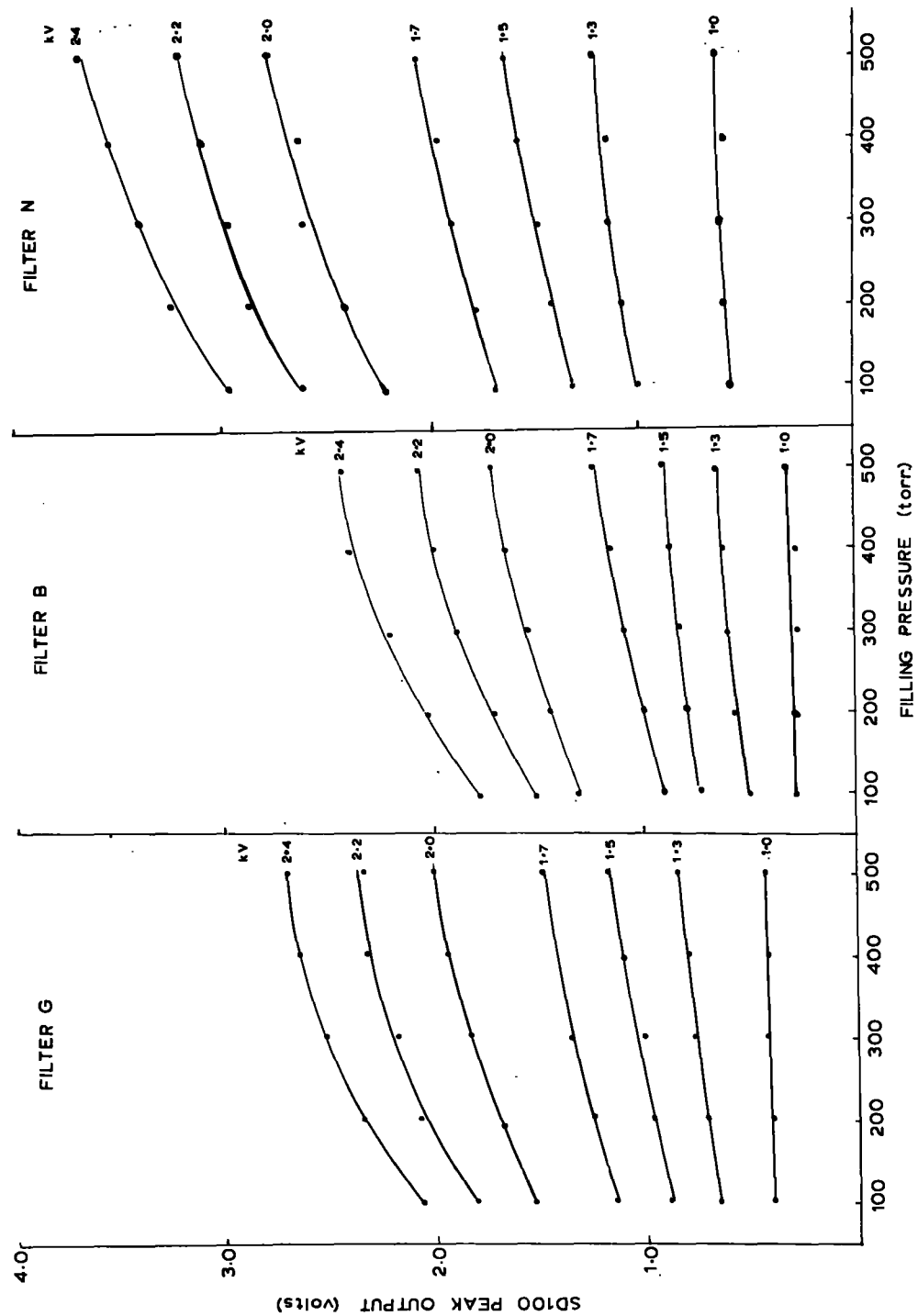

Figure 18: VARIATION OF PEAK LIGHT OUTPUT WITH FILLING PRESSURE

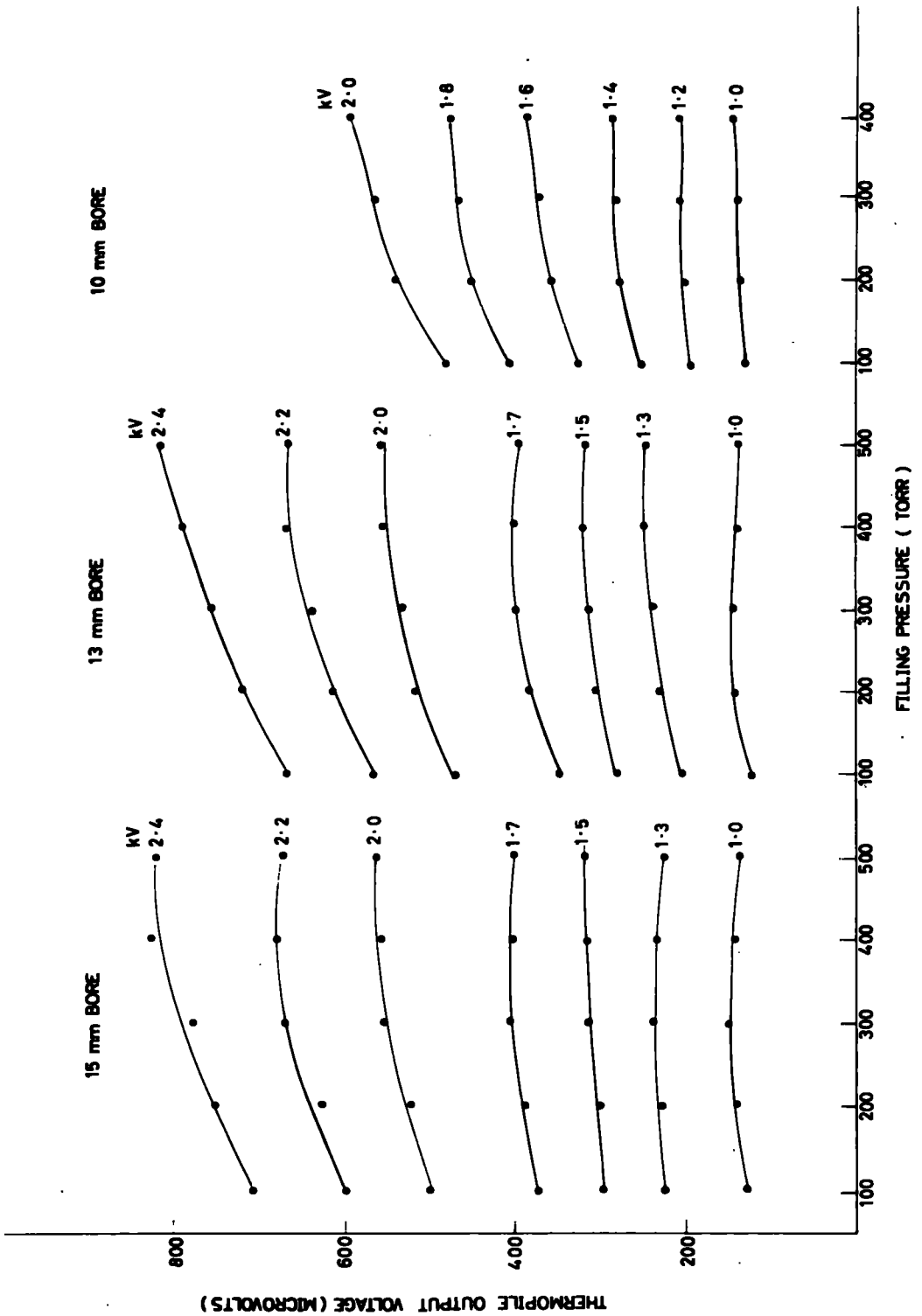

Figure 19: VARIATION OF TOTAL RADIATED ENERGY WITH FILLING PRESSURE

the tube for d 15cm.

Early results gave unreal efficiency figures - in some cases over 100%. Possible explanations for this anomaly were:-

a) An inaccurate thermopile calibration factor.
b) Variation in emission along the length of the flash tube.
c) Spurious reflection from some part of the protective box which could increase the thermopile reading.

The first was eliminated by use of an identical thermopile with a slightly different calibration factor. Both instruments gave the same efficiency value. A piece of black card placed behind the flash tube caused a reduction in thermopile output. The tube and 1cm slit were therefore set up without the box as in figure 20. There was no variation in output with slit position along the length of the discharge.

The thermopile output with the 1cm slit is too low for accurate measurement at low energy input. Measurements with and without the slit were compared with d accurately set at 16cm. Table I shows a mean reduction in thermopile output of 10.2% when the slit is used. This factor did not vary with tube size. Tube efficiency is therefore calculated from:-

$$\eta = \frac{1.14\ V_t\ 0.102 \times 256}{\frac{1}{2}CV^2}$$

$$= \frac{2.97\ V_t}{\frac{1}{2}CV^2}$$ where V_t is the thermopile output voltage with no slit at d = 16cm.

V_t was measured using different inductors with changes in bank capacity and voltage. It was found that inductance variation between 100μH and 450μH did not affect V_t. The results for all inductors are shown in Table II. These results show:-

a) For a fixed capacity, voltage variation between 1.0 and 2.4KV does not affect the efficiency (within the limits of experimental error).

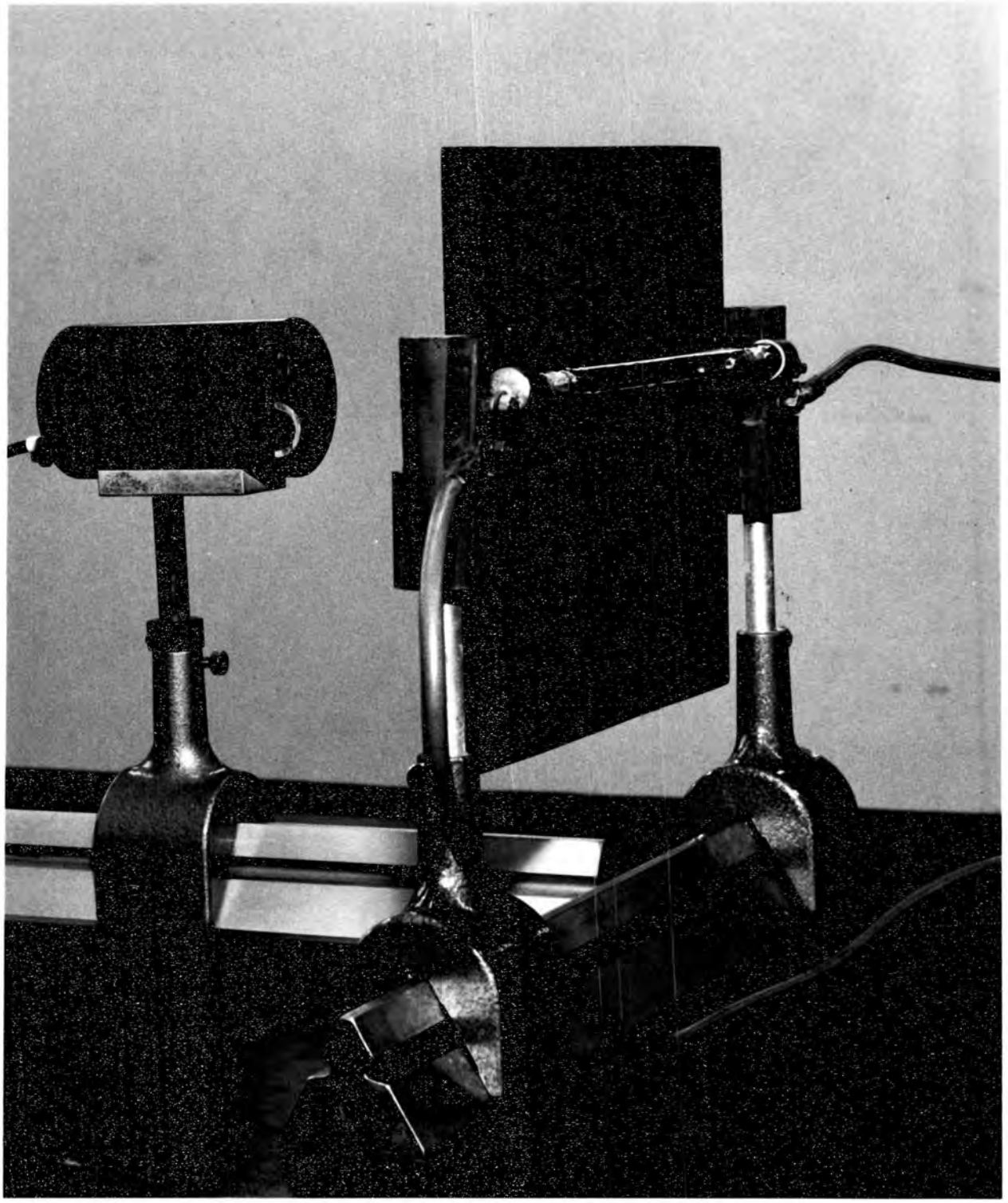

Figure 20: DETERMINATION OF LAMP EFFICIENCY

L = 450μH C = 4000μFd d = 16cm

Bank Voltage KV	Energy Stored Joules	Thermopile output voltage V			Efficiency η%
		without 1cm slit Vt	with 1cm slit Vp	$\frac{Vp}{Vt}$ %	
1.0	2000	54	5.5	10.2	80
1.3	3380	90	9.0	10.0	79
1.5	4500	128	13.0	10.15	84
1.7	5780	160	16.5	10.3	82
2.0	8000	214	22.0	10.3	79
2.2	9680	269	26.5	9.85	80
2.4	11520	312	33.0	10.6	80
		Mean		10.2	80.5

Table I: EFFICIENCY CALCULATION

Energy input Win = $\frac{1}{2}$ CV² joules. 100μH<L<450μH

Vt values are the mean of 5 readings to nearest integer.

CμFd	4000			3500			3000			2500		
Tube Bore	Win j	Vt μV	η %	Win j	Vt μV	η %	Win j	Vt μV	η %	Win j	Vt μV	η %
10mm	2000	52	77	1750	46	78	1500	42	83	1250	33	78
	4500	111	73	3934	94	71	3372	91	80	2810	73	77
	8000	203	75	7000	179	76	6000	150	74	5000	134	79
	-	-	-	10080	248	73	8640	218	75	7200	180	74
		Mean	75			74½			78			77
13mm	2000	57½	85	1750	48	81	1500	43	86	1250	35	83
	4500	123	81	3934	95	71	3372	98	86	2810	80	84
	8000	225	83	7000	196	83	6000	170	84	5000	138	82
	11520	332	85	10080	282	83	8640	240	82	7200	220	83
		Mean	83½			79½			84½			83
15mm	2000	54	80	1750	51	86	1500	45	89	1250	33	78
	4500	127	83	3934	103	78	3372	94	83	2810	81	85
	8000	214	79	7000	186	79	6000	158	78	5000	140	83
	11520	312	80	10080	275	81	8640	236	81	7200	180	77
		Mean	80½			80½			84			81
CμFd	2000			1500			1000			500		
10mm	1000	26	77	750	20	79	500	13	77	250	-	-
	2248	60	79	1686	45	79	1124	29	76	562	13½	71
	4000	104	76	3000	77	76	2000	52	77	1000	24	71
	5760	151	78	4320	109	75	2880	72	74	1440	34	70
		Mean	77½			77			76			71
13mm	1000	28	83	750	20	79	500	11	65	250	-	-
	2248	58	77	1686	42	75	1124	27	71	562	11	58
	4000	99	73	3000	71	70	2000	45	66	1000	21½	64
	5760	145	75	4320	105	72	2880	69	71	1440	31	64
		Mean	77			74			68			62
15mm	1000	25	76	750	17	67	500	11	65	250	-	-
	2248	58	76	1686	42	75	1124	25	66	562	12	63
	4000	106	78	3000	71	70	2000	46	68	1000	20½	61
	5760	140	72	4320	106	73	2880	69	71	1440	30	62
		Mean	75½			71			67½			62

Table II: VARIATION OF EFFICIENCY WITH OPERATING CONDITIONS

b) For all tubes, efficiency is lower when lightly loaded. The gas discharge probably does not entirely fill the tube bore below 1000 joules input.

c) The efficiency of the 13mm and 15mm tubes is similar.

The 10mm bore tube is more efficient at energy inputs up to about 4kJ and less efficient above this.

The absolute value of efficiency of 83% for the 13mm bore tube at 5kJ input is in reasonable agreement with the results of GONCZ and NEWELL (1966). They used a spectroradiometer to measure an efficiency of 65% in the spectral range 0.35μ to 1.1μ for a similar tube.

5.4 Variation of Flash Duration and Light Intensity with Circuit Parameters

The flash duration measured using either filter B or G is equal. Periods measured using filter N are approximately 100 microseconds longer due to continued infra-red emission after cessation of the discharge. Filter G is used when monitoring variations in intensity and flash duration with circuit parameters for tubes filled at 400 torr.

The results of these measurements using the 100μH, 235μH and 450μH inductors with different capacitance value are shown in Tables III and IV and graphically in figures 21, 22 and 23.

It can be seen that:-

a) The flash duration is almost independent of bank voltage and tube bore.

b) The 13mm and 15mm bore tubes display very nearly identical characteristics.

c) The graphs (figures 22 and 23) show that a decreasing increment of light intensity occurs with increasing capacity at a fixed voltage and inductance. This effect is most apparent with the 10mm bore tube. For C <2000μ Fd (E = 5000 joules), the green light intensity of the 10mm tube is greater than the intensity of the 13mm or 15mm bore tube. For C>3500μFd, the intensity of the 10mm tube is less.

Filter G

Distance of photodiode from tube axis = 24cm

Readings in microseconds

Capacity μFd	Inductance 450μH				235μH				100μH			
	Bank Voltage (kilovolts)											
	1.0	1.5	2.0	2.4	1.0	1.5	2.0	2.4	1.0	1.5	2.0	2.4
					15mm Bore							
500	1040	1010	995	980	705	690	690	690	490	490	482	482
1000	1425	1400	1400	1400	1010	980	980	995	665	650	655	665
1500	1760	1730	1690	1730	1220	1210	1200	1225	840	855	840	868
2000	2000	1980	1970	2000	1425	1400	1410	1425	1020	994	1020	1035
2500	2240	2210	2210	2210	1550	1550	1570	1620	1120	1120	1160	1185
3000	2420	2370	2450	2480	1725	1725	1760	1830	1200	1215	1240	-
3500	2620	2590	2620	2660	1865	1865	1930	2000	1340	1320	1380	-
4000	2780	2760	2820	2930	2030	2030	2070	2170	1410	1410	1490	-
					13mm Bore							
500	1020	994	994	994	718	690	690	690	510	484	455	455
1000	1450	1450	1410	1410	1020	993	993	993	690	685	685	685
1500	1720	1690	1690	1690	1260	1230	1260	1260	855	855	855	885
2000	2040	2000	2000	2000	1465	1420	1410	1476	965	994	1040	1100
2500	2320	2250	2280	2280	1620	1590	1690	1690	1130	1160	1160	1215
3000	2415	2415	2450	2520	1760	1760	1790	1790	1255	1240	1270	-
3500	2620	2620	2700	2700	1930	1970	1930	2000	1365	1365	1405	-
4000	2760	2800	2830	3000	2000	2000	2070	-	1450	1450	1520	-
					10mm Bore							
500	1005	965	965	965	705	677	677	677	490	468	468	482
1000	1420	1380	1380	1420	1010	966	980	980	705	677	705	712
1500	1760	1730	1730	1760	1225	1210	1225	1270	895	855	882	910
2000	2000	2000	2000	2070	1460	1420	1445	1500	1035	995	1050	-
2500	2250	2250	2280	2350	1655	1620	1655	-	1212	1170	1185	-
3000	2450	2450	2550	2590	1830	1790	1865	-	1295	1295	-	-
3500	2690	2690	2760	2830	1965	1930	2000	-	1410	1410	-	-
4000	2930	2860	2960	-	2140	2140	2170	-	1545	1545	-	-

Table III Variation of Flash Duration with Circuit Parameters

Filter G

Distance of photodiode from tube axis = 24cm

Readings in volts ∝ peak light intensity

Capacity μFd	Inductance 450μH				235μH				100μH			
	Bank Voltage (kilovolts)											
	1.0	1.5	2.0	2.4	1.0	1.5	2.0	2.4	1.0	1.5	2.0	2.4
					15mm Bore							
500	0.1	0.24	0.45	0.65	0.15	0.39	0.73	1.05	0.24	0.6	1.19	1.8
1000	0.17	0.4	0.8	1.17	0.28	0.70	1.31	1.9	0.41	1.1	2.03	2.94
1500	0.24	0.64	1.12	1.68	0.38	0.95	1.76	2.52	0.56	1.48	2.69	3.61
2000	0.29	0.76	1.38	2.03	0.45	1.17	2.14	2.95	0.68	1.78	3.1	4.07
2500	0.34	0.9	1.63	2.33	0.52	1.37	2.42	3.23	0.79	2.07	3.46	4.4
3000	0.4	1.03	1.82	2.62	0.58	1.55	2.68	3.54	0.89	2.38	3.72	-
3500	0.45	1.16	2.00	2.76	0.65	1.66	2.9	3.8	0.96	2.55	3.98	-
4000	0.46	1.23	2.14	2.97	0.69	1.76	3.07	3.93	1.02	2.65	4.17	-
					13mm Bore							
500	0.1	0.27	0.49	0.73	0.17	0.43	0.77	1.16	0.25	0.68	1.24	1.86
1000	0.19	0.49	0.9	1.33	0.3	0.77	1.41	1.91	0.43	1.16	2.1	2.9
1500	0.26	0.65	1.2	1.72	0.37	0.98	1.79	2.52	0.54	1.45	2.62	3.51
2000	0.33	0.79	1.41	2.07	0.44	1.16	2.03	2.88	0.65	1.69	3.0	3.93
2500	0.35	0.94	1.72	2.38	0.5	1.35	2.47	3.31	0.72	1.93	3.24	4.13
3000	0.41	1.05	1.86	2.59	0.58	1.48	2.62	3.5	0.8	2.17	3.66	-
3500	0.44	1.15	2.0	2.76	0.6	1.57	2.72	3.59	0.81	2.21	3.72	-
4000	0.47	1.2	2.14	2.93	0.63	1.75	2.96	-	0.94	2.48	3.87	-
					10mm Bore							
500	0.12	0.3	0.56	0.84	0.19	0.48	0.91	1.38	0.26	0.73	1.41	2.1
1000	0.21	0.53	1.0	1.47	0.3	0.8	1.52	2.21	0.4	1.2	2.24	3.14
1500	0.25	0.69	1.3	1.88	0.37	1.05	1.93	2.73	0.57	1.54	2.79	3.61
2000	0.34	0.84	1.57	2.21	0.45	1.23	2.24	3.0	0.62	1.79	3.17	-
2500	0.36	0.98	1.76	2.45	0.5	1.38	2.39	-	0.68	2.0	3.31	-
3000	0.39	1.05	1.86	2.58	0.52	1.47	2.55	-	0.73	2.14	-	-
3500	0.41	1.1	2.02	2.68	0.56	1.59	2.62	-	0.75	2.19	-	-
4000	0.44	1.2	2.15	-	0.57	1.64	2.69	-	0.76	2.3	-	-

Table IV Variation in Peak Light Output with Circuit Parameters

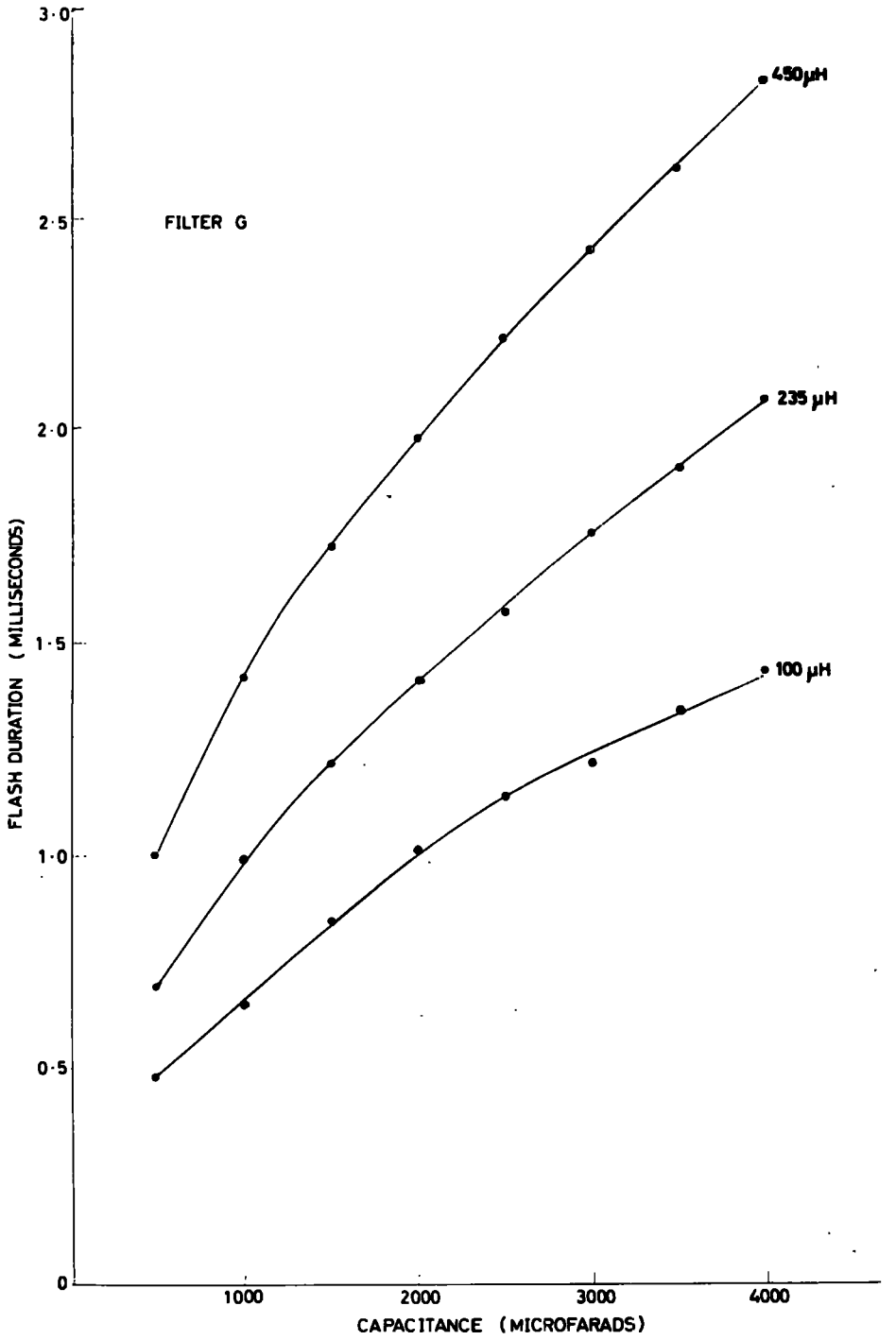

Figure 21: VARIATION OF FLASH DURATION WITH CAPACITANCE

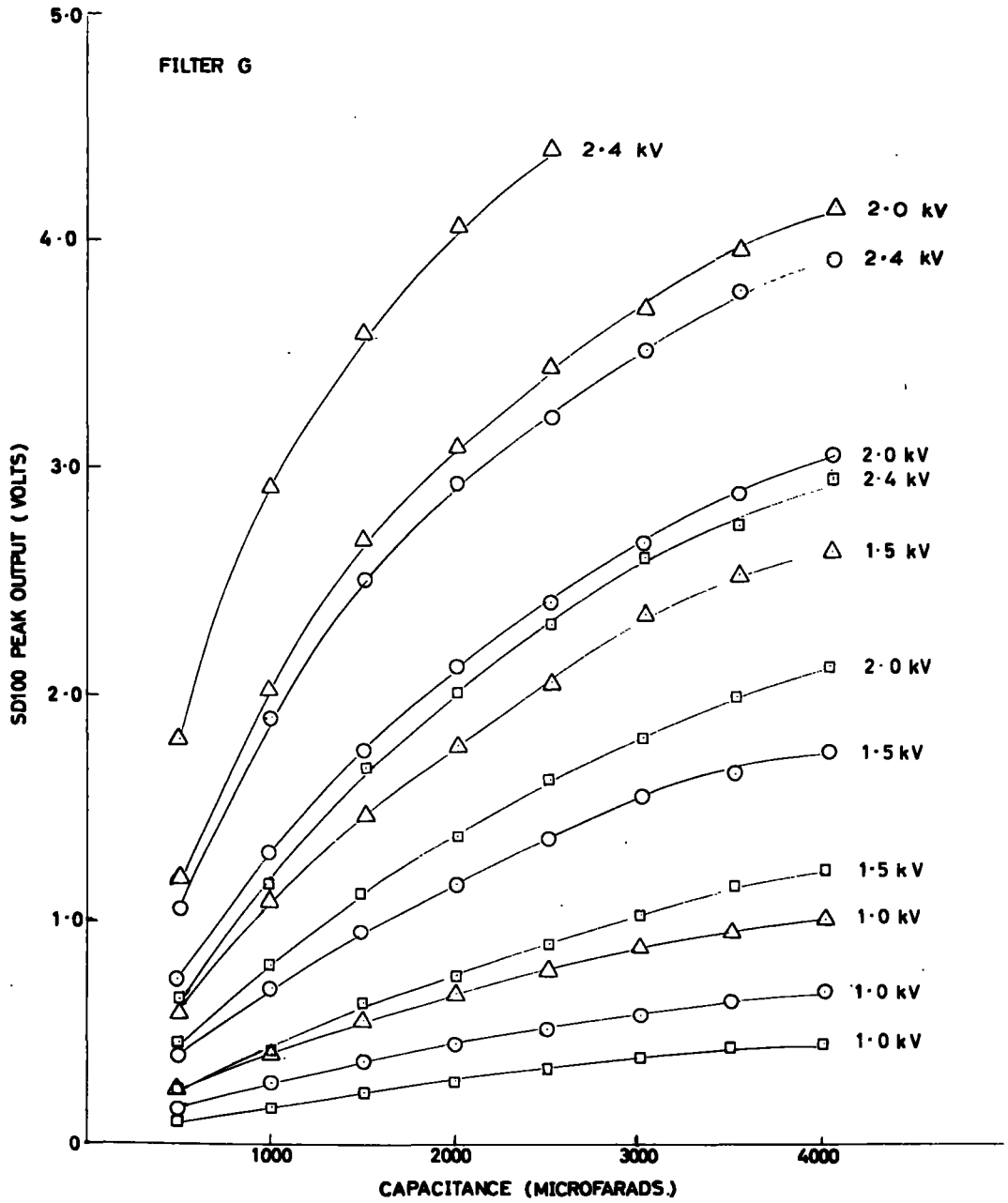

Figure 22: VARIATION OF PEAK GREEN LIGHT INTENSITY WITH CAPACITY (13mm AND 15mm BORE TUBING)

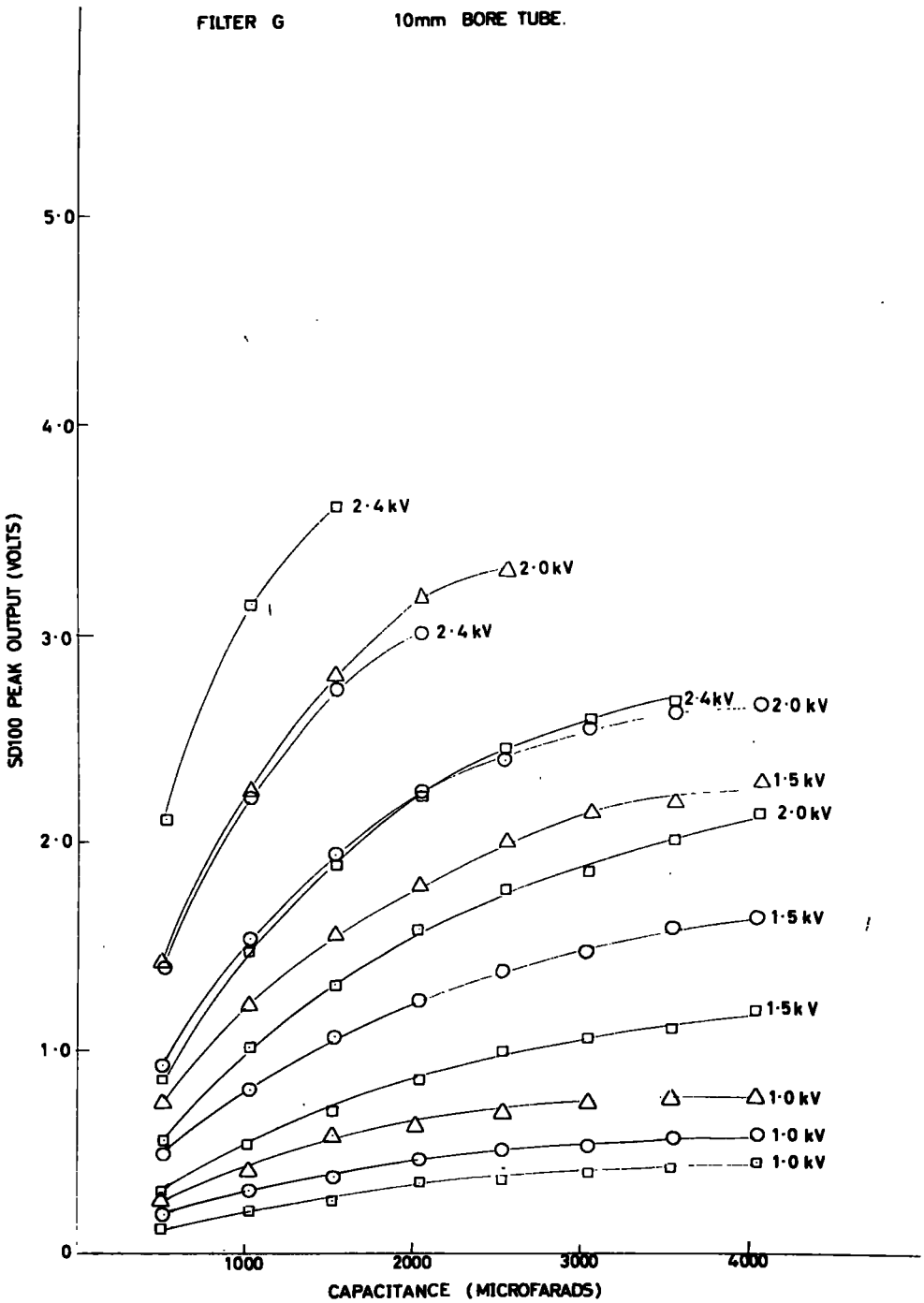

SERIES INDUCTANCE Δ = 100μH. O = 235μH. □ = 450μH.

Figure 23: VARIATION OF PEAK GREEN LIGHT INTENSITY WITH CAPACITY (10mm BORE TUBING)

d) The peak light intensity is increased and the flash duration decreased by a factor 2 (approximately) when the series inductance is changed from 450μH to 100μH.

5.5 Wall Loading and Life Characteristics

Life tests were performed on the 10mm and 13mm bore tubes at various wall loadings. Two types of failure mechanism were found. At a high wall loading, the tube failed due to the envelope shattering. A low wall loading caused a reduction in peak light intensity due to electrode erosion (mainly the cathode). It is possible for the two types of failure mechanism to combine if excessive deposition of electrode material provides a localised tracking path at the inner wall surface. This has never happened with thoriated tungsten electrodes.

A loading of 51kW/sq cm caused a 13mm bore tube to shatter after 1714 discharges with a light output reduction of 8%. Several tubes were tested at this loading for a recommended life of 1000 discharges without failure. Raising the loading to 57kW/sq cm caused the tube to shatter after 950 discharges. A reduced loading of 26.5kW/sq cm permitted the tube to be run for 10^4 discharges before reduction in light output of more than 10%. A 10mm bore tube ran for over 5000 discharges at 48kW/sq cm and for 10^4 discharges at 33kW/sq cm. The circuit parameters producing these wall loadings are shown in table V.

Tube bore (mm)	13			10		
Energy input (joules)	10^4	5000	4000	5000	5000	3000
Capacitor bank (μFd)	4000	4000	2000	2000	4000	2000
Bank voltage (kV)	2.24	1.58	2.0	2.24	1.58	1.73
Series inductance (μH)	450	450	100	450	450	100
Flash duration (msec)	2.9	2.8	1.04	2.0	2.9	1.0
Wall loading (kw/sq cm)	51	26.5	57	48	33	57.5
Minimum life	1000	10^4	500	3000	10^4	500
Minimum operating voltage	1.0kV (depending on trigger pulse)					
Trigger voltage (peak)	25-40 kV					

Table V Lamp Operating Conditions

Chapter 6. Ruby Laser Rod Production and Appraisal

6.1 Ruby Boule Growth

The method used for boule production is basically that invented by VERNEUIL (1904). However, the original method although simple in principle has been refined to permit a reasonable yield of large crystals.

Finely divided alumina doped with trivalent chromium oxide (0.05% by weight) is discharged from a hopper by sonic agitation, dropped through an oxygen-hydrogen flame and crystallised on a seed rod of known crystallographic orientation which is withdrawn progressively as the crystal grows. In this work, the seeds used were of 90° orientation, i.e. with the crystallographic c-axis normal to the direction of growth. In effect, the growth takes place by crystallisation from a molten film on the surface of the boule which is maintained at the melting point (2040°C) by the oxy-hydrogen flame. The growing boule is normally surrounded by a shield of refractory material to reduce heat losses and to minimise thermal gradients.

For good crystal growth it is essential to maintain the growth conditions constant. The flame composition and its configuration, the powder feed rate and the position of the crystal relative to the flame are perhaps the most important operating parameters.

In the equipment used for crystal growing, burner gases are carefully metered and the powder feed and boule retraction are automatically interdependent. The position of the boule in the refractory shield is maintained constant by a photo-electric cell control system which also governs the powder feed rate. The growing boule is also rotated to reduce thermal gradients. Figure 24 is a schematic diagram of the growth equipment.

The three stages in boule growth are;

a) Adjustment of the flame, the powder feed and the retraction rate to increase the seed size from $\frac{1}{8}$" diameter to the required boule diameter;

b) growing the required crystal length;

A Diagrammatic Representation of the Verneuil Crystal Growing Equipment.

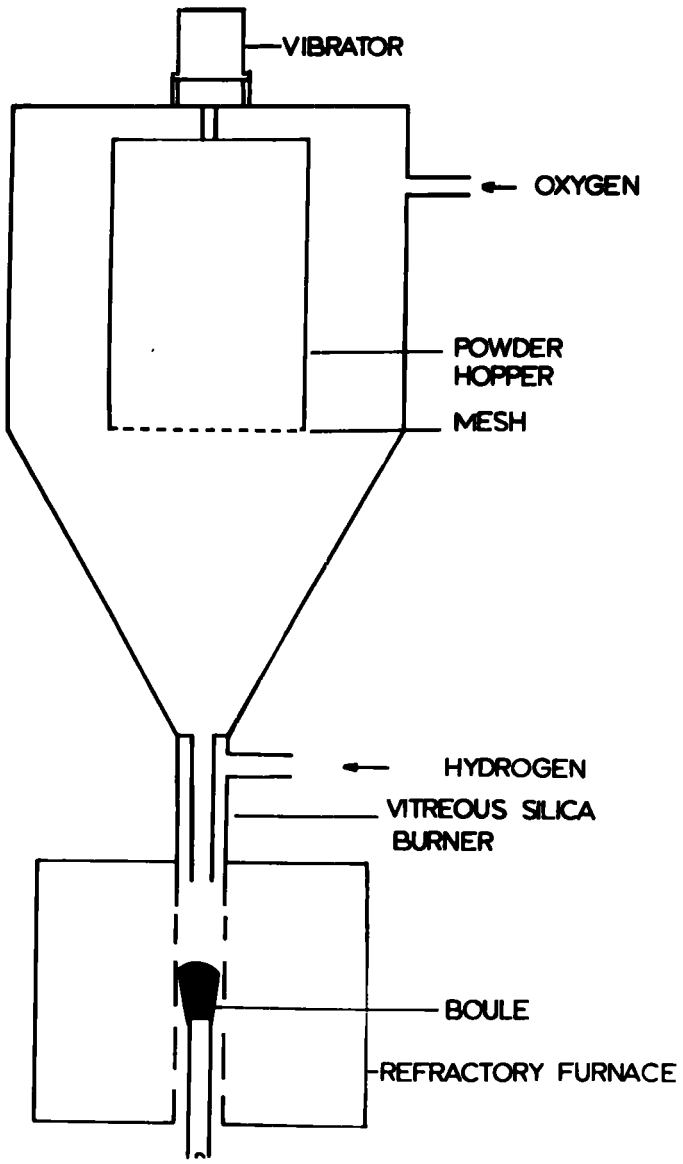

Figure 24: VERNEUIL GROWTH EQUIPMENT

c) shutting off the powder feed and gas supplies simultaneously when the required crystal length has been achieved, and then in the case of larger crystals, allowing the boule to cool naturally within the refractory shield.

Since boules are considerably stressed due to the thermal environment during growth, it is necessary to anneal them in order to avoid fractures in the course of machining. Boules used in this work have been annealed by maintaining them at 1850°C for about 36 hours and then cooling down very slowly.

The advantages of the Verneuil process are a relatively fast rate of growth (typically 6mm/hour for a $\frac{5}{8}$" diameter boule) and the ease of production of large crystals. The main disadvantages are; (a) the wide range in optical quality of the boules. Generally, the yield of very good quality crystals is low, and (b) the boules can contain small bubbles and particles of unfused raw material.

The lack of reproducibility inherent in the process has led to a study of each boule produced in order to correlate the crystal quality with the operational parameters during growth. This thesis, however, considers only with the correlation of crystal quality with laser performance.

6.2 Examination of Boule Optical Quality

The optical properties considered most important in a laser crystal are:

a) material parameters which contribute directly to the attenuation of a light beam, such as the density of scattering centres, and

b) variations in the refractive index which lead to wavefront distortions in the laser beam, i.e. a large beam divergence angle and an uneven distribution of the output energy over the beam cross-section.

The annealed boule is first inspected visually for macroscopic defects such as strain cracks and large bubbles or inclusions. The top and bottom of the boule are then cut at 90° to its geometrical axis and the cut faces rough polished flat and parallel to within a few minutes of arc. The cylindrical surface is also buffed to remove the thin opaque film of unfused material. (See figure 25).

In these experiments, the degree of scatter has been estimated qualitatively by placing the boule in the parallel beam of a 6328Å Helium-Neon gas laser. The cylindrical surface of the boule is moistened with methylene iodide. The scattering centres are illuminated and the best portion marked. Areas with a high degree of scatter are cut out and the faces repolished before interferometric examination.

A standard Twyman-Green interferometer is used to measure variations in refractive index of the boule. The interferometer light source is a 1 milliwatt 6328Å gas laser. High contrast interference fringes can be obtained from boules up to twelve inches in length. The interferometer mirrors are set to compensate for the physical wedge angle of the boule end faces. Since the gas laser beam is plane polarised, the crystal is rotated to obtain interferograms with light polarised perpendicular to and parallel with the c-axis. (Ordinary and extraordinary rays).

The area of boule with minimum scatter and fringe variation is selected and this portion cut and ground to produce a ruby rod of the desired size. Measurement between crossed polaroids ensures that the geometrical axis of the rod is maintained parallel to the c-axis plane.

6.3 Laser Rod Fabrication

The geometrical specification for the B.E.F. (both ends flat) laser rods used in this work is as follows:-

a) The end faces of the rod should be flat to within one tenth of a wavelength of light (6328Å)

b) The end faces must be perpendicular to the rod axis within one minute of arc.

c) The end faces are parallel to better than five seconds of arc.

d) The degree of surface finish of the ends must be high. Any scratches or polishing marks will contribute to the scattering loss of the material.

In addition, a normal tolerance on rod length of -0.000" + 0.020" and on rod diameter of -0.000" + 0.001" is required. The cylindrical surface

may have either a fine ground or a clear polished finish.

For polishing the end faces, a cylindrical jig is used whose central hole is at 90° ± ½' to the top jig face. The ruby rod is honed to a tight push fit in the jig and then waxed in. Ruby rod offcuts cemented around the jig circumference act as outriggers and stabilise the assembly during grinding and polishing. The rod face is ground on flat cast iron laps with 45μ, 25μ and 14μ diamond compounds successively. The end face of the rod is maintained at an angle of 90° ± ½' to the rod axis by measurement with an autocollimator between the upper reflecting jig surface and an optically flat mirror in contact with the rod face. The jig and autocollimator set up is shown in Figure 26.

Polishing of the end face is carried out on flat tin laps using 6μ then $^1/_{10}\mu$ diamond compound. The main problem associated with the polishing is lap contamination by abrasive particles larger than 6μ or $^1/_{10}\mu$. These obviously cause sleaks and scratches and absolute cleanliness is essential to attain the high standard of surface finish required.

The rod face is inspected for flatness by interferometric comparison with one of the Twyman-Green interferometer mirrors (flat to $\lambda/_{20}$ over 3" diameter) and for surface finish by viewing with a microscope.

The rod is then turned in the jig and the opposite face ground and polished as before. During grinding the parallelism of the faces is checked to within 30 seconds of arc using the autocollimator set-up. Corrections are applied by adjustment of the pressure point on the jig.

At the polishing stage, the readings for correction of end face parallelism are obtained using a double-ended Fizeau interferometer. This interferometer, specially constructed for wedge angle measurements, is capable of an accuracy in reading of ± 1 second of arc for rods up to $12\frac{1}{2}$" long x ½" diameter. The experimental arrangement is shown in Figure 27 and consists essentially of optical flats 1 and 2 in micrometer controlled precision mountings. Flat 2 is wedge shaped to avoid interference fringes between its front and back face. Flat 1 is figured on the back face and acts also as a collimating lens. The single mode gas laser beam allows one to obtain interference fringes between flats 1 and 2 up to the maximum length of the optical bench (2 metres). The pinhole P_1 forms an aperture close to the diffraction limited spot size for the focussing lens L_1.

Figure 26: POLISHING JIG AND AUTOCOLLIMATOR

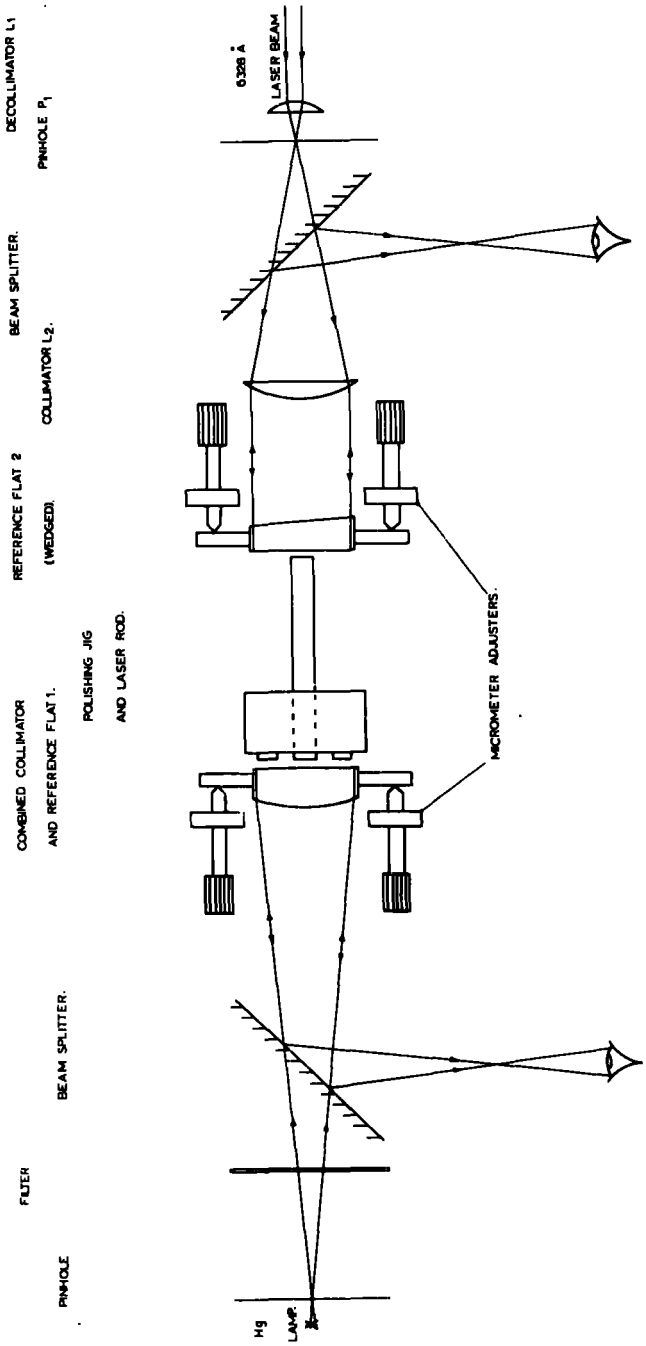

Figure 27: DOUBLE FIZEAU INTERFEROMETER

This acts as a spatial filter and smooths the intensity distribution across the gas laser beam wavefront (SPECTRA-PHYSICS 1966). The lens L_2 expands the beam to the diameter of the optical flats (35mm). The mercury lamp with flat 1 is set up as a standard Fizeau interferometer.

The laser rod is placed close to flat 1 which is adjusted to obtain interference fringes between the flat and the rod face. This flat is adjusted to set these fringes at extinction indicating parallelism between the flat and the rod face. Using the gas laser source, fringes between the flat 2 and the opposite end of the rod are set to extinction. The jig is now removed and fringes between flats 1 and 2 indicate the degree of parallelism of the rod. If F is the number of fringes visible across the 35mm diameter flats, the wedge angle of the rod, θ, is given by;

$$\theta = \frac{F\,\lambda}{2D} \quad \text{radians}$$

which for λ = 6328Å and D = 35mm becomes

$$\theta = 1.86\,F \text{ seconds}$$

Parallelisms to within the 5 seconds of arc tolerance requirements are easily measured since the extinction settings can be made to within $\frac{1}{4}$ fringe.

Rods with a linear refractive index variation may also be polished with the end faces out of parallel so that the physical wedge compensates for the optical wedge due to the material inhomogeneity. These correction measurements are obtained using the Twyman-Green interferometer. All rods used in these experiments have their end faces polished parallel since optical correction can also be achieved by off-setting the external reflectors.

After final inspection, the rod is carefully removed from the jig and all traces of the holding wax dissolved with a suitable solvent. For a high power laser system, clear sapphire sleeves polished to a close fit on the cylindrical surface are used to mount the rod in the laser cavity.

6.4. Optical Appraisal of Laser Rods

The finished laser rod is set up on the Twyman-Green interferometer and the o-ray and e-ray interferograms recorded. A fringe count across the aperture

of the rod is then determined from the o-ray interferogram, this being the polarisation direction of the laser beam from a 90° rod. The optical quality is assessed by the number of fringes per inch length per inch diameter. For Verneuil material, an average fringe count is 6fr/in/in (20 fringes across a ½" diameter rod, 6½" long). The yield of rods with fringe counts less than 3fr/in/in is low. The degree of c-axis misorientation can be obtained from the fringe difference between the o-ray and e-ray interferograms although the fringe patterns are usually too complicated for this measurement.

The rod is illuminated through the ends by a gas laser beam and the scatter centres counted. The degree of scatter for a good rod compared with a poor one is shown in Figure 28.

POOR ROD

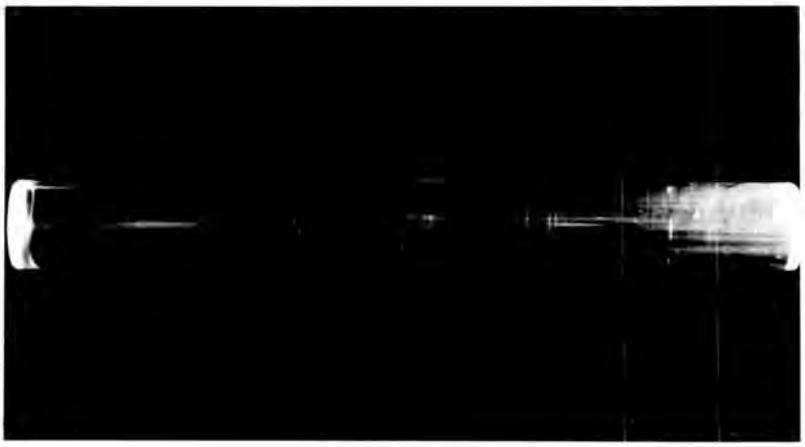

GOOD ROD

Figure 28: ILLUMINATION OF SCATTER CENTRES BY A GAS LASER BEAM

Chapter 7. Laser System

7.1 Radiation Transfer from Flash Lamp to Ruby Rod

The most usual and generally the most efficient system employed for concentration of the radiation from a linear flash tube onto a ruby rod consists of an elliptical cylinder with the lamp placed along one focal line and the laser rod along the other. This configuration is based on the fact that rays originating from one focus of an ellipse are reflected into the other. In these experiments, two main factors had to be considered when determining the size of ellipse to be used; the capacity of the only available lathe capable of machining an accurate ellipse limited the outside diameter of the cylinder to 10cm and the minimum separation of the flash lamp with insulators and ruby rod with external reflectors was 3.85cm. The elliptical reflector was therefore made to the following dimensions:

Major axis 2a	=	7.6 cm
Separation of foci D = 2ae	=	3.85 cm
$\therefore$ Eccentricity e	=	0.506 cm
Minor axis 2b	=	6.56 cm

To provide a split reflector permitting ease of access to the laser rod, a $6\frac{1}{2}$" long x $4\frac{1}{2}$" diameter aluminum bar was slit lengthwise and the sawn edges milled. The two pieces were dowelled, clamped together and the external machined to 4" diameter. The blank was bored to a diameter near to the minor axis and set up in a lathe on which the boring tool followed an elliptical former of the correct size. The machined surface was then polished to a mirror finish whose measured reflectivity was between 65% at 4000 Å and 72% at 5500 Å. Vacuum deposition of aluminium on this surface increases the reflectivity in the pumping bands to about 92% but the coating deteriorates rapidly under the intense radiation from the flash tube. Electrolytic polishing and then anodising produces a more

durable highly reflecting surface but the equipment for this was not available. In these experiments, the cavity reflectance was maintained within a few percent of 72% by dismantling the system and re-polishing at frequent intervals (after 50 discharges).

Increased pumping efficiency may also be obtained by using an elliptically formed glass cylinder with a dielectric coated reflecting surface giving a reflectance of between 85% and 97% in the ruby pump bands. These coatings also transmit unwanted infra-red radiation which heats up the ruby and reduces efficiency. Both types of cavity have been compared by WHITEMAN (1966).

The elliptical reflector is fitted with polished aluminium end plates accurately machined and dowelled to the end faces of the cavity to ensure precise positioning of the foci. The dimensions of the machined cavity are accurate to within $\frac{1}{4}$ mm. The flash tube is mounted in Tufnol insulators screwed to the cavity end plates. The bore of the insulator is lined with alumina tube to prevent carbonisation of the Tufnol by the lamp radiation and a consequent reduction in cavity reflectivity. Close fitting sapphire sleeves are essential for mounting the ruby rod in the end plate. Damage occurs at the edge chamfer of the rod end face if metal holders are used and the polished sleeves also permit excitation of the whole rod.

Figure 29 shows the reflecting cavity complete with ruby rod and flash tube.

7.2. The Effect of Flash Tube Diameter on Cavity Efficiency

The pumping efficiency E of an elliptical cylinder reflector is given by (BOWNESS 1965):

$$E = \frac{100}{\pi} \left[\alpha_o + \frac{T_2}{T_1} \theta_o \right]$$

where T_1 = flash tube radius

T_2 = crystal radius

α_o and θ_o are angles measured from the lamp and crystal axis respectively to any point P_o on the ellipse (see figure 30).

The crystal is assumed to absorb all the useful pumping energy incident upon it and the reflectivity of the cavity wall to be 100%.

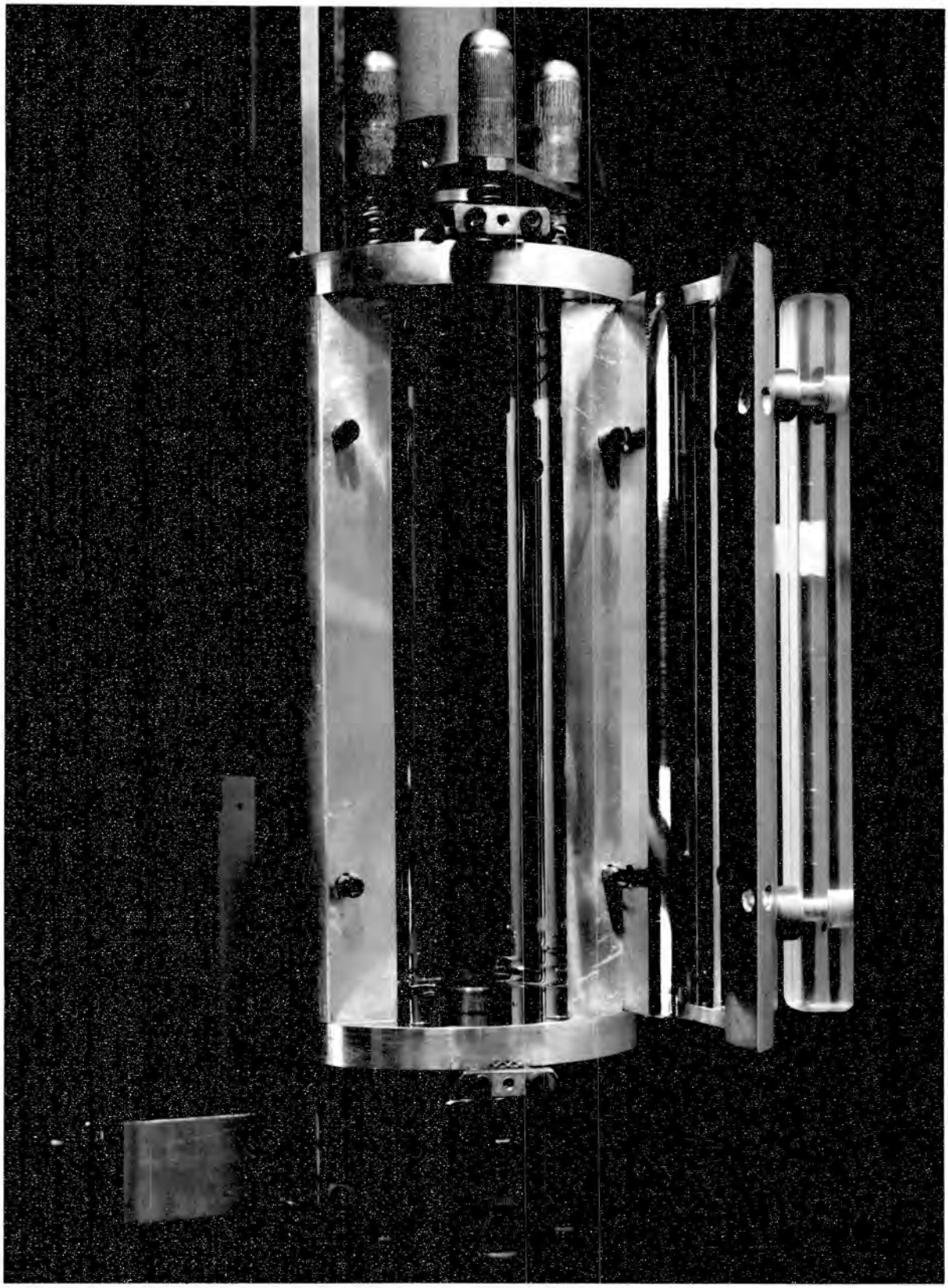

Figure 29: INTERIOR OF ELLIPTICAL PUMPING REFLECTOR

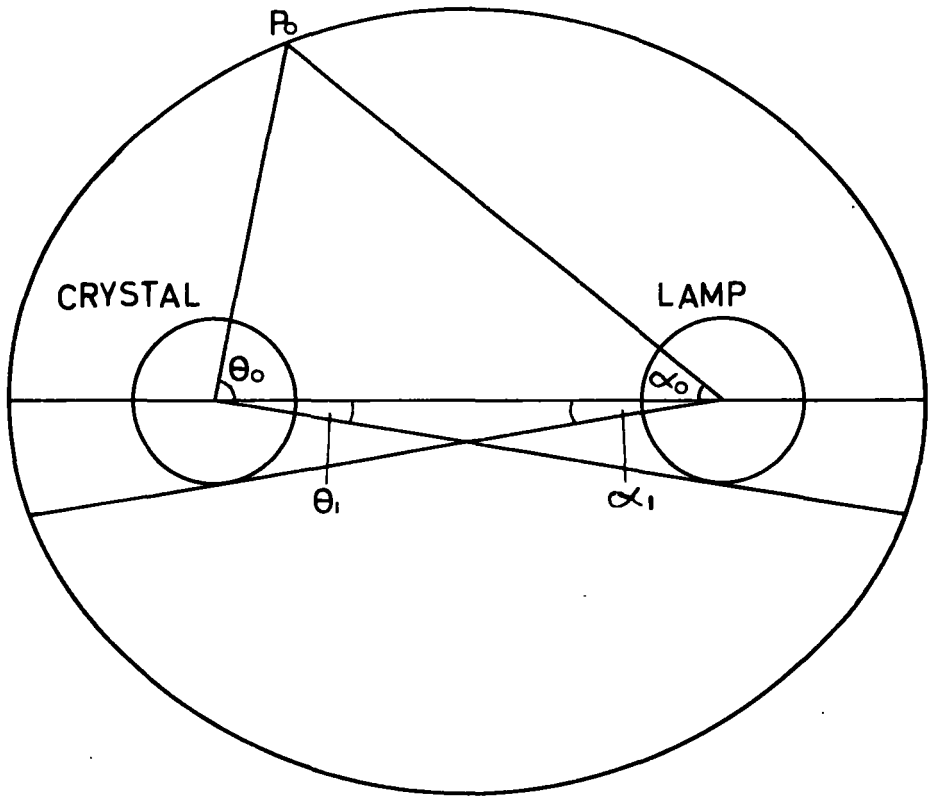

Figure 30: CROSS-SECTION OF ELLIPTICAL REFLECTOR

Since some of the reflecting surface behind the lamp is screened from the crystal by the lamp itself, the angle θ_o must be reduced by θ_1 where

$$\sin \theta_1 = \frac{T_1}{2ae} \tag{7.1}$$

θ_1 is the angle subtended at the crystal by the lamp.

$$\therefore E = \frac{100}{\pi} \left[\alpha_o + \frac{T_2}{T_1} \left(\theta_o - \theta_1 \right) \right] \tag{7.2}$$

No correction is applied to allow for the finite crystal size since all energy falling on it directly is assumed to have been collected.

α_o and θ_o may be calculated from the following equations dependent on the properties of an ellipse,

$$\cos \alpha_o = \frac{1}{e} \left[1 - \frac{1-e^2}{2} \left(1 + \frac{T_2}{T_1} \right) \right] \tag{7.3}$$

$$\sin \theta_o = \frac{T_1}{T_2} \sin \alpha_o \tag{7.4}$$

For a = 3.8 cm and e = 0.506 cm, the equations give efficiency values of 70%, 62%, and 55% for the 10 mm, 13 mm and 15 mm bore tubes respectively with a 12.7 mm diameter ruby rod. Increased overall efficiency is possible either by increasing the size of the ellipse or by reducing the separation of the foci.

A paper by KAMIRYO et al (1965) considers the effect of wall reflectivity on pumping efficiency. Exact efficiency values are difficult to obtain from this paper since no equations are given. A graph of cavity efficiency against cavity reflectivity and dimensional parameters indicates efficiency values of 40%, 37% and 35% for the 10mm, 13mm and 15mm bore tubes for a wall reflectivity of 80%.

For a wall reflectivity of 70%, the effect of the lamp size on the radiation transfer efficiency will therefore be small.

7.3 Series Impulse Triggering

Breakdown of the narrow air gap between the cavity end plate and the flash tube trigger wire caused a loss of trigger pulse energy and frequent misfiring of the flash tube. The addition of a quartz insulating sleeve at the point did not entirely solve the problem. A method of series impulse triggering whereby the trigger pulse is applied directly to the flash tube electrodes via a small isolating capacitor worked satisfactorily (CHERNOCH and TITTEL 1965). The modified flash tube circuit is shown in figure 31. An adjustable spark gap with tungsten electrodes generates a high frequency pulse train in the trigger circuit. The main current limiting inductor L also serves to block the high frequency trigger pulse from the energy storage capacitors C. The coupling capacitor c isolates the main bank voltage from the trigger transformer. This alteration in triggering method made no detectable change to the flash tube main discharge wave form.

7.4 Fabry-Perot Cavity Reflectors

The last stage in the energy conversion process of the laser is the Fabry-Perot cavity which provides positive feedback to the amplifying medium and increases the system gain. As a result of the spontaneous and stimulated emission in the laser material, a light wave is generated in the resonant cavity. The light that does not pass through the side of the rod is reflected back and forth between the mirrors. If a light wave of intensity I_o is incident upon the crystal of length L, the intensity after one pass through the material is given by:

$$I = I_o \exp \beta L.$$

where β is the gain per pass of the rod at the stimulated emission frequency. The gain of the laser rod is therefore:

$$G = \frac{I}{I_o} \exp \beta L.$$

One of the Fabry-Perot reflectors is usually made as near 100% reflectivity as possible, the other must be partially transmitting to obtain an output

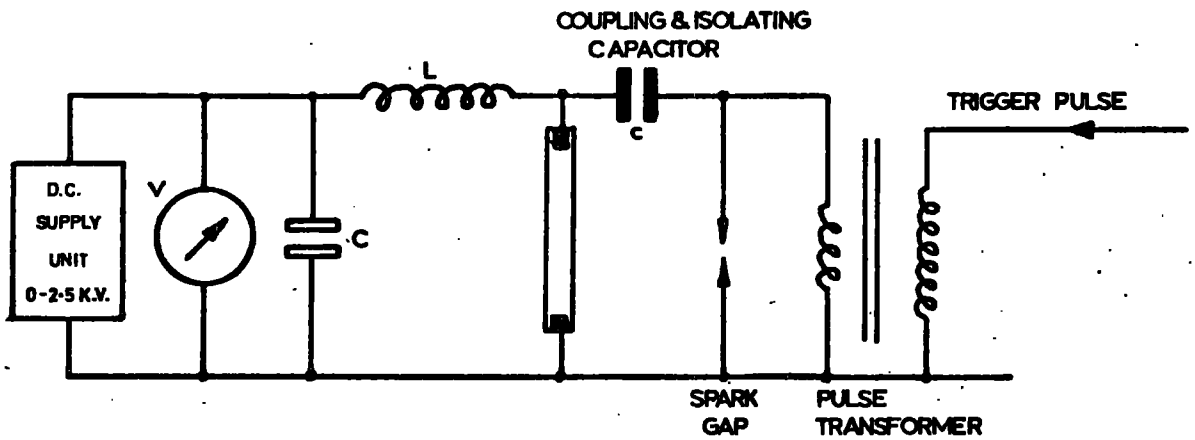

FIGURE 31. SERIES TRIGGER FLASHTUBE CIRCUIT.

from the system. If the reflectivity of this mirror is R, the system gain during a double pass in the laser material is given by:

$$G = R \exp 2\beta L.$$

The loss coefficient per double pass through the system due to the external reflector is defined as $\gamma = -\ln R^{\frac{1}{2}}$ and the system gain becomes:

$$G = \exp 2(\beta L - \gamma)$$

If G<1, the laser oscillations will die out and if G>1 oscillations will grow. The system will be at threshold of oscillation when:

$$\beta = \frac{\gamma}{L} \qquad (7.5)$$

The gain in the laser material, the length of active medium and the mirror reflectivity are thus interdependent. If R = 100% none of the output energy can emerge while if R has a value defined by equation (7.5) the system will only be at the oscillation threshold. Between these two values is a reflectivity for which the system output and efficiency is a maximum. The optimum reflectivity for a $6\frac{1}{2}$" long x $\frac{1}{2}$" diameter laser rod has been determined by WHITEMAN (1966). A reflector of between 15% and 20% reflectivity gives the maximum output.

The optical elements are usually fabricated from an optically homogeneous synthetic vitreous silica e.g. Spectrosil*. The mirror blanks are polished flat to $\lambda/_{10}$ over the working area and coated with a vacuum deposited, multi-layer dielectric film having the required transmission and reflection characteristics at the laser wave-length. Considerable difficulty has been experienced in obtaining reflectors capable of withstanding high energy laser pulses. In most cases, the reflectors suffer damage well below the figure claimed by the manufacturers, probably due to residual absorption in the multi-layer coating. The transmitting reflector suffered damage at energies as low as 20 joules in 1 millisecond (≈40kw/sq.cm). The problem is not as serious with the maximum reflectivity mirror (typically 99.8% at 6943 Å) although damage occurred to one sample after 20 shots at a power

---

* Spectrosil is a registered trade mark of Thermal Syndicate Limited.

level of 60kw/sq. cm.

Since the required transmission value is in the region of 80%, a sapphire disc was used as the transmitting reflector. The disc faces are polished flat to $\lambda/_{10}$ and are parallel to within 1 second of arc. The measured reflectivity is 15% which together with the 7% reflection at the ruby/air interface gives a total combined reflectivity of 21%. This reflector showed no signs of damage up to the maximum power level of about 250kw/sq. cm achieved in these experiments.

A right-angled Spectrosil prism was also used as the maximum reflectivity element. The 90^{o} and 45^{o} angles are polished accurately to within 2 arc seconds. The disadvantage of the prism is that it must be aligned with the ruby rod end face by an image reflected through the rod. With a poor rod, image distortion makes alignment difficult. The prism/sapphire disc combination is used when comparing flash tubes at high energy levels with a given ruby rod and the di-electric reflector/sapphire combination is used to compare the characteristics of ruby rods at a lower energy input.

The reflectors are fixed into mountings controlled by precision threaded adjusting nuts on studs attached to the cavity end plates (see Figure 29). The reflectors are aligned using a Hilger and Watts, Angle Dekkor autocollimator as follows:

(a) the 100% reflector is aligned parallel to one ruby rod end face by adjusting the mirror until the images from faces A and B coincide (see Figure 32);

(b) the autocollimator is then set up to view the reflected image of its scale from face C;

(c) the sapphire disc can then be set so that the image from face D coincides with that from C i.e. the reflectors are parallel to each other if the rod faces are parallel. Alternatively, the sapphire disc can be set so that the image from face D coincides with the image from face A seen through the laser rod i.e. the reflectors compensate for the optical wedge due to material inhomogeneity.

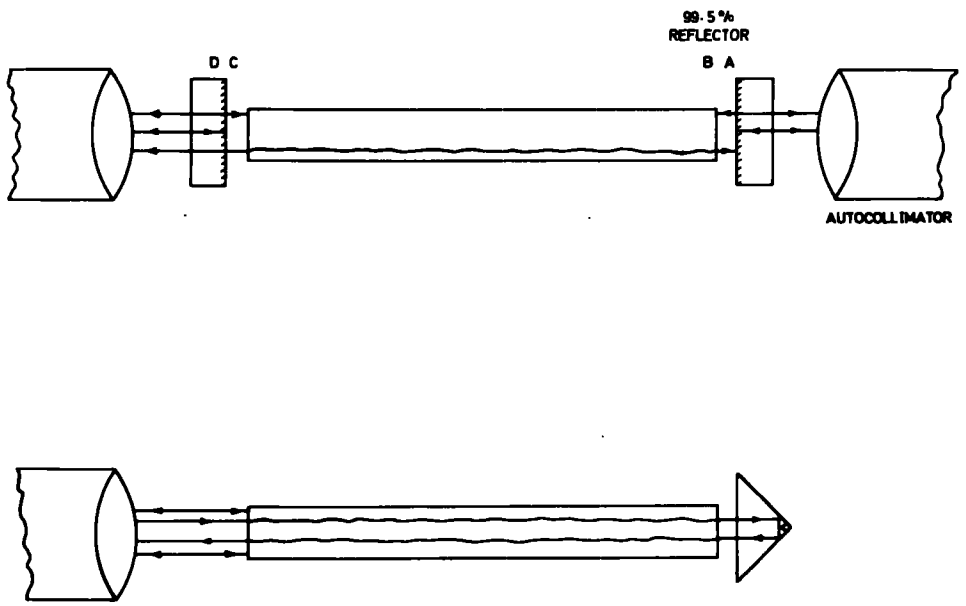

Figure 32: FABRY-PEROT REFLECTOR ALIGNMENT

The sapphire flat or 100% dielectric reflector can be aligned parallel to the end faces within 10 arc seconds. Because of the distortion of the auto-collimator graticule viewed through the rod, the alignment accuracy using this image is 30 to 60 seconds depending on the rod optical quality. The reflecting prism can only be aligned through a good rod. The effect of adjusting the mirror alignment to compensate for the optical wedge of the material on the laser output will be examined in Chapter 8.

The length of the Fabry-Perot cavity in these experiments is about 21 cm. (rod length 16.5 cm) The cavity length, laser threshold, output beam divergence and energy output are interdependent. LISITSA et al (1966) found that increased cavity length for a fixed laser rod length results in an increase in threshold energy and a reduction in beam divergence and output energy.

7.5 Emission Structure of the Laser Output

Figure 33 shows a typical wave form of the light output from the ruby laser. Fluorescence begins immediately after the start of the pumping pulse and when the required population inversion is achieved, stimulated emission amplification occurs resulting in sharp spikes in the output wave form of about 1 microsecond duration. This relaxation oscillation effect occurs because the rate of depletion of the metastable level exceeds the rate at which the level is populated by the excitation process. The gain of the laser material is reduced below the oscillation theshold until the population inversion is re-established.

Additionally, the Fabry-Perot resonator has a large number of possible modes of oscillation each giving different light amplification characteristics. A complicated interaction takes place between the stimulated emission from the atoms of the laser material and these cavity modes. Each mode may be regarded as an almost independent oscillator whose quality factor, Q, is defined by:

$$Q = \frac{2\pi \upsilon_o E}{P_d}$$

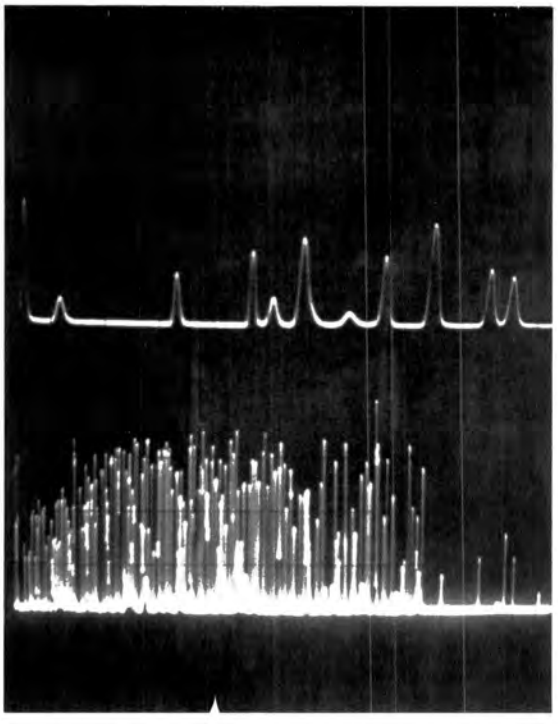

Top trace : 2μsec/cm

Bottom trace : 50μsec/cm

Figure 33: LASER OUTPUT WAVE FORM

where υ_o is the resonant cavity frequency, E is the energy, and P_d is the rate at which energy is dissipated in the oscillator (LENGYL 1966). A high Q represents low dissipation and narrow line-width. The highly directional beam from a laser is due to a high Q value for the axial modes.

The irregular pulsations of the output are the result of variation in uniformity of the pumping radiation in the rod giving rise to varying stimulated emission rates and the excitation of different modes of oscillation. The number of excited modes also increases with energy input above threshold.

Since the excitation of any particular mode is largly influenced by minor irregularities in the laser material, only the highest quality crystals produce output wave-forms with regular spiking. Spiking behaviour has been extensively studied by TANG, STATZ and De MARS (1963 and 1964) who demonstrated regular spiking of the output of a ruby laser operating in a single mode.

The integrated output energy of the system is measured with the ballistic thermopile system described in Chapter 3.5. A lens is used to converge the output beam into the $\frac{3}{8}$" diameter thermopile aperture. The lens and thermopile were maintained at a fixed distance from each other and from the laser system. The experimental layout is shown in Figure 34.

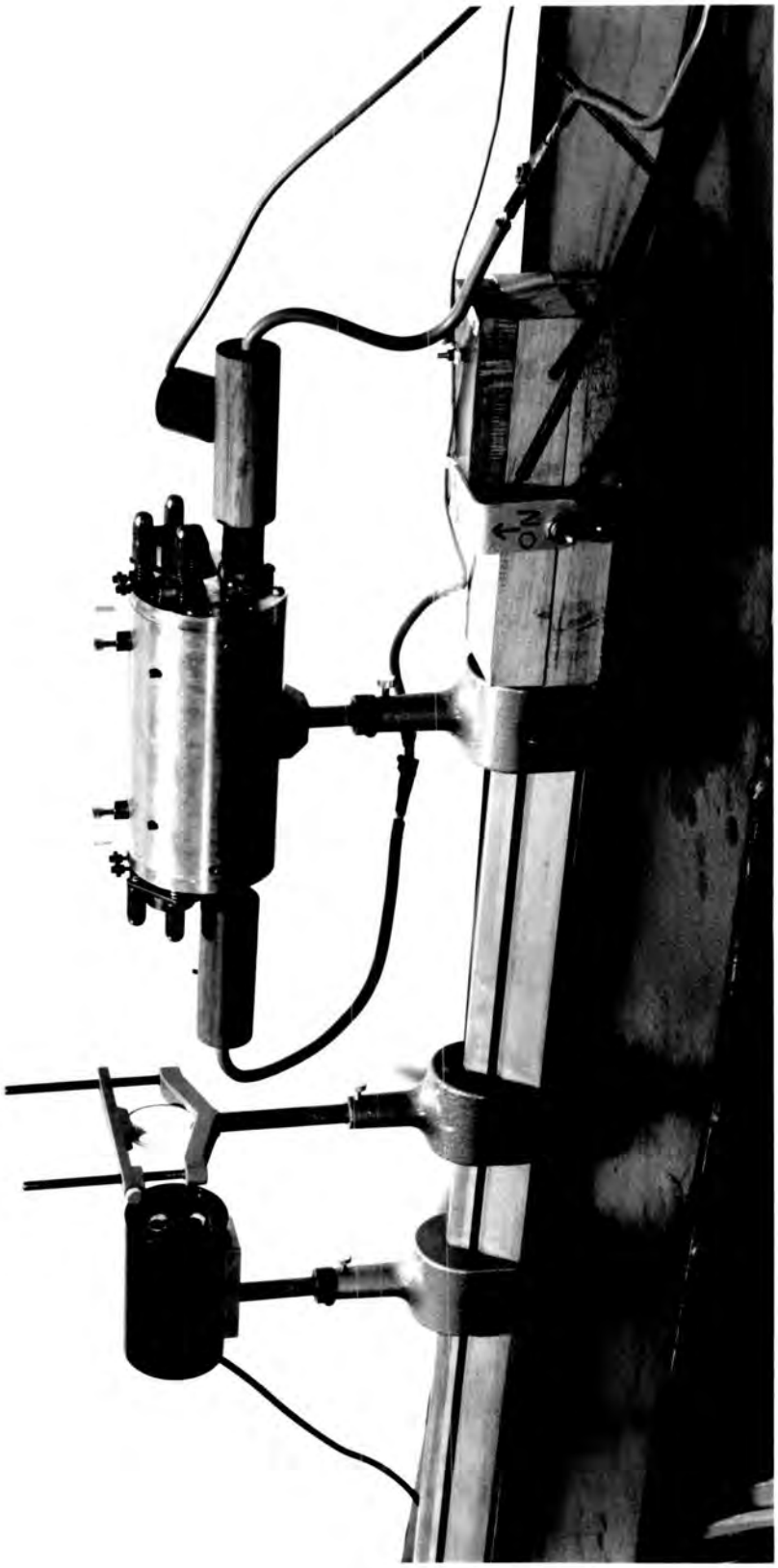

Figure 34: LASER SYSTEM AND T.R.G. THERMOPILE

Chapter 8. Results of Experiments on the Laser System

8.1 Experimental Conditions

All measurements of laser output energy were made under controlled conditions after consideration of the following parameters:

a) Increased ruby temperature reduces the output energy mainly due to a broadening of the laser line-width. This factor has been examined by WHITEMAN (1966) who used a water jacket to maintain the ruby rod at a given temperature. For a high repetition rate, a water cooled ruby rod is essential.

In these experiments, the ruby rod was maintained at about room temperature by a stream of dry nitrogen gas flowing through the elliptical reflector. Investigations of the reduction of output energy with increasing repetition rate at the maximum energy input to the system showed the necessity for an interval between measurements of 15 minutes to allow the rod and cavity to cool. Discharges at shorter intervals gave reduced outputs. In general, the output was measured at 30 minute intervals for inputs above 6000 joules and 15 minute intervals for lower inputs.

b) The pumping efficiency of the laser cavity depends on the orientation of the c-axis of the ruby with respect to the flash tube. Since the wall reflectivity of the pumping reflector is not 100%, maximum absorption of the direct radiation from the flash tube will occur when the c-axis plane is parallel to the direction of the incident radiation (See figure 3). For the 90^{o} orientation rods used in this work, the c-axis was thus set parallel to the plane passing through the rod and tube axis. The output with the c-axis at 90^{o} to this plane is about 25% less.

c) To check the effect of possible deterioration of the elliptical pumping reflector or external mirrors, the first measurement was repeated at the end of a series of results. If the two measurements differed by more than 10%, the laser cavity was repolished and the

series repeated. When the prism is used the results are very reproducible; two measurements under the same conditions at an 18 month interval gave the same result.

To avoid damage to the di-electric coated mirror, the energy input to the system was limited to 8000 joules in a period of about 2.5 milliseconds (450 μH series inductance). With the best laser rod, the corresponding energy output was in the region of 60 joules, a power level of about 25 kW/sq.cm. Figure 35 shows the type of damage to the coating caused after a few shots at a power level of 60 kW/sq.cm. Atmospheric dust settling on the coating may be partly responsible for this by providing a localised absorption centre with heating of the coating at that point. For long life of a dielectric coated reflector, the system should be hermetically sealed.

8.2 Comparison of the Output Characteristics of Six Ruby Rods

In this experiment, the 13 mm bore lamp was used because of its known life characteristics and a lower wall loading than the 10 mm bore lamp. The series inductor was 450 μH and bank capacity 4000 μFd. to obtain a maximum flash duration, a low wall loading and minimum lamp deterioration. The maximum reflectivity mirror and sapphire disc formed the Fabry-Perot cavity.

The variation of output energy with input energy for each rod is shown in Figure 36. The results show a linear relationship between output and input energy at energy outputs above about 5 joules. Nearer the laser threshold the efficiency falls off. For 516, the threshold energy under these conditions is about 1600 joules, a capacitor bank voltage of 900 volts. The slope efficiency is nearly the same for each rod, probably a function of the laser system itself. A different dielectric coated reflector gave at first a greater slope efficiency (14 joules/kJ input) for 516, but this mirror was damaged by the laser radiation after a few shots. The slope efficiency has a value between 10 and 12 joules output per 1000 joules input above threshold, about 1%.

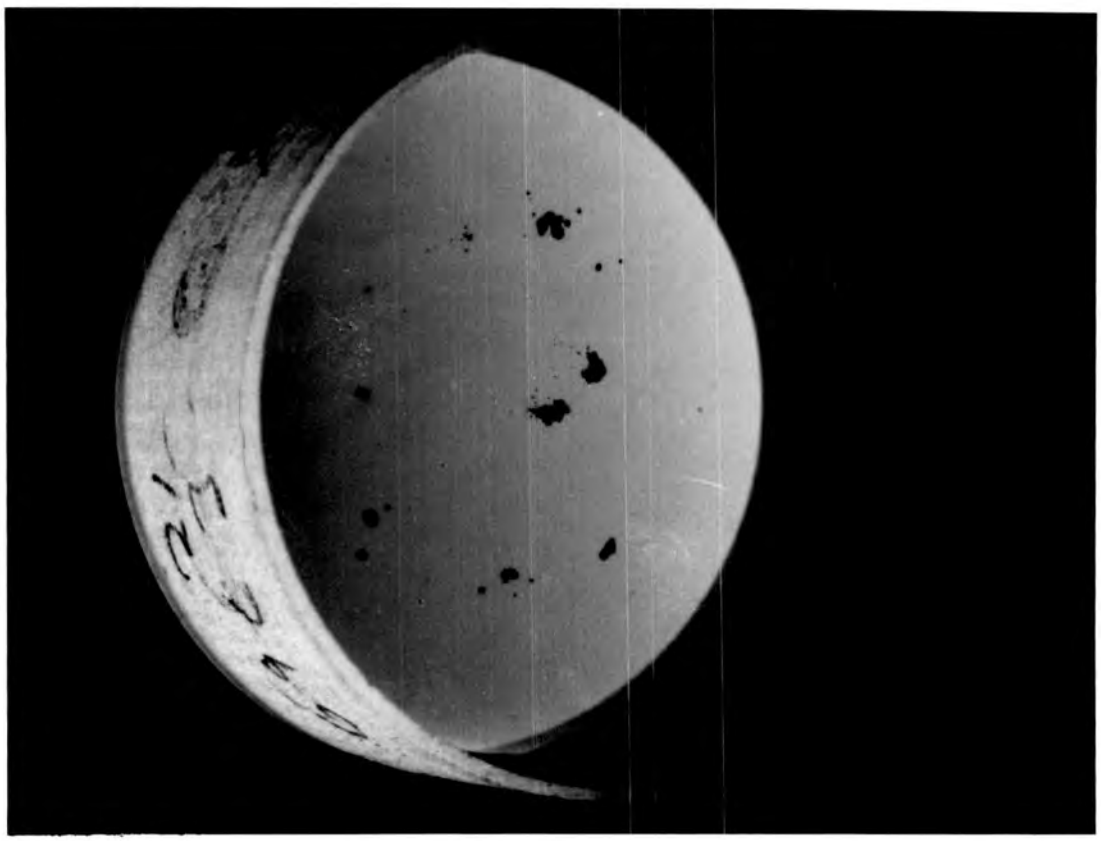

Figure 35: DAMAGE TO DIELECTRIC COATED REFLECTOR

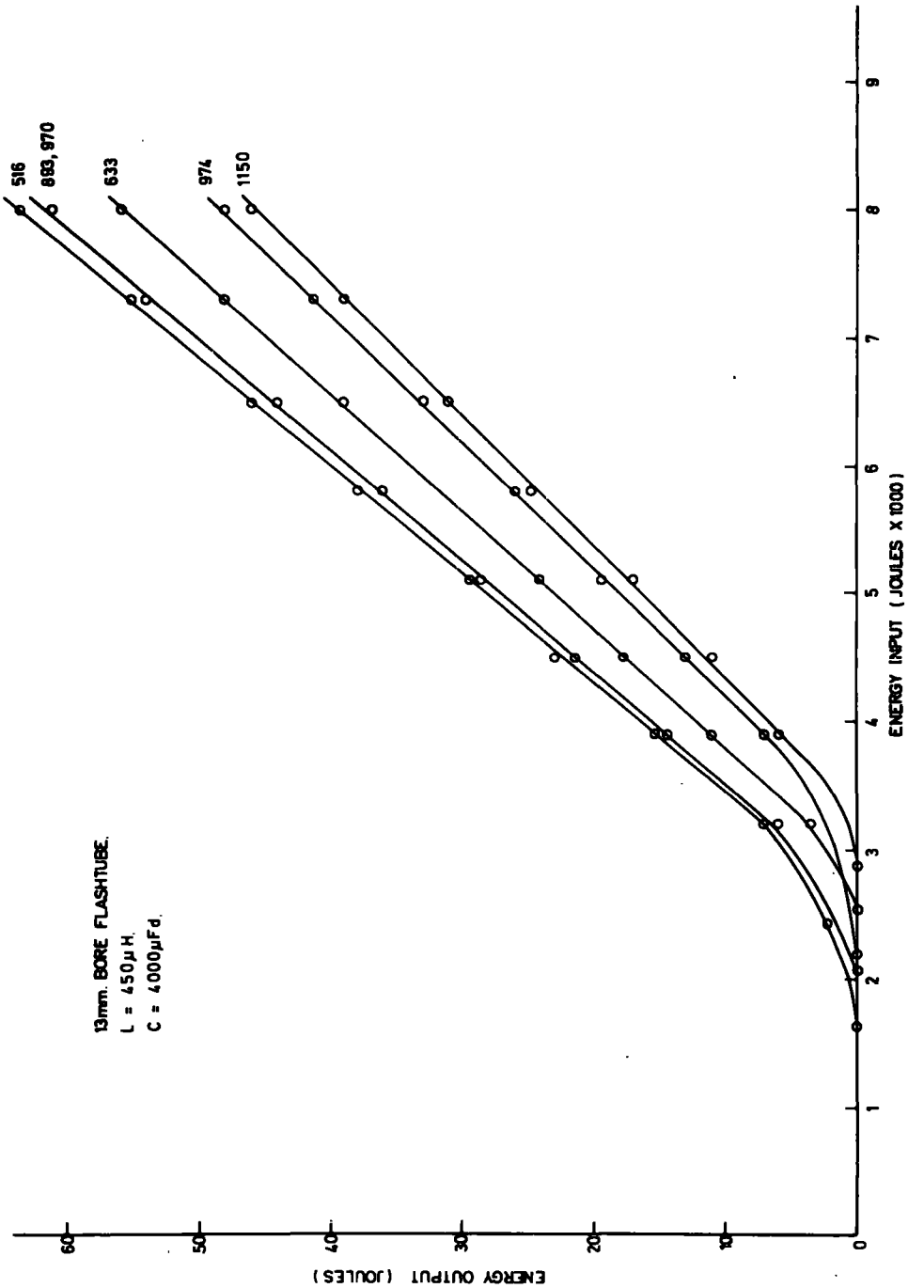

Figure 36: VARIATION OF ENERGY OUTPUT OF DIFFERENT RUBY RODS

The Twyman-Green interferograms (o-ray) of the rods are shown in Figure 37 and the optical characteristics of the rods are set out in the following table:

Rod Number	Fringe Count /in/in	Number of Scatter Centres	Optical Wedge	Threshold joules	Energy Output (8 kJ Input)
516	12	13 large, many small	<10 seconds	1620	63.5
633	33	many small	low, indeterminate	2640	56
893	33	1 large, 14 medium	"	2000	61
970	41	3 large, 10 medium	about 1 minute	2200	61
974	60	2 medium, many small	indeterminate	2200	48
1150	12	clean material	<10 seconds	2880	46

Table VI

Large scatter centres are defined by a dimension of 2 mm or greater in any direction, small scatter centres are less than $^1/_{10}$ mm in size. Since it is impossible to obtain rods of similar optical quality with varying degree of scatter, the effect of scatter on laser performance cannot be determined. Rod 516, despite the many scatter centres, gives the best laser performance. EDWARDS (1967) placed fused silica plates within the Fabry-Perot cavity to provide an artificial scattering loss. Provided the reflectivity of the mirrors was adjusted to compensate for the inserted scattering loss, up to 70% of the output energy of a loss-free resonator could be obtained. In the case of a Q-switched laser (HELLWARTH 1961) where high intensity, short flash duration pumping pulses are used, the laser rod operates at a higher power density. Scatter centres lower the internal damage threshold of the material (PASHKOV and ZVEREV 1966) in this type of laser.

From Figure 36 and the preceeding table, it can be seen that the laser performance is independant of the optical quality. Although the best rod, 516, gives the greatest output energy, the next best, 1150, gives the least. This experiment shows that there can be no substitute for measurement of the actual performance of a ruby rod when selecting rods to provide specified laser outputs from a given laser system.

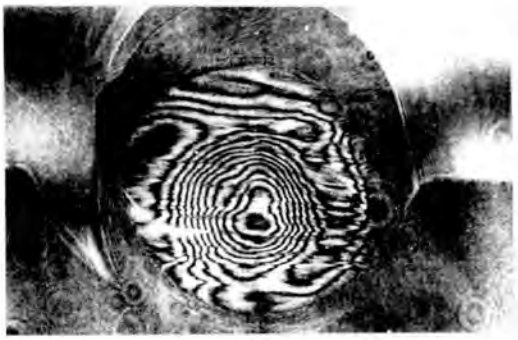

516

633

893

970

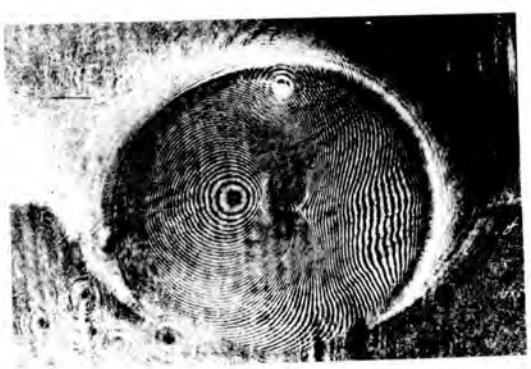

974

1150

Figure 37: TWYMAN-GREEN INTERFEROGRAMS

8.3 Variation of Laser Peformance with Lamp Parameters

In this experiment rod 516 was used to determine the effect on the laser system performance of flash tube size, inductance variation and capacity of the condenser bank. The prism was used in place of the dielectric coated reflector to allow an input energy of up to 10000 joules. One ruby rod used in early experiments suffered considerable damage to the fine ground cylindrical surface after about thirty shots at an input energy above 8000 joules and measurements at high energy input were therefore limited. The damage effect is discussed in the next section.

The results for a capacitor bank of 4000 μFd. are shown graphically for each flash tube in figures 38, 39 and 40 for a 100 μH, 235 μH and 450 μH series inductance respectively. From the flash tube results (Chapter 5) the corresponding flash durations are in the rgion of 1.5, 2.0 and 3.0 milliseconds. Figures 38 to 40 show for each tube a linear relationship between output and input energy above threshold. In each case, the shorter flash duration when the 100 μH inductor is used results in an increased slope efficiency and a lower laser threshold. The 10 mm bore tube is the most efficient and the 13 mm bore tube equally or slightly more efficient than the 15 mm tube.

For the same energy input to the flash tube, reduction of the bank capacity to 2000 μFd. neccessitates a higher bank voltage and results in a shorter flash duration and increased peak intensity. Figure 41 shows the input/output relationship with the 100 μH and 450 μH series inductors and the 10 mm and 13 mm bore tubes.

The slope efficiencies in joules/kilojoule above threshold in figures 38 to 41 and the corresponding laser thresholds are given in the following table, together with the laser output for 4000 joules and 5760 joules total input.

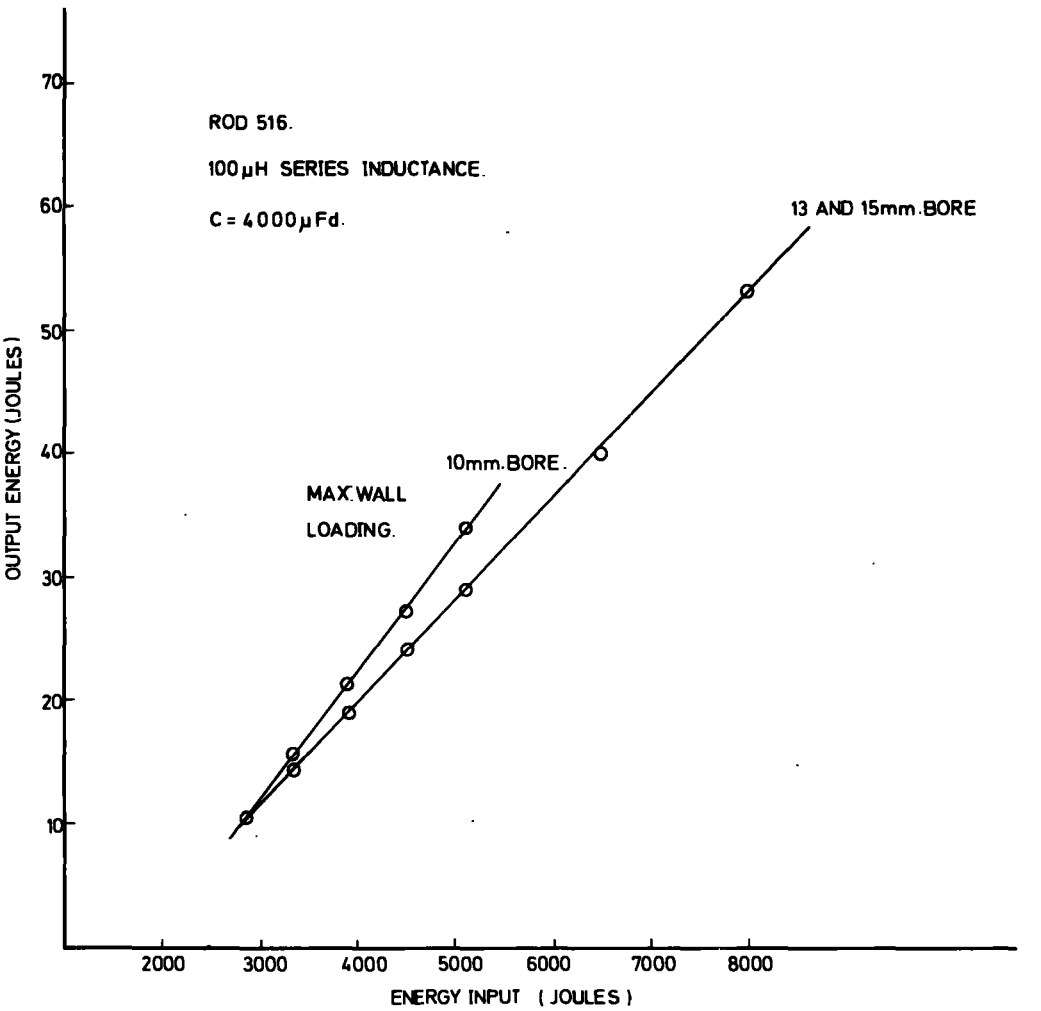

Figure 38: VARIATION OF LASER OUTPUT WITH LAMP AND CIRCUIT PARAMETERS

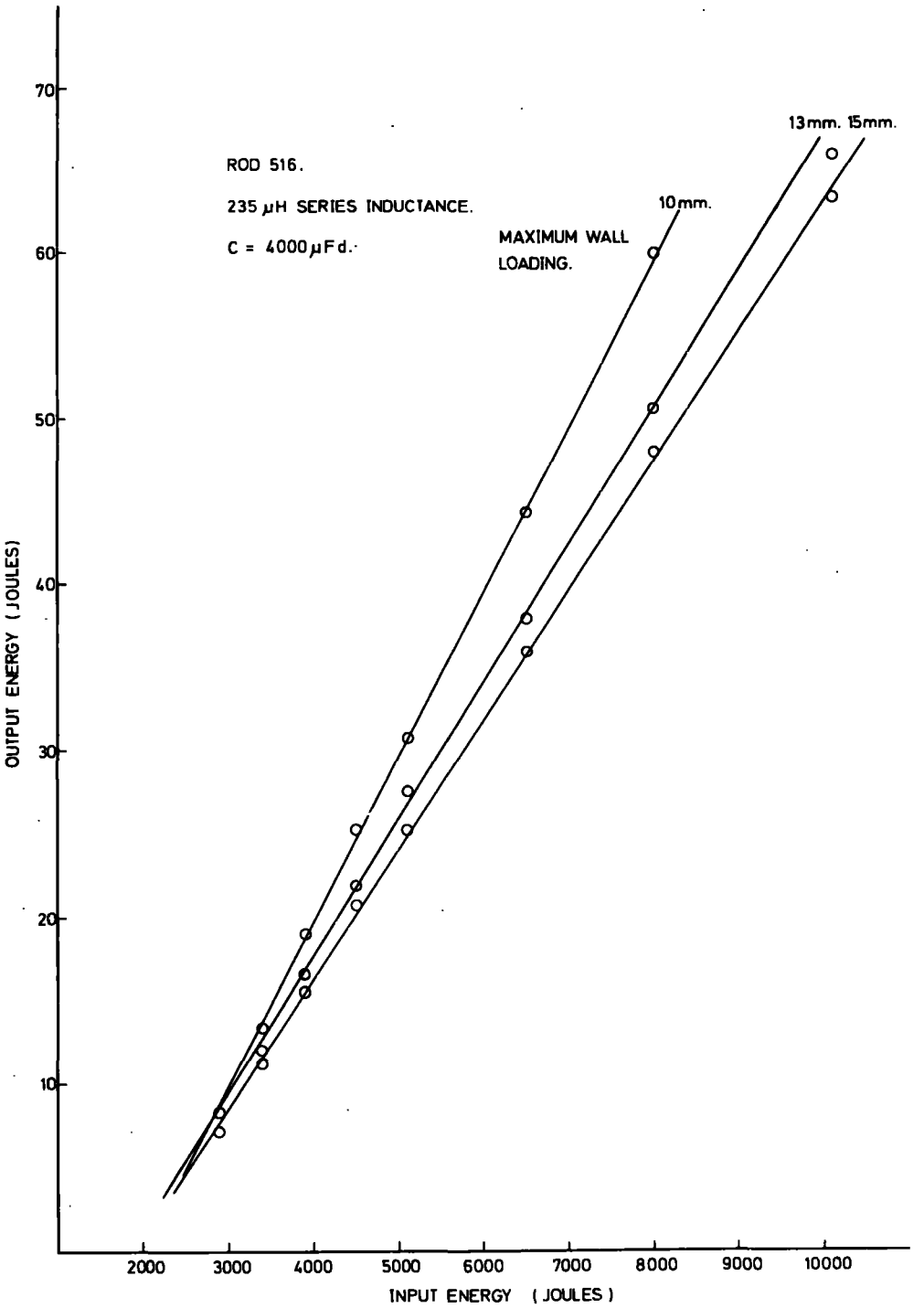

Figure 39: VARIATION OF LASER OUTPUT WITH LAMP AND CIRCUIT PARAMETERS

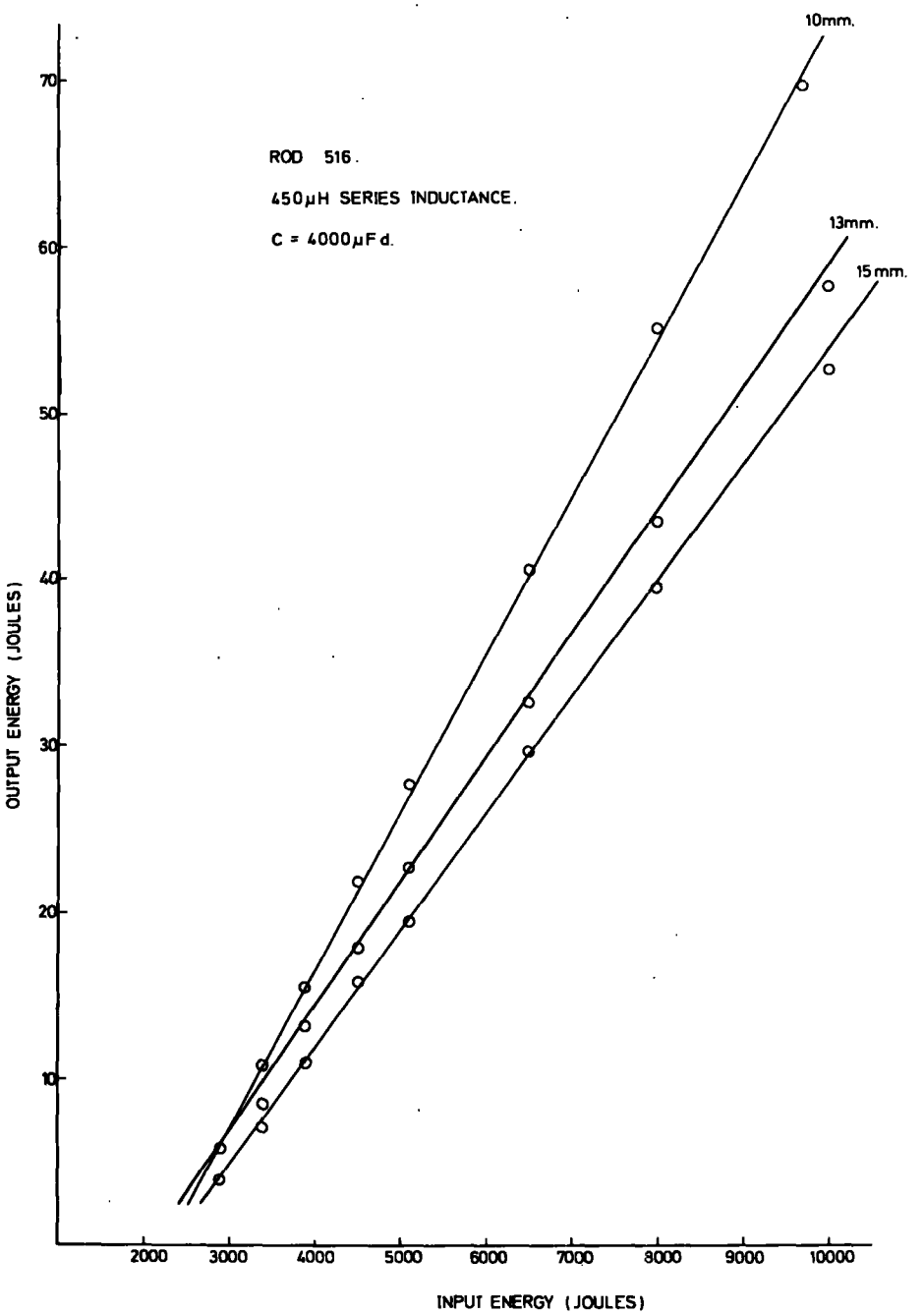

Figure 40: VARIATION OF LASER OUTPUT WITH LAMP AND CIRCUIT PARAMETERS

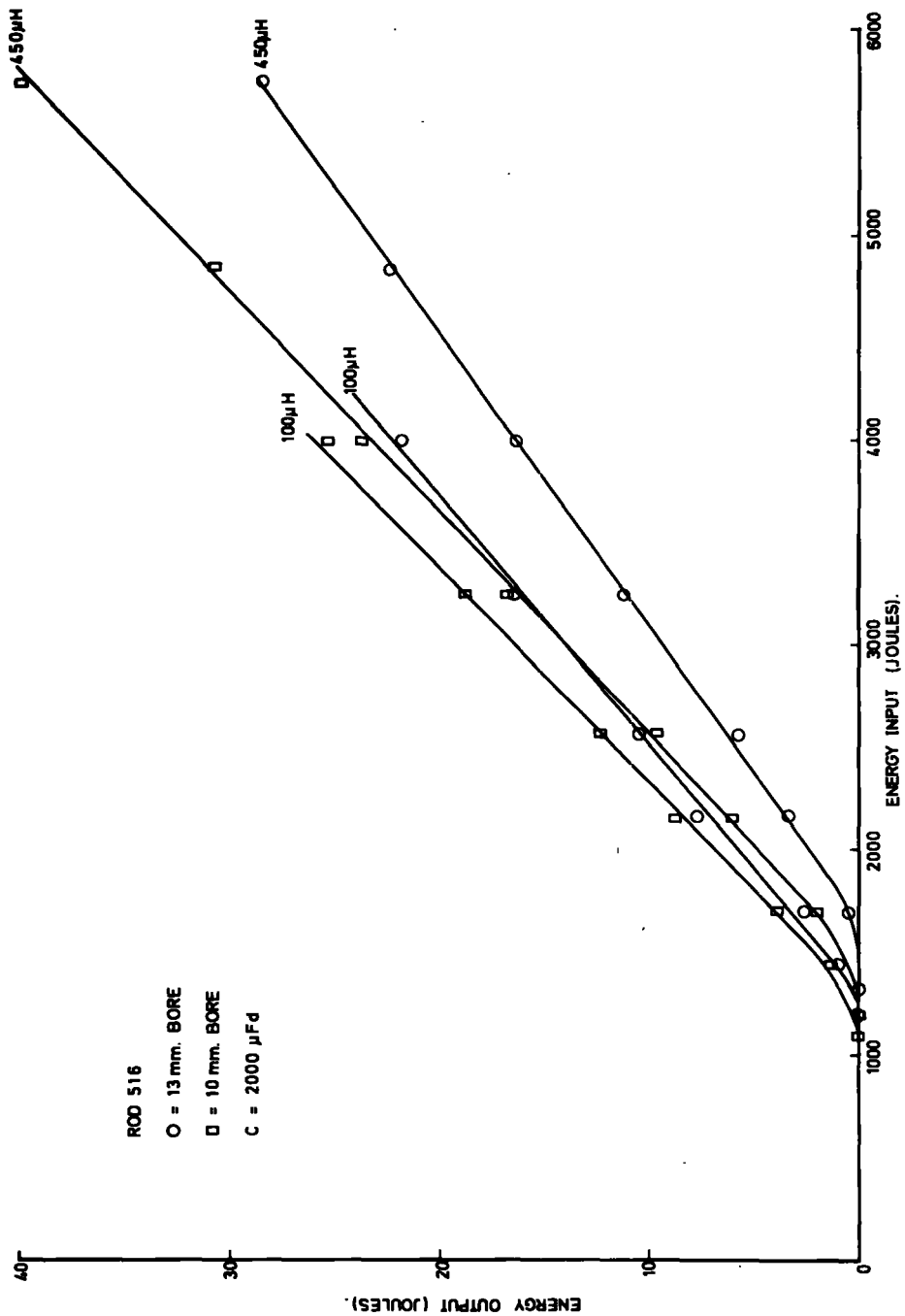

Figure 41: VARIATION OF LASER OUTPUT WITH LAMP AND CIRCUIT PARAMETERS

Slope Efficiency (joules/kJ)									
Tube bore	10 mm			13 mm			15 mm		
Inductance	100	235	450	100	235	450	100	235	450
C = 4000 μFd	10.4	10.0	9.25	8.3	8.25	7.5	8.0	7.5	7.0
C = 2000 μFd	9.6	-	9.2	8.2	-	7.0	-	-	-
Threshold Energy (joules)									
C = 4000 μFd	1450	1620	2000	1620	2000	2000	1620	2000	2200
C = 2000 μFd	1100	-	1210	1210	-	1320	-	-	-
Output for 4000 joules input (joules)									
C = 4000 μFd	22.2	-	16.5	19.8	-	14			
C = 2000 μFd	25.4	-	23.7	21.8	-	16.4			
Output for 5760 joules input (joules)									
C = 4000 μFd	-	-	33	-	-	27.2			
C = 2000 μFd	-	-	40	-	-	28.4			

Table VII

The slope efficiency with the dielectric mirror is 12 joules/kJ compared with 7.5 joules/kJ under the same conditions with the prism.

The slope efficiency with a capacity of 4000 μFd is slightly less than the slope efficiency with 8000 μFd. This is in agreement with the total lamp efficiency measurements of Table II (Chapter 5) for the 13 mm bore lamp.

Table II shows the 10 mm bore tube to be less efficient than the 13 mm and 15 mm tubes at an energy input above 4 kJ. All laser output results show the opposite. The lamp efficiency measurements do not, however, consider the spectral distribution of the radiation and the 10 mm bore tube is possibly more efficient at the ruby absorption wavelengths with its total efficiency slightly less. The calculated cavity pumping efficiency is also slightly greater for the 10 mm bore lamp.

The laser threshold is lower when the 2000 μFd bank is used and is also reduced when the inductance is reduced. The shorter flash duration results in a pulse of greater intensity for a given energy. This follows from theoretical considerations of the pumping intensity and laser losses, since it is a minimum pumping intensity not merely energy input that is required at threshold to overcome the photon losses of the Fabry-Perot cavity. The threshold energy values given are accurate to the nearest 50 volts (an energy difference of 220 joules between 1.0 and 1.05 kV with C = 4000 μFd) and correspond to the appearance of a lasing filament visible as an intense spot on a diffuse screen 30 cm from the end of the rod.

The increased slope efficiency with decreasing flash duration and consequent increase of peak intensity also follows from theory because the Fabry-Perot cavity loss affects the stimulated photon intensity with a large population inversion less than it would with a small one.

Operation with a smaller capacitor bank results in a lower threshold and the energy output for a given input is higher (Table VII) despite the slight decrease in slope efficiency. Since the difference in cost between a 2000 μFd and 4000 μFd capacitor bank and power supply unit is in the region of £500, the capacity value is an important design parameter.

The following operating conditions all produce a laser output of 25.4 joules with the 10 mm bore tube.

a) C = 2000 μFd, V = 2.0 kV, L = 100 μH, Flash duration = 1.05 milliseconds, Energy input 4000 joules, Wall loading 73.5 kW/sq.cm.

b) C = 2000 μFd, V = 2.05 kV, L = 450 μH, Flash duration = 2.0 milliseconds, Energy input 4200 joules, Wall loading 40.2 kW/sq.cm.

c) C = 4000 μFd, V = 1.5 kV, L = 235 μH, Flash duration = 2.14 milliseconds, Energy input 4500 joules, Wall loading 40.2 kw/sq.cm.

Although a is the most efficient, the lamp wall loading is excessively high and would result in a very short lamp life. b is slightly less efficient but the lower lamp wall loading is obviously advantageous, and the output is obtained with a smaller capacitor bank than c. The maximum working voltage of the capacitors (2.5 kV) would, however, limit the energy output of the system in b to about 30 joules (N.B. with the prism reflector).

To sum up, for maximum efficiency the system is operated with a low bank capacity, high bank voltage and short flash duration and as low a flash tube wall loading as possible.

The 10 mm bore and 13 mm bore lamps are listed in the commercial range of Thermal Syndicate Limited, reference numbers T/E6/94 No. 2 and T/E6/79 No. 2 respectively.

8.4 The Effect of Polishing the Cylindrical Surface of the Rod

During early experiments with the laser system, the fine ground cylindrical surface of a rod suffered damage after about thirty exposures to the excitation energy at lamp inputs above 8000 joules. Small chips of material became detached from the ruby opposite the lamp (See figure 42). To rule out the possibility of surface strain caused by grinding the rod from the boule, rod blanks were annealed after finishing the cylindrical surface and before the end faces were polished. This procedure did not prevent damage.

The damaged laser rod was examined by x-ray at the University of Durham for crystallographic perfection. (G.L. STURGESS - Private communication). Grain misorientation of the order of $\frac{1}{2}^{o}$ - 1^{o} was detected in the damaged area although examination of the surrounding crystal showed points of good material. Further exposure of the rod to the high intensity pumping radiation caused damage at the points of good material so it is probable that the misorientation was induced by the radiation damage.

In order to determine the effect of the rod surface finish on the damage, the cylindrical surface of rod 516 was given a highly polished surface finish. The polished rod was exposed to a flash energy of 10 kJ input for about fifty shots, the only sign of surface damage after this test being a small matt area. Since this area appeared to have a carbon deposit, it is presumed that a dirt particle (probably deposited by the nitrogen cooling gas) was vapourised to form a small area of absorption.

A $\frac{1}{4}$" thick sample slice of ruby was polished for spectrophotometric examination. One face of the sample was then given the same 14 micron matt surface finish as the laser rods and the transmission characteristics again measured. The ultra-violet transmission of the sample dropped from about 50% to 1% and the infra-red transmission dropped from about 50% to an average of 10% when the face of the sample was fine ground. This

Figure 42: LASER ROD SURFACE DAMAGE

additional absorption or scattering is occuring in a surface layer only about 20 microns thick and it is therefore not surprising that surface damage occurs with a high energy flux.

The damage does not occur when the rod is surrounded by a water cooling jacket. (D.H. ARBIB, G. and E. BRADLEY LTD., Private communication). Since water absorbs infra-red energy above about 1.5 micron and has a fairly good ultra-violet transmission, it is probable that the infra-red component of the flash tube radiation is mainly responsible for the surface damage.

A polished cylindrical surface on the rod causes a marked decrease in efficiency. Figure 43 compares the output characteristic of rod 516 with a polished and fine ground barrel. With the prism and sapphire disc reflectors, the laser output with a polished barrel saturates at about 8 joules for 5 kJ input and above, irrespective of the circuit inductance. A similar result was obtained with a dielectric coated mirror used in place of the prism, although the output with the mirror is increased to about 12 joules for 5 kJ input. The outputs of the rod with fine ground barrel are 23 joules and 28 joules with the prism and mirror respectively for 5 kJ input.

Possible explanations for the reduced efficiency are:

a) The polished cylindrical surface increases the activity of spurious modes due to internal reflection at the walls (see section 1.4). In this event the beam divergence should be larger, a factor which is discussed in Chapter 9.

b) The fine ground cylindrical surface reduces the heating effect on the bulk of the rod by the pumping pulse due to the reduced infra-red transmission. This seems unlikely to affect the temperature of the material during a 3 millisecond pumping pulse enough to account for the differences in output.

c) A paper by GREENE, EMMETT and SCHAWLOW (1966) states that intense ultra-violet pump light is detrimental to ruby laser output. Measurements on a similar flash tube with a spectroradiometer (GONCZ and NEWELL 1966) indicate that about 20% of the lamps energy output is in the ultra-violet region between 0.2 and

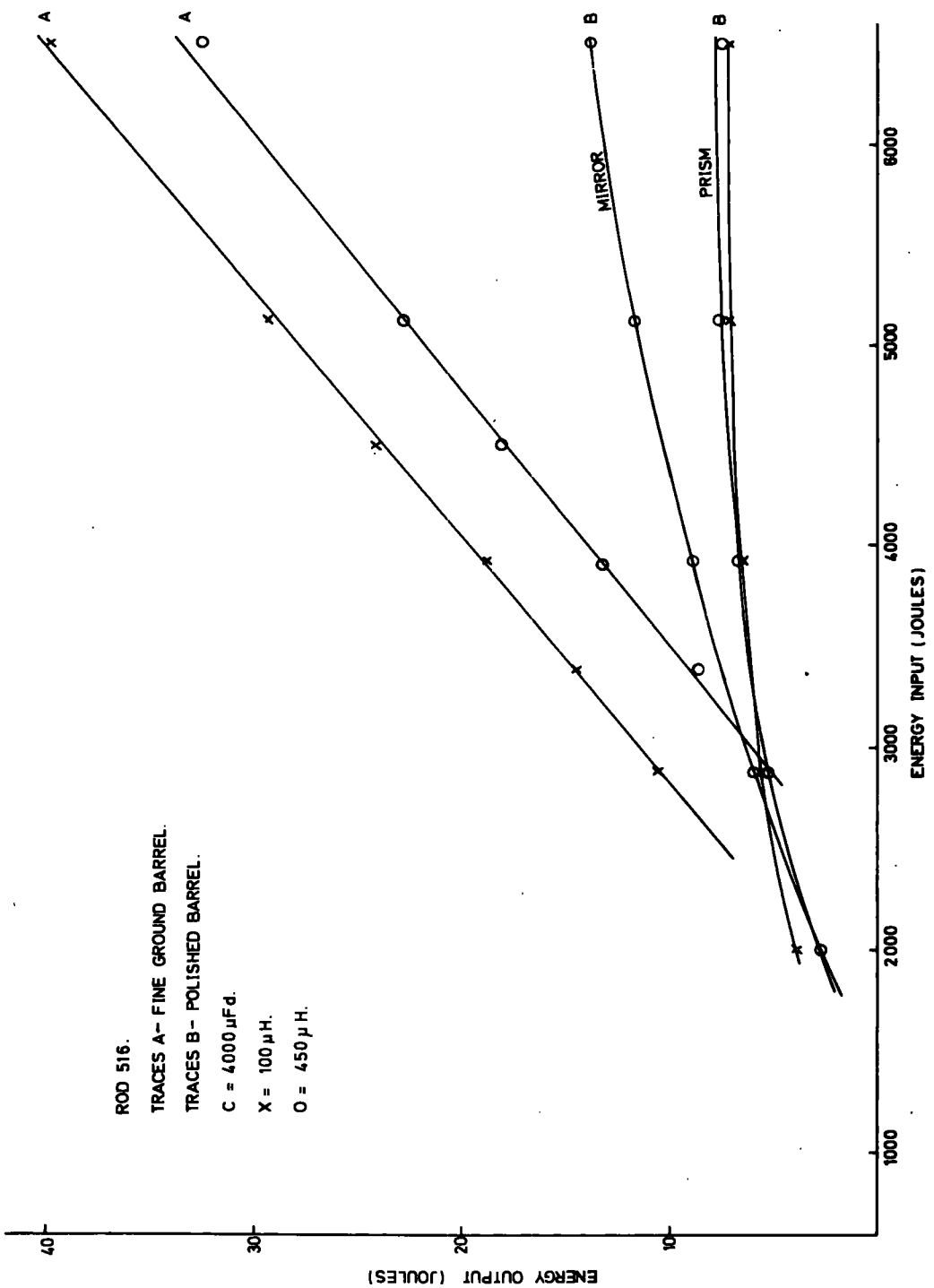

Figure 43: EFFECT OF POLISHED BARREL ON ENERGY OUTPUT

0.35 micron when the lamp is operated at a high current density.

Further experiments would be necessary to filter out the ultra-violet and infra-red components of the lamp radiation and observe whether polishing of the cylindrical surface has the same effect on the laser output. Since the addition of a water cooling jacket eliminates the surface damage effect with a fine ground rod, there is no point in using a rod with a polished barrel and the above experiment would be of academic interest only.

8.5 The Effect of Optical Correction by Mirror Alignment

Only two of the laser rods used had well defined optical wedges, 970 and 974. Alignment of the far mirror through 974 proved impossible due to the considerable distortion of the autocollimator image seen through the rod. Rod 970 possessed a well defined optical wedge with no gross distortion of the graticule image. The mirror was offset horizontally from the parallel position by 3 minutes of arc to make the image from the end of the rod and that through the rod coincide.

Figure 44 shows energy output versus energy input with parallel and offset mirror alignment for rod 970. The results show that the output is slight increased when the reflector is aligned to compensate for the optical wedge of the crystal. The slope efficiency and the laser threshold were unchanged.

To provide further information, another rod (B) with a clearly defined optical wedge was obtained. With this rod, it was necessary to move the mirror 1 minute horizontally and 4 minutes vertically to the compensated position. The output in the compensated position was increased by 8½% of that obtained with the mirror aligned parallel to the end of the rod.

If the energy output at a set input is plotted against the alignment, the peak of the graph corresponds to the optically corrected position. The effect of mirror alignment on the output of these particular rods is not critical, the energy being within 80% of the peak value over several minutes of misalignment. To polish a rod of this optical quality to a highly accurate

end face parallelism is therefore a costly waste of effort. Optical correction by polishing the end faces several minutes out of parallel to compensate for the optical wedge produces more efficient operation. This factor is of greater importance with smaller rods where dielectric coatings deposited on the end faces of the rod form the reflectors.

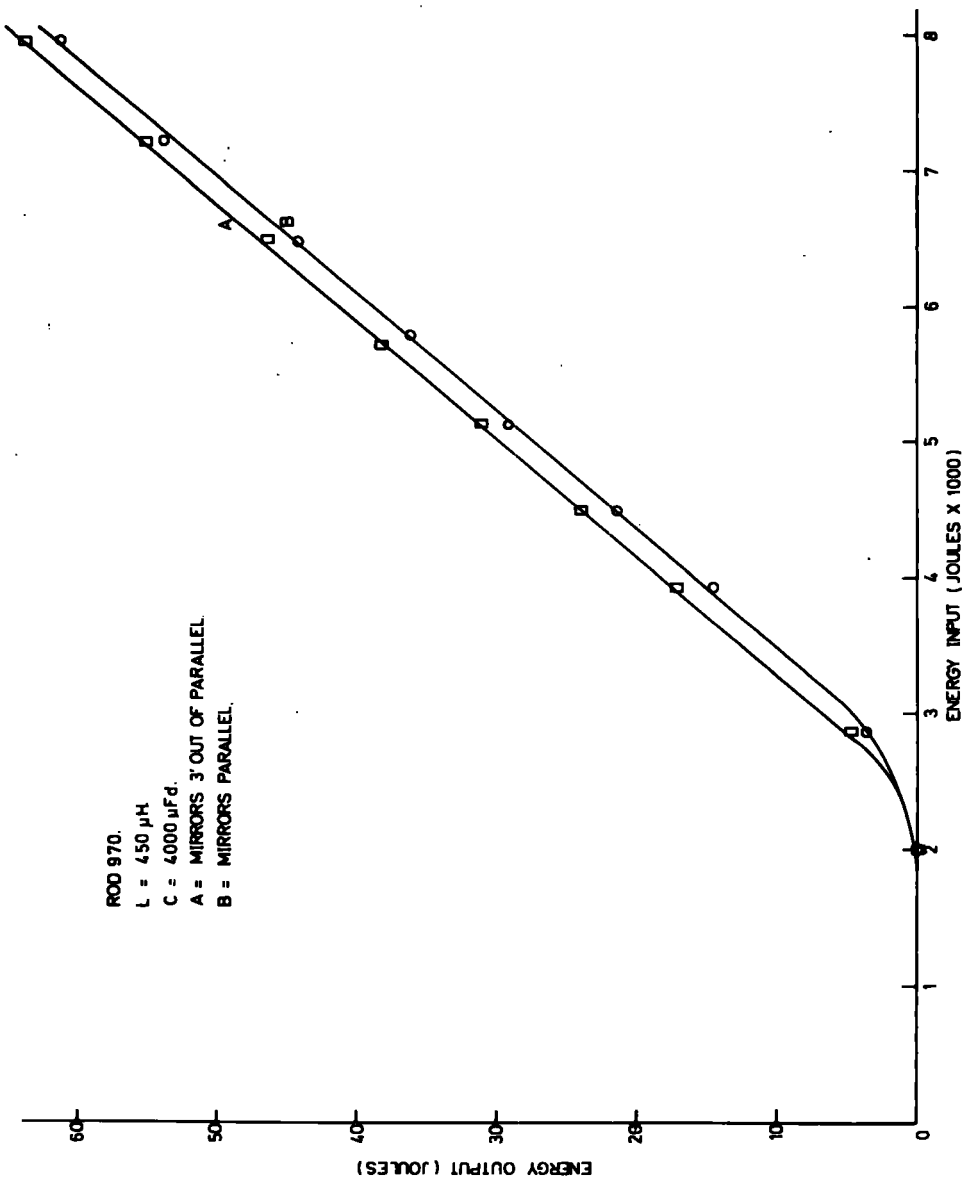

Figure 44: EFFECT OF OPTICAL WEDGE COMPENSATION

Chapter 9. Output Beam Divergence

9.1 Theoretical Considerations

The energy contained in a given cone angle must be carefully considered in the design of a laser system. The beam divergence is dependent on the crystal perfection, geometry of the system, external mirror reflectivity and degree of excitation of the rod. Near the laser threshold stimulated emission amplification occurs only in the low loss axial modes. The beam divergence will increase with increasing energy input above threshold as higher loss non-axial modes may be excited.

From beam divergence measurements on 37 rods 2" long x $\frac{1}{4}$" diameter, KELLINGTON and KATZMAN (1965) concluded that the probability of obtaining the smallest possible beam divergence is increased but not guaranteed by selecting a rod with the best optical quality. Their measured values in the 1 to 4 milliradian region (total divergence angle) were obtained with a reflector spacing of 40 cm. These figures are much greater than the value according to diffraction theory which for a plane wave front of circular aperture d passing through a perfect material gives a beam divergence for a zone containing 83% of the beam energy of:

$$\phi = \frac{1.22\lambda}{d} \quad \text{radians}$$

For d = 1 cm and λ = 6943Å, the diffraction limited beam divergence would be 8.5×10^{-2} milliradians.

In a non-ideal material the plane wave front is distorted due to variations in the optical path length and the beam divergence increases. Optical path length variations in ruby are due to refractive index changes caused by variable composition, misorientation and strain. If it is assumed that the beam is not diffraction limited and that refractive index variations are symmetric about the axis of the beam, it can be shown (CHARVAT, SMITH and NESTOR 1966) that the beam divergence of an imperfect material is given by:

$$\theta = 4 \frac{L}{D} (\Delta n) \text{ radians} \qquad (9.1)$$

where θ is the beam half angle, L the length and D the diameter of the crystal and Δn the index change across the radius.

The dependence of $\Delta\eta$ on misorientation, strain and variation in chromium content has been estimated from available data in the literature (NESTOR 1964)

Beam divergence depends on these factors as follows:

$$\theta = 1.2 \times 10^{-2} \frac{L}{D} \Delta C \qquad (9.2)$$

where ΔC is the weight % Cr_2O_3 variation

$$\theta = 1.0 \times 10^{-5} \frac{L}{D} \psi^2 \qquad (9.3)$$

where ψ is the degree of misorientation for a 90° rod (ψ in degrees)

$$\theta = 4.0 \times 10^{-7} \frac{L}{D} S \qquad (9.4)$$

where S is the residual strain in p.s.i.

Radial temperature variation is also considered, and if ΔT (°C) is the radial temperature variation in the rod then,

$$\theta = 8.8 \times 10^{-5} \frac{L}{D} \Delta T \qquad (9.5)$$

The thermal gradients that evolve during the pumping pulse can contribute significantly to the beam divergence.

The net beam divergence will depend on the contribution from all the above sources. One source may predominate.

In these experiments, the Twyman-Green interferometer is used to assess optical path differences in the laser rod. Specifying the crystallographic and temperature variation that will produce a displacement of one fringe in a Twyman-Green interferogram of the rod (NESTOR 1964) gives the following values (taking λ = 7000Å, with L in cm):

$$\Delta C = \frac{1.2 \times 10^{-2}}{L}$$

$$\psi = \frac{3.7}{\sqrt{L}} \quad \text{(for a 90° rod)}$$

$$\Delta S = \frac{350}{L}$$

$$\Delta T = \frac{1.6}{L}$$

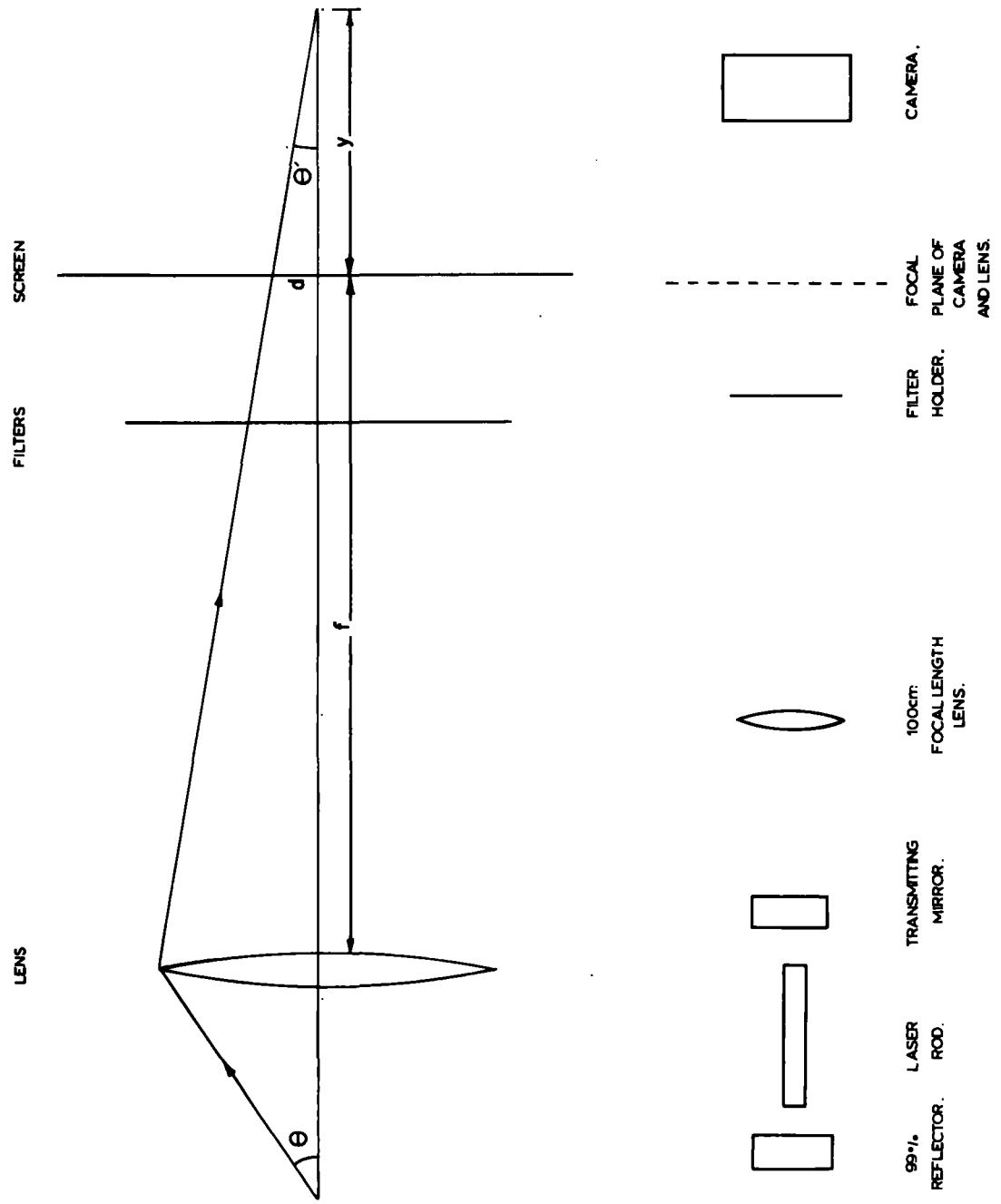

Figure 45: MEASUREMENT OF BEAM DIVERGENCE

Referring to figure 45, if θ is the half angle beam divergence, then by the Helmholtz equation,

$$\frac{\tan \theta}{\tan \theta'} = \frac{y}{f}$$

where f is the focal length of the lens.
For small angles, $\theta = \tan \theta$ and $\tan \theta' = d/y$ where d is the radius of the beam, then:

$$\theta = \frac{d}{f} \text{ radians}$$

For f = 100 cm, measurement of the spot diameter in millimetres gives the whole divergence angle of the beam, i.e. 2θ.

9.3 Results

The Fabry-Perot cavity was formed by the maximum reflectivity mirror and the opposite ruby-air interface.

The beam divergence at the same energy output was measured for the six ruby rods. The values are shown in the following table:

Rod Number	Radial Index Variation $\Delta n \times 10^{-5}$	Beam Energy Joules	Spot Size on Film mm	Beam Divergence θ milliradians
633	6.3	18.1	23	11.5
893	6.3	18.0	22	11.0
970	7.85	17.5	23	11.5
974	11.5	18.5	23	11.5
1150	2.3	19.0	21	10.5
516	2.3	19.0	17.5	8.7
13 mm bore flash tube L = 450μH C = 4000μFd				

The radial refractive index variation was calculated from the number of Twyman-Green fringes visible in the O-ray interferogram of the rod. (See figure 37). The calculated beam divergence is computed using equation (9.1), although these figures can only be meaningful for rods having a symmetric fringe pattern, viz: 516, 893, 633.

Rod Number	633	893	970	974	1150	516
Calculated Divergence	3.3	3.3	4.1	6.0	1.2	1.2
Measured Divergence	11.5	11.0	11.5	11.5	10.5	8.7

These figures show that there is little difference in beam divergence with optical quality for rods 633, 893, 970 and 974 with fringe counts of 10, 10, $12\frac{1}{2}$ and $18\frac{1}{2}$ fringes/in/in respectively. The two better quality rods 1150 and 516 (both 3.8 fr/in/in) have a lower beam divergence. Rod 516 has a more symmetric interferometric pattern, the lowest fringe count and the lowest beam divergence of the six rods. The difference between the calculated values and the higher measured values can easily be accounted for by temperature variation during pumping.

The three best rods, 516, 893, and 1150 were used in further experiments to measure the variation of beam divergence with energy output. For each rod, energy output and beam divergence were measured with and without the sapphire reflector. These results are shown graphically in figure 46. In each case the increased Fabry-Perot cavity length when using the sapphire reflector results in a reduced beam divergence. The beam divergence increases with increasing energy input, this effect being more apparent up to $1\frac{1}{2}$ times the threshold energy.

The effect of a polished lateral surface on 516 was also studied. With only the maximum reflectivity mirror, the energy output is reduced to below 1 joule for 8,000 joules input and the beam would not mark the film. With the sapphire disc and mirror, measurable spots were obtained. From the graph (Figure 46), it can be seen that the beam divergence of 516 with a polished barrel was the lowest measured in these experiments, although the energy conversion efficiency of the rod in this condition is substantially reduced. (This effect was discussed in Chapter 8.4). This reduced divergence is the opposite of the expected result, since the effect of polishing the lateral surface is more likely to increase the beam divergence due to the possible excitation of transverse modes resulting from total internal reflection at the polished surface. However, it is possible that a strong focussing action occurs due to the polished rod side making the excitation of axial modes more likely.

The low efficiency characteristic of 516 with polished barrel is probably due to the heating effect suggested in Chapter 8.4, rather than the excitation of transverse modes which would give a high beam divergence.

9.4 Conclusion

Within the accuracy of these experiments, the results agree with the theoretical considerations of decreased beam divergence with an increased Fabry-Perot cavity length and an increased beam divergence with increasing energy input. The main result is that the rods giving the lowest beam divergence are of the best optical quality.

For the poorer quality rods, variation of beam divergence with optical quality is not significant.

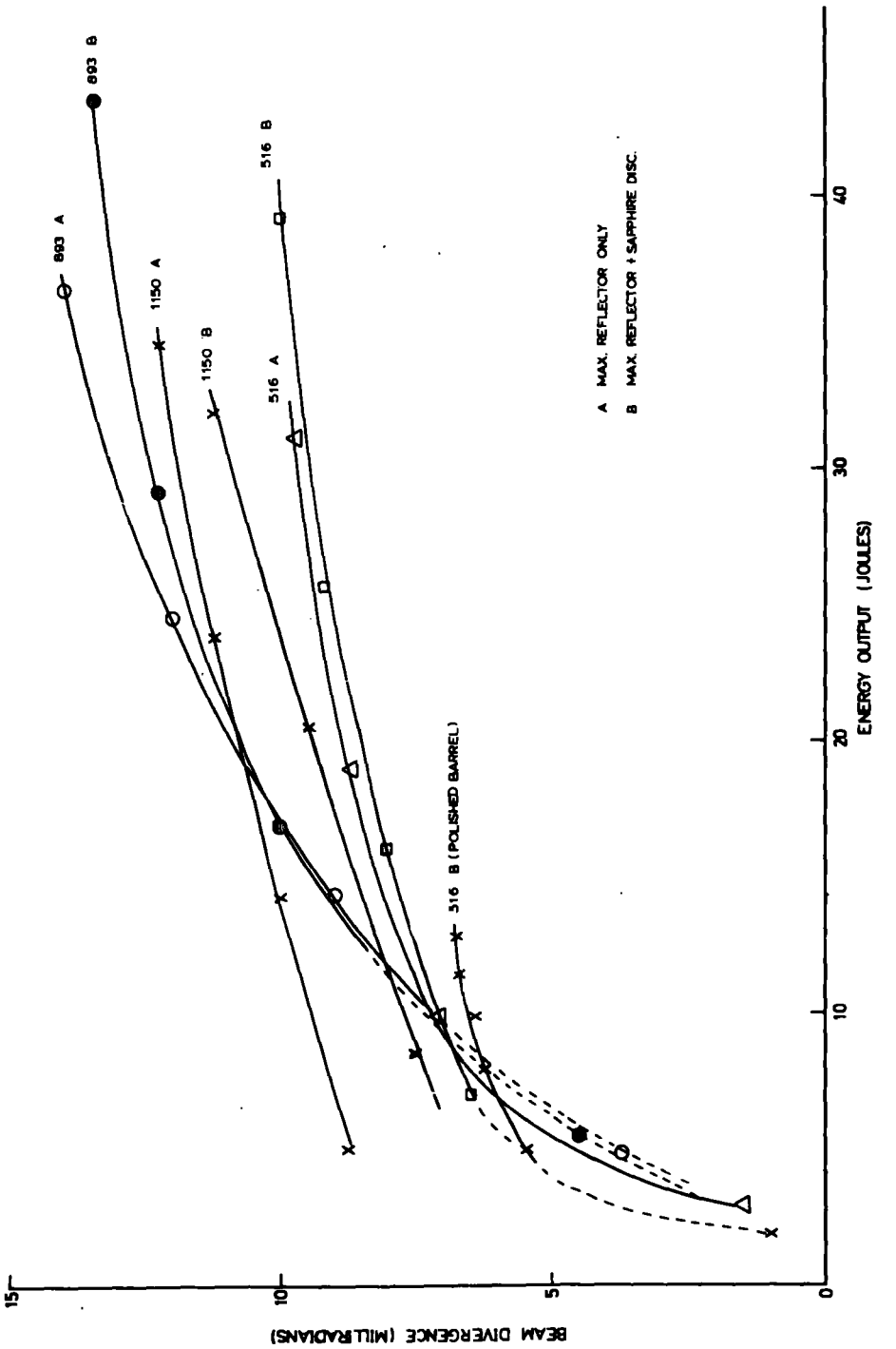

Figure 46: VARIATION OF BEAM DIVERGENCE WITH ENERGY OUTPUT

REFERENCES

BORN M. and WOLF E. 1959	Principles of Optics (Pergamon Press), P.322.
BOWNESS C. 1965	Applied Optics 4 (1), P. 103.
BOWNESS C. and MISSIO D.V. 1963	Raytheon Electronic Progress VII, 6. (Jan. - Feb. 1963)
CHARVAT F.R. SMITH J.C., and NESTOR O.H. 1966	Proc. Int. Conference on Crystal Growth. 20th - 24th June, 1966 (Pergamon Press) P. 45.
CHERNOCH J.P. and TITTEL K.F. 1965	Rev. Sci. Instr. 36 (3). P.392.
CIFTAN M. et al 1961	Proc. I.R.E. 49. P. 960.
CONGLETON R.S. et al 1963	Quantum Electronics III Volume II, (Columbia University Press) P. 1415.
EDWARDS J.G. 1967	Applied Optics 6 (6) P.1011
GONCZ J.H. and NEWELL P.B. 1966	J.O.S.A. 56 (1). P.87.
GREENE R.L., EMMETT J.L. and SCHAWLOW A.L. 1966	Applied Optics 5 (2). P.350.
GUREVICH I.M. and CHARNAYA F.A. 1963	Optics and Spectroscopy 14 (4). P.297.
HELLWARTH R.W. 1961	Advances in Quantum Electronics (Columbia University Press). P.344.
KAISER W. and KECK M.J. 1962	J. Appl. Phys. 33. P.762.
KAMIRYO K. et al 1965	Proc. I.E.E.E. 53 (11). P.1750.
KELLINGTON C.M. and KATZMAN M. 1965	J. Appl. Phys. 36. P.2910.
LENGYL B.A. 1966	Introduction to Laser Physics. (John Wiley and Sons Inc.). P.80.
LISITSA M.P. et al 1966	Optics and Spectroscopy 21 (1). P.41.
MAIMAN T.H. 1960	Brit. Commun. and Electronics 7. P.674.
MAIMAN T.H. 1964	Microwaves July 1964.
MARSHAK I.S. 1956	Proc. 3rd Int. Congress on High Speed Photography (Edited by R.B. Collins) Sept. 1956. P.30.
NELSON D.F. and BOYLE W.S. 1962	Applied Optics 4. P.531.

NESTOR O.H. 1963-1964	Annual Summary Report on Czochralski Ruby. U.S.A. Contract NONR-4132 (00) Union Carbide Ltd., Linde Division.
PASHKOV V.A. and ZVEREV G.M. 1967	Soviet Physics J.E.T.P. 24 (3). P.516.
ROESS D. and ZEIDLER G. 1966	Electronics Sept. 5 1966. P.115.
SIMS S.D., STEIN A. and ROTH C. 1966	Applied Optics 5 (4). P.621.
SOFFER B.H. and HOSKINS R.H. 1965	Appl. Phys. Letters 6. P.200.
SPECTRA-PHYSICS INC. 1966	Mountain View, California U.S.A. Laser Technical Bulletin No. 5 and Data Sheet on Model 331 Beam Expanding Telescope.
TANG C.L., STATZ H. and De MARS G. 1963 and 1964	J. Appl. Phys. 34. P.2289 1963 Appl. Phys. Lett. 2. P.222 1963 Phys. Rev. 136, A1-8, 1964
VEDUTA A.P. et al 1965	Soviet Phys. J.E.T.P. 21 (1). P.59.
VERNEUIL A. 1904	Am.Chem.Phys. 3. P.20.
WHITEMAN P. 1966	M.Sc. Thesis. University of Durham.
YARIV A. and GORDON J.P.	Proc. I.E.E.E. 51 (1). P.4.